FACULTY
OF MATHEMATICS
AND PHYSICS
Charles University

DOCTORAL THESIS

Mariia Uzhytchak M. Sc.

Influence of functionalized nanoparticles of different sizes, materials, and surface properties on cellular machinery

FZU - Institute of Physics of the Czech Academy of Sciences, Department of optical and biophysical systems, Laboratory of Biophysics

Supervisor of the doctoral thesis: Oleg Lunov, Ph.D.
Study program: P4F4 Biophysics, chemical and macromolecular physics

Praha 2024

I declare that I carried out this doctoral thesis independently, and only with the cited sources, literature, and other professional sources. It has not been used to obtain another or the same degree. I understand that my work relates to the rights and obligations under Act No. 121/2000 Sb., the Copyright Act, as amended, in particular the fact that the Charles University has the right to conclude a license agreement on the use of this work as a school work pursuant to Section 60 subsection 1 of the Copyright Act.

In . . . . . date . . . . . .

. . . . . .

Author's signature

Dedication.

This dissertation stands as a milestone in my academic journey and a testament to the profound impact of those whose support and guidance have illuminated my path.

Foremost, my sincere gratitude is reserved for Dr. Oleg Lunov, whose mentorship exceeded the boundaries of conventional academia, bringing a sense of joy and enlightenment to both my scientific endeavors and my life in broader terms. Oleg has been more than a supervisor to me. He stands as an example of an excellent scientist, my close friend, and a beacon of inspiration. His unconditional support has been a constant source of strength and encouragement throughout my academic voyage. Every day, he challenged me to overcome my limits, fostering my growth as a scientist and a person. Special appreciation goes next to Dr. Mariia Lunova, by being equally influential, she graciously shared her knowledge and insight, enriching my professional path and personal development. I am deeply grateful for their support, guidance, and encouragement, which have been instrumental in my achievements.

In parallel, I extend my profound appreciation to Dr. Alexander Dejneka, the head of our department, whose leadership and insightful conversations have significantly contributed to my understanding of life, human behavior, and the subtle art of navigating interpersonal relationships.

To my family, whose patience, love, and belief in my pursuits have been the silent, steadfast pillars upon which I have leaned during moments of doubt and celebration alike, I owe an immeasurable debt of gratitude. Your sacrifices and unwavering faith in me have been the bedrock of my resilience and determination.

Lastly, I would like to acknowledge a somewhat unconventional recipient of gratitude—myself. This journey has been a testament to the power of perseverance, the importance of seeking reasons to continue, to fight, and to

find the strength within to overcome challenges, no matter the odds. This dedication, therefore, is also a recognition of my own journey, of never yielding to despair and always striving towards the light of knowledge and understanding.

In sum, this thesis does not simply represent the culmination of years of research; it embodies a journey enriched by those who have inspired, supported, and believed in me. To all of you, I extend my deepest thanks.

Title: Influence of functionalized nanoparticles of different sizes, material, and surface properties on cellular machinery

Author: Mariia Uzhytchak

Department: Department of Optical and Biophysical Systems, Institute of Physics of the Czech Academy of Sciences

Supervisor: Mgr. Oleg Lunov, PhD., Department of Optical and Biophysical Systems, Institute of Physics of the Czech Academy of Sciences

Abstract:

Last few decades nanoparticles (NPs) have emerged as promising tools in the nanomedicine field as theranostic agents. The influence of functionalized nanoparticles with different sizes, material compositions, and surface properties on cellular machinery has attracted significant research interest. Understanding these influences is crucial for the development of safe and effective nanomedicines. This study aims to explore the impact of functionalized nanoparticles on cellular machinery and kinetics. Hereby, the thesis is focused on the importance of gaining knowledge in the field of nanomedicine while considering potential harms associated with nanomaterials application.

Keywords: cell culture, cell signaling, cytotoxicity, nanoparticles, drug delivery

Název: Vliv funkcionalizovaných nanočástic různé velikosti, složení a povrchových vlastností na buněčné funkce

Autor: Mariia Uzhytchak

Oddělení: Oddělení optických a biofyzikálních systémů, Fyzikální ústav Akademie věd České republiky

Vedoucí práce: Mgr. Oleg Lunov, PhD., Oddělení optických a biofyzikálních systémů, Fyzikální ústav Akademie věd České republiky

Abstrakt:

V posledních několika desetiletích se nanočástice (NP) ukázaly jako perspektivní nástroje v oblasti nanomedicíny jako teranostické agenty. Vliv funkčně modifikovaných nanočástic s různými velikostmi, materiálovým složením a povrchovými vlastnostmi na buněčný aparát přitahuje značný výzkumný zájem. Porozumění těmto vlivům je klíčové pro vývoj bezpečných a účinných nanoléčiv. Tato studie si klade za cíl prozkoumat vliv funkčně modifikovaných nanočástic na buněčný aparát a kinetiku. Práce se zaměřuje na získání znalostí v oblasti nanomedicíny s ohledem na potenciální nežádoucí účinky spojené s aplikací nanomateriálů.

Klíčová slova: kultivace buněk, buněčné signalizace, cytotoxicita, nanočástice, doručování léčiv

Content

1. Introduction

1.1 Basics of Biomedical Nanotechnology:

1.1.1 Definitions of Nano-drugs (Nanomedicines)

Over the last several decades biomedical nanotechnology has been established as an interdisciplinary field that merges principles and methods of nanotechnology with biomedical sciences, aiming to develop innovative solutions for medical applications. Nano-drugs or nanomedicines have unique physicochemical properties, high reactivity, and most importantly biocompatibility which allows them to enhance drug delivery, and overall therapeutic efficacy and reduce side effects compared to conventional drugs. Due to their specificity and certain benefits, nano-drugs have the potential to significantly boost nanoscience research for the further improvement of diagnostics and treatment.

The terminology "nanoparticle" and "nanomedicine" itself has been debatable and needs thoughtful consideration in its integrity [1, 2]. However, according to the U.S. Food and Drug Administration (FDA), nanomedicine is defined as *"(1) whether a material or end product is engineered to have at least one external dimension, or an internal or surface structure, in the nanoscale range (approximately 1 nm to 100 nm). (2) whether a material or end product is engineered to exhibit properties or phenomena, including physical or chemical properties or biological effects, that are attributable to its dimension(s), even if these dimensions fall outside the nanoscale range, up to one micrometer (1,000 nm)."* [3, 4] Concurrently, the European Medicines Agency (EMA) identifies nanomedicine as *"the application of nanotechnology in view of making a medical diagnosis or treating or preventing diseases. It exploits the improved and often novel physical, chemical and biological properties of materials at*

nanometer scale". [3] So far, the EMA specifies the nanometer scale as the range of 0.2 nm to 100 nm. Those definitions emphasize the importance of size-dependent properties and effects associated with nanomedicines. Both agencies approve newly discovered nanodrugs, regulate nanomedicine safety usage, and their potential harm to the organism. It is important to note that the precise definitions of "nano", "nanotechnology", and "nanomedicine" vary among different sources and regulatory agencies, which can create challenges and discrepancies in research and terminology. Nevertheless, efforts have been made to regulate and unify the terminology and experimental approaches to enhance the understanding and reproducibility of nanomedicine research.

1.1.2 Overview of biomedical applications of nanoparticles.

The rapid development of nanoparticles in biomedicine has significantly transformed medical science, representing innovative methodologies for diagnosis, imaging, personalized therapies, and effective drug delivery within the last several decades (Figure 1). Due to nanomedicine's unique properties such as size, charge, surface and core compositions, origin, both natural and synthetic, toxicity effect, and many others, it became a powerful tool for a variety of biomedical applications. Nanoparticles have been extensively used as drug delivery agents due to their ability to encapsulate drugs, both hydrophobic and hydrophilic, protecting them from degradation and enhancing their properties. Nanoparticles offer controlled release, prolonged circulation in the bloodstream, biodegradability, and targeted drug delivery to specific tissue sites and cells, minimizing toxic effects [5-7].

Moreover, nanoparticles can be designed to recognize and bind to specific tissue sites and cell types. This targeted delivery is pivotal in reducing off-target effect, and cytotoxicity and enhancing the therapeutic index of various drugs. [8], [5, 9]. Since nanoparticles are abundantly employed in cancer treatment for

targeted drug delivery and imaging, they are facing various drawbacks in their utilization. NPs usually accumulate in tumor tissues due to the enhanced permeability and retention (EPR) effect - a phenomenon where nanoparticles mostly accumulate in tumor tissue, enabling the delivery of chemotherapeutics directly to the cancer cells while not affecting healthy tissues. Furthermore, the variability of nanoparticles allows them to be conjugated with imaging agents, enhancing the contrast and resolution of various imaging techniques, such as magnetic resonance imaging (MRI), computed tomography (CT), and ultrasound. Consequently, a variety of nanoparticles serve these purposes. Quantum dots, for instance, are nanoscale semiconductors that emit light, utilized in fluorescence microscopy and in vivo tracking. Superparamagnetic iron oxide nanoparticles (SPIONs) improve magnetic resonance imaging (MRI) due to their magnetic characteristics. Gold nanoparticles are preferably used in certain computed tomography (CT) scans and photoacoustic imaging for their distinctive optical qualities. Moreover, targeted imaging is achieved by attaching nanoparticles to antibodies that track and localize cancer cells, thus upgrading diagnostic accuracy and treatment. Functionalized nanoparticles can target specific biomarkers, allowing for early disease detection, accurate diagnosis, and monitoring of disease progression [5, 6, 10, 11].

However, theranostic nanoparticles combine therapeutic and diagnostic properties in a single nano model. [5, 6]. They enable simultaneous imaging of disease sites and the delivery of therapeutic agents, facilitating real-time monitoring of treatment responses. In this regard, nanotechnology has provided a flexible platform for the innovation of vaccines using nanoparticles as carriers for antigens or adjuvants. This has significant implications for the field of immunotherapy, where the goal is to train the immune system to recognize and fight pathogens and tumor cells more effectively. Thus, nanoparticles can also be engineered to simulate the size and surface patterns of pathogens, which can enhance the recognition and uptake by antigen-presenting cells (APCs), leading

to a stronger and more specific immune response. The surface of nanoparticles can be modified with targeting ligands that can further stimulate the immune system or direct the nanoparticle to a specific region of interest.

The recent development of COVID-19 vaccines has demonstrated the power of nanoparticle-based vaccines. This novel approach has several benefits over traditional vaccine methods. It allows rapid development and production, which was crucial in response to the pandemic. The stability and efficacy of mRNA are significantly enhanced by the encapsulation within lipid nanoparticles (LNPs), ensuring that the mRNA remains intact until it is taken up by the cells after vaccination. Besides, being employed for vaccine delivery, nanoparticles can transport genetic material, such as DNA, mRNA, or small interfering RNA (siRNA) into a patient's cells to treat a disease. The genetic material needs to reach the target cells and be expressed without being degraded by the patient natural immune responses. Once inside the target cells, the genetic material can be released to produce the desired therapeutic effect — either by correcting a genetic mutation, silencing a harmful gene, or providing a new function to the cell.

Within the field of tissue engineering and regenerative medicine, nanotechnology also plays an important role. Nanoscale materials are engineered to simulate the extracellular matrix, providing an optimal surface for cells to adhere, proliferate, and differentiate. This approach allows the restoration of tissues and organs compromised by injury or disease. Neuroscience has also benefited from nanotechnology's advancements. Nanoparticles have the unique capability to go through the blood-brain barrier (BBB), which is a big challenge for conventional drug delivery systems currently. This feature holds transformative potential for treating neurological conditions and targeting brain tumors with remarkable precision. Nanoparticles, such as nanosilver, have been used in wound healing to accelerate natural tissue regeneration processes by preventing infection and promoting tissue healing. Nanoparticles have extended

their usage to intracellular sensing and monitoring, where they function as probes within the cellular matrix. By entering cells and demonstrating intracellular changes.

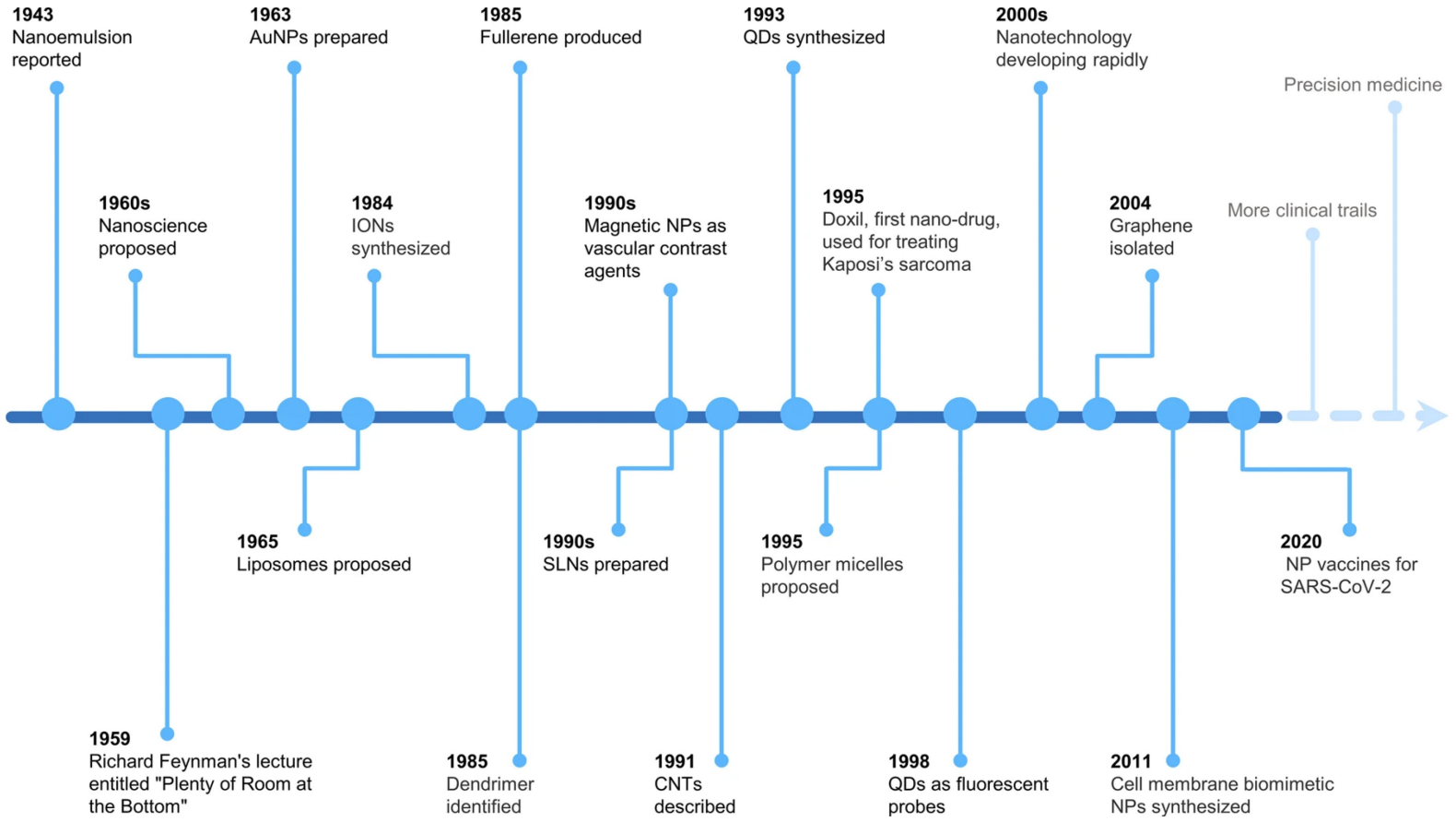

Figure 1. Historical timeline of major nanomedicine development. *Reprinted from Xu, H., Li, S. & Liu, YS. Nanoparticles in the diagnosis and treatment of vascular aging and related diseases. Sig Transduct Target Ther 7, 231 (2022). https://doi.org/10.1038/s41392-022-01082-z*

1.1.3 Types of nano-drugs. Current status

Currently, several types of nano-drugs are utilized in biomedical research and treatment, having their specific characteristics and distinct applications [6, 12-17].

One of the most frequently used nanocarriers in clinical research are lipid-based nanoparticles (LNPs), such as liposomes and solid lipid nanoparticles (SLNs). Their lipid bilayers encapsulate drug molecules within their liquid core or a specific lipid matrix, making them quite adaptable for various pharmacological and biomedical purposes. LNPs might offer controlled release, improved drug stability, and targeted drug delivery to specific tissues or cells [6, 12-17].

Polymer-based nanoparticles (NPs) – another big group of widely used NPs, specifically poly(ethylene glycol) (PEG) NPs, are primarily used as delivery agents for various therapeutic agents. These NPs can be formed from either natural or synthetic polymers and are capable of encapsulating a wide range of compounds, including both hydrophobic and hydrophilic substances. However, challenges such as aggregation and overall toxicity limit their clinical application, as evidenced by the few FDA/EMA-approved polymer NP-based nanomedicines [6, 12-17].

Carbon-based nanomaterials, such as carbon nanotubes and graphene, have unique properties that make them promising agents for drug delivery. They have high surface areas and can be functionalized with drugs or targeting ligands. Carbon nanomaterials can penetrate cellular membranes and deliver drugs intracellularly.

Inorganic-based NPs, usually metallic nanoparticles, including gold, iron, and silver nanoparticles, possess distinct physicochemical properties that enable various therapeutic applications. They can be surface-functionalized to carry drugs and target specific cells or tissues. Metallic nanoparticles also have imaging capabilities, making them valuable for diagnostic purposes in clinics [8], [6, 12-17].

Superparamagnetic iron oxide nanoparticles (SPIONs) have been explored for liver imaging in patients with suspected hepatocellular carcinoma (HCC). However, in 2013, the FDA issued a safety communication stating that certain types of SPIONs used for liver imaging should not be used in patients with moderate-to-severe kidney impairment due to the risk of nephrogenic systemic fibrosis (NSF), a rare but serious condition. This led to the withdrawal of some SPION-based contrast agents from the market [31-35].

There have been several examples of successful development and clinical application of nanoparticles within the past few years. In order to understand the complexity and challenges within this field some nanomedicines have been presented below (Table 1).

Doxil (Liposomal Doxorubicin) is a liposomal formulation of the chemotherapy drug doxorubicin. It was one of the first FDA-approved nanomedicines and has been used for the treatment of ovarian cancer, multiple myeloma, and Kaposi's sarcoma [18]. Liposomal encapsulation helps reduce the general toxicity of doxorubicin and improves its delivery to tumor cells, enhancing its therapeutic efficacy. Another successful example is Abraxane (Nab-Paclitaxel), it is a nanoparticle albumin-bound formulation of the chemotherapy drug paclitaxel. It is approved for the treatment of breast cancer, non-small cell lung cancer, and pancreatic cancer. The albumin-bound nanoparticles facilitate the delivery of paclitaxel to tumor cells, improving drug solubility and reducing the need for toxic solvents used in the conventional formulation. Further, we have, Onivyde (Irinotecan liposome injection) a liposomal formulation of the chemotherapy drug irinotecan. It is used in combination with other anticancer agents for the treatment of metastatic pancreatic cancer. Liposomal encapsulation helps improve drug stability and allows for sustained release, leading to enhanced drug accumulation in tumor tissues. One of the recently released drugs is Vyxeos (liposome-encapsulated daunorubicin and cytarabine), which is a liposomal

formulation that combines two chemotherapy drugs, daunorubicin and cytarabine. It is approved for the treatment of certain types of acute myeloid leukemia (AML). The liposomal delivery system enables a synergistic ratio of the two drugs, enhancing their effectiveness against AML cells. Another example of a single-stranded oligonucleotide nanoparticle is Defitelio (Defibrotide Sodium) which is a complex compound of sodium salt formulation of defibrotide. It is approved for the treatment of hepatic veno-occlusive disease (VOD) with renal or pulmonary dysfunction after hematopoietic stem cell transplantation. Defitelio's mechanism of action involves stabilizing endothelial cells and reducing inflammation and coagulation in the affected blood vessels.

In general, the field of nanomedicine has seen a surge in research and development, evidenced by the significant number of nanomedicines currently in phase Ⅱ clinical trials for a variety of diseases, particularly cancers and infectious diseases. Over 60 nanomedicines have already received FDA approval, marking a significant milestone in the field [6, 7, 12-17].

There has been an exponential growth in nanomedicine research, with a substantial increase in publications and ongoing clinical trials since 2015. This growth is indicative of fundamental, translational, and product-oriented research. Various nanocarrier drug delivery systems (NDDSs), made from a variety of materials discussed earlier, are at the forefront of this research. However, the translation of these NDDSs into commercial products faces challenges related to toxicity, manufacturability, instability, affordability, and quality control.

A critical aspect of nanomedicine development is understanding the *in vivo* fate and safety to ensure their successful clinical translation for patients. This understanding is crucial for overcoming the challenges in drug loading, off-target issues, safety concerns, and the complexity of clinical translation in general.

Table 1. Current list of EMA or FDA-approved nanomedicines.

Drug name	Company	Approved application	Date of first approval	Average diameter (nm)
Lipid-based nanomedicines				
Doxil	Janssen	Ovarian cancer; HIV-associated Kaposi's sarcoma; Multiple myeloma	1995 (FDA) 1996 EMA)	~87 [18]
AmBisome	Gilead Sciences	Fungal/protozoal infections	1997 (FDA)	<100 [19]
Myocet	Teva UK	Treatment of metastatic breast cancer	2000 EMA)	100-230 [20]
Marqibo	Acrotech Biopharma	Philadelphia chromosome-negative acute lymphoblastic leukemia	2012 (FDA)	~100 [21]
Onivyde	Ipsen	Metastatic pancreatic cancer	2015 (FDA) 2016 EMA)	~110 [22]
Vyxeos	Jazz Pharmaceuticals	Acute myeloid leukaemia	2017 (FDA) 2018 (EMA)	~100 [23]
Onpattro	Alnylam Pharmaceuticals	Transthyretin-mediated amyloidosis	2018 (FDA) 2018 (EMA)	~100 [24]
Polymer-based nanomedicines				
Abraxane	Celgene	Advanced non-small cell lung cancer; Metastatic breast cancer; Metastatic pancreatic cancer	2005 (FDA) 2008 EMA)	~130 [25]
Inorganic-based nanomedicines				
Feraheme	AMAG	Iron deficiency in patients with chronic kidney disease	2009 (FDA)	~ 23 [26]
Injectafer	American Regent	Iron deficient anemia	2013 (FDA)	~ 31 [27]

While nanomedicine holds great promise, there have been instances where nanomedicines were withdrawn from the market or faced with regulatory challenges (Figure 2). Here are a few examples of nanomedicines that faced issues and were subsequently withdrawn [28-30]

DepoCyt (liposomal cytarabine), a liposomal formulation of cytarabine that was used for the treatment of lymphomatous meningitis, faced issues related to drug safety and regulatory concerns. In 2006, the FDA required labeling changes for DepoCyt due to reports of increased mortality associated with its use. While the product was not officially withdrawn, its use became more restricted due to safety concerns.

Caldolor (ibuprofen lipid injectable emulsion) an injectable formulation of ibuprofen for the treatment of pain and fever, faced regulatory challenges related to its manufacturing process. In 2014, the FDA issued a warning letter to the manufacturer, Cumberland Pharmaceuticals, citing significant deviations from current good manufacturing practices (cGMP). As a result, the company voluntarily recalled Caldolor from the pharmaceutical market.

Feraheme (ferumoxytol), is an iron oxide nanoparticle formulation used as an intravenous contrast agent for magnetic resonance imaging (MRI) and the treatment of iron deficiency anemia in patients with chronic kidney disease [7, 36-39]. The nanoparticles provide a high payload of iron, allowing for improved imaging contrast and efficient iron supplementation [40, 41].

To summarize, it is crucial to address any potential risks associated with nanomedicines and meet the regulatory requirements to ensure patient safety.

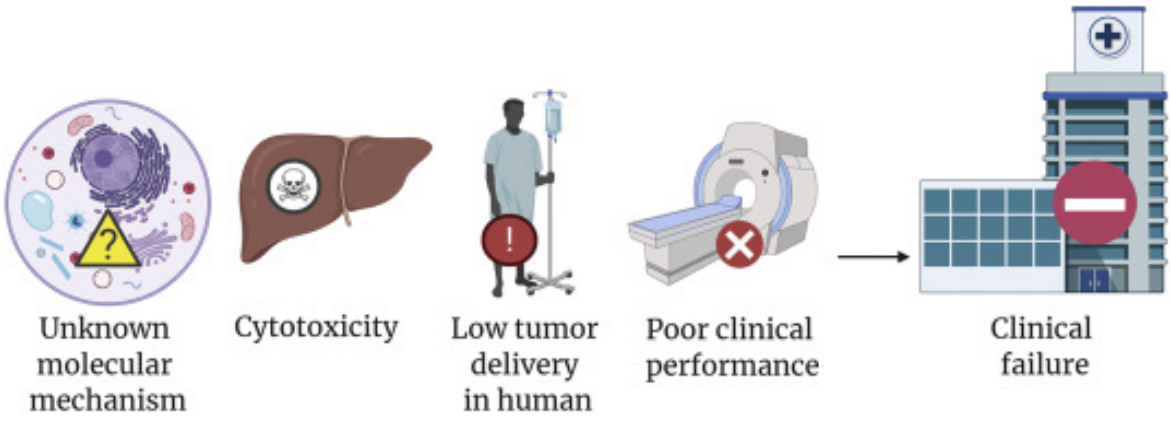

Figure 2. Summary of reasons that resulted in IONPs clinical failure. *Reprinted from Adam Frtús, Barbora Smolková, Mariia Uzhytchak, Mariia Lunova, Milan Jirsa, Šárka Kubinová, Alexandr Dejneka, Oleg Lunov. Analyzing the mechanisms of iron oxide nanoparticles interactions with cells: A road from failure to success in clinical applications. Journal of Controlled Release, Volume 328, 2020, Pages 59-77, ISSN 0168-3659. https://doi.org/10.1016/j.jconrel.2020.08.036*

1.2 Iron oxide nanoparticles in biomedical applications

1.2.1 Types of iron oxide nanoparticles utilized in biomedical applications.

Iron oxide nanoparticles (IONPs) are widely used in biomedical applications due to their unique magnetic properties, biocompatibility, and simple functionalization. Several types such as magnetite (Fe_3O_4) and maghemite (γ-Fe_2O_3) nanoparticles have unique properties due to their superparamagnetic nature, high magnetic susceptibility, and stability in biological environment. Both are typically used in magnetic resonance imaging (MRI) contrast enhancement, hyperthermia therapy, drug delivery, and bioseparation. Additionally, maghemite IONPs are usually smaller and more uniform in their size compared to magnetite and have better stability. Another example of IONPs is hematite (α-Fe_2O_3) IONPs with antiferromagnetic properties, which make them less magnetic than magnetite and maghemite, and thus more biocompatible. However, hematite IONPs are less common in biomedical applications due to lower magnetic properties but used in photothermal therapy and as a catalyst in biosensing. Another big group of IONPs is ferrites (MFe_2O_4, where M = Co, Ni, Zn, etc.). Since ferrites are mixed iron oxides with other metal ions,

their properties vary depending on the metal ion but generally exhibit superparamagnetic properties. The application covers targeted drug delivery, magnetic hyperthermia, and utilization as contrast agents in MRI (Figure 3).

Each type of iron oxide nanoparticle can be further modified with various coatings (like silica, dextran, or polymers) to enhance biocompatibility, prevent aggregation, and allow for functionalization with targeting molecules or drugs (Table 2). The choice of nanoparticle type and coating depends on the specific biomedical application and the required properties for that application. This work is focused mainly on magnetite and maghemite IONPs, which will be discussed further.

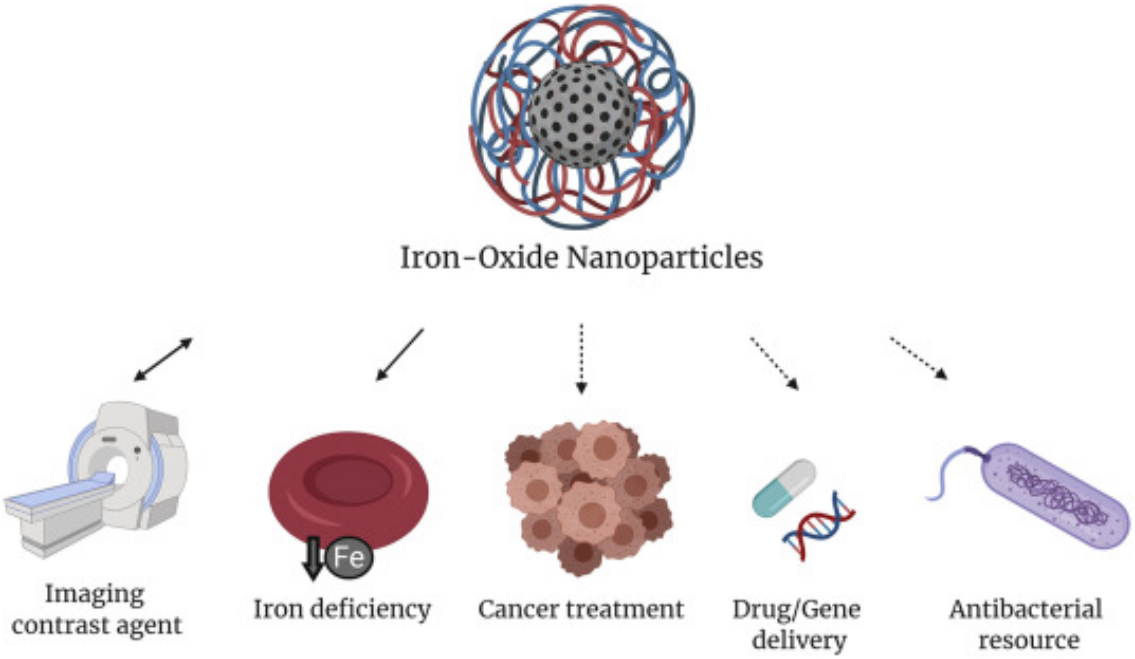

Figure 3. Summary of IONP clinical applications. Dashed arrows represent applications under development; solid arrows – approved applications; double-headed arrows – approved but lately discontinued applications. *Reprinted from Adam Frtús, Barbora Smolková, Mariia Uzhytchak, Mariia Lunova, Milan Jirsa, Šárka Kubinová, Alexandr Dejneka, Oleg Lunov. Analyzing the mechanisms of iron oxide nanoparticles interactions with cells: A road from failure to success in clinical applications. Journal of Controlled Release, Volume 328, 2020, Pages 59-77, ISSN 0168-3659.* https://doi.org/10.1016/j.jconrel.2020.08.036

Table 2. Summary of physicochemical characteristics of most frequently studied IONPs, for detailes see Appendix V.

Core composition	Core size (nm)	Hydrodynamic size (nm)	Coating	Morphology	MS (emu/g)	Targeting ligand
Hematite(α-Fe2O3) Magnetite (Fe3O4) Maghemite(γ-Fe2O3)	4-40	7-3500	Polyethylene glycol Polyvinylpyrrolidone Polyvinyl alcohol Polyacrylic acid Poly(N-isopropylacryl amide) Dextran Gelatin Chitosan Carboxydextran Silica Aminosilane Carboxylmethyl-dextran	Spherical Cubic Rods Wires	10-90	Transferrin Lactoferrin Transforming growth factor-α (TGF-α) Nerve growth factor (NGF) Ceruloplasmin Pullulan Elastin Albumin Tat-peptide RGD peptide Folic acid

MS - Saturation magnetization

1.2.2 IONPs interactions with cells

Once entering a biological environment, NPs initial interaction starts not primarily with the cells but with the surrounding biomolecules, specifically by the formation of the protein corona, which subsequently affects various cellular pathways and responses [7, 8, 42-46]. This process is happening due to proteins and amino acids present in the biological fluids, which are rapidly attached to the organic surface of the NPs [47]. The protein corona composition can vary depending mostly on the biochemical content environment and the duration of exposure. This process is crucial as it fundamentally influences the physicochemical properties, morphology, and functions of the nanoparticles from the perspective of the intracellular environment. In general, the nature of the protein corona determines how cells recognize and internalize the nanoparticles. Certain proteins can facilitate recognition by specific cell receptors, leading to more efficient uptake of the nanoparticles via different types of endocytosis. This cellular uptake is critical in applications like targeted drug delivery or imaging, where the nanoparticles need to reach specific intracellular locations [48-52].

Once inside the cell, the fate of IONPs is determined by various factors. Aggregation of nanoparticles can occur, influenced by the intracellular environment's ionic strength and pH. This aggregation can affect the nanoparticles' stability and, consequently, their function within the cell. For instance, aggregated nanoparticles might be less effective in drug delivery applications or could induce unexpected cellular responses [6, 10, 48-53].

Internalized nanoparticles can also activate various cellular pathways. Their presence within the cell can trigger responses like oxidative stress, inflammation, or even apoptosis, depending on the particle size, coating, and concentration. These responses are part of the

natural cell's defense mechanism against foreign objects. Understanding and controlling these responses are crucial for the safe application of IONPs in diagnostics and treatment. Furthermore, the redistribution of nanoparticles within the cell, and their following clearance, is a crucial aspect of their interaction with cells. The nanoparticles can be transported to different cellular compartments, where they may have different effects. The efficiency and type of clearance, whether through exocytosis or degradation within lysosomes, can impact the cell's metabolism and the overall biocompatibility of the nanoparticles [48-52, 54-56]. Certain types of NP-cell interactions are presented in Table 3.

In summary, the interaction of iron oxide nanoparticles with cells is a complex process that starts with the formation of the protein corona and extends to various cellular responses, including uptake, activation of cellular pathways, aggregation, redistribution, and clearance. Each step in this interaction has implications for both the efficacy of the nanoparticles in biomedical applications and their safety profile. Understanding these interactions in detail is crucial for advancing the use of IONPs in therapeutic and diagnostic applications, particularly in fields like cancer therapy and imaging [57].

Table 3. Summary of cellular signaling pathways affected by IONPs.

IONPs	*Cell model*	*Signaling pathways*	*Biological effect*	*Ref.*
α-Fe_2O_3 **Fe_3O_4**	*PC12*	WB: ↑LC3-II ↑caspase-3 ↓cytochrome c ↓p62 WB: ↑LC3-II ↑caspase-3 ↓p62	Oxidative stress, autophagic activity, and cell death	58]
SEI-10 (PEI coating) **SMG-10** (PEG coating) **SMG-30** (PEG coating)	*SKOV-3*	WB: ↓Bcl-2 ↓Bax ↓cyclin D WB: ↑LC3B-II ↓Bax ↓cyclin D WB: ↑LC3B-II ↓Bcl-2 ↓Bax ↓cyclin D	ROS production, autophagy, and apoptosis	59]
Fe_3O_4 **Fe_3O_4@PDA**	*MSCs*	FC: ↑SPF ↑PIndex ELISA: ↑VEGF qPCR, WB: ↑c-Met ↑CCR1 ↑CXCR4 qPCR: ↑TGF-β ↑IL-10 ↓TNF-α ↓COX-2 FC: ↑SPF ↑PIndex ELISA: ↑VEGF qPCR, WB: ↑c-Met ↑CCR1 ↑CXCR4 qPCR: ↑TGF-β ↑IL-10 ↓TNF-α ↓COX-2	Cell migration	60]
Fe_2O_3 @D-SiO_2 **Fe_3O_4 @D-SiO_2**	*RAW264.7* *RAW264.7* *C57BL/6*	qPCR: ↓CD206 qPCR: ↑NF-kB ↑IRF5 ↑IL23 ↓Arg-1 ↓CD206 ↑CD86 ↑CD64 WB: ↑Ferritin ↓Tumor volume	ROS production, M1 macrophage polarization	61]
Ferumoxytol (Feraheme) **Ferucarbotran** (Resovist)	*BMMs (BALB/c mice)* *BMMs (BALB/c mice)*	qPCR: ↓RANK ↓Nfatc1 ↓Acp5 ↓Calcr ↓Ctsk ↓c-Src ↓CYLD ↑p62 qPCR: ↓RANK ↓Nfatc1 ↓Acp5 ↓Calcr ↓Ctsk ↓c-Src WB:	Inhibitory effect on osteoclastogenesis	62]

	RAW 264.7	↓P-JNK ↑JNK ↓P-p38 ↓p38 ↓P-Erk1/2 ↓Erk1/2 ↓P-p65 ↓p65 ↑IκBα ↓CYLD ↑p62 WB: ↓P-JNK ↑JNK ↓P-p38 ↓P-Erk1/2 ↓P-p65 ↑IκBα		
USPIO-NPs **SPIO-NPs**	*L02*	qPCR: ↑IL1B ↑IL6 ↑IL18 ↑TNFSF12 ↑TNFRSF12 ↑JAK1 ↑STAT5B ↑SAA1 ↑SAA2 ↑CXCL14 ↑HSPA5 ↑EIF2AK3 ↑ATF4 ELISA: ↑IL6 WB: ↑BiP ↑PERK ↑ATF4 qPCR: ↑STAT5B ↑CXCL14 ELISA: ↑IL6 WB: ↓PERK ↑ATF4	Inflammation and cell death	63]
SPIONs	*PC12* *C57BL/6J* (Striatum) *C57BL/6J* (Hippocampus)	WB: ↓TH ↑P-JNK ↓T-JNK WB: ↑P-JNK ↓T-JNK WB: ↑P-JNK ↑T-JNK	Apoptosis	64]
SPIONs (carboxydextran coated)	*J774.2* *RAW264.7*	FC: ↑IL-1a ↑IL-10 ↑IL-1b ↑IL-27 ↑INF-b ↓MHCII ↓Arg-1 ↓CD163 FC: ↑IL-1a ↑IL-10 ↑IL-1b ↑IL-27 ↑INF-b	Transient phenotypic changes of macrophages	65]
Ferucarbotran with PMF (carboxydextran coated)	*HuH7*	IS: ↑Annexin V IF: → LAMP1 Cathepsin B ←	ROS production and apoptosis	66]
Resovist (carboxydextran coated)	*RAW264* *HeLa*	WB: ↑P62 ↑LC3-I ↑LC3-II ↓ATG5/12 WB: ↑LC3-II	Autophagy	67]

Feraheme (polyglucose sorbitol carboxymethylether coated)	*BMMs* *293T* *Ana-1* *RAW264* *HeLa* *BMMs* *293T* *Ana-1*	WB: ↑P62 ↑LC3-II WB: ↓P62 ↑LC3-I WB: ↑P62 ↑LC3-I ↑LC3-II WB: ↑P62↑LC3-I ↑LC3-II WB: ↑LC3-II WB: ↑P62 ↑LC3-I ↑LC3-II WB: ↑P62 WB: ↑P62 ↑LC3-II		
SPIO nanocomposites	*HepG2*	WB: ↓Bcl-2 ↑Bax ↑caspase-3 qPCR: ↓HSPA9 ↓GLRX5 ↑MT1X ↑MT1F↑MT2A ↓ND4L ↓NDUFA4 ↓ND2 ↓ CytB ↓MT-CO1 ↓MT-CO2 ↓MT-CO3 ↓ATP6 ↓ATP8	Oxidative stress and cell death	68]
Magnetic IONPs-trastuzumab half-chains	*MDA-MB-453* *SKBR3*	WB: ↑pY1248-HER2/ HER2 ratio ↑p27Kip1	Cell cycle arrest	[69, 70]
mIONPsp-Xcc (LOS) (TLR4 agonist)	*B16-F10*	FC: ↓PD-1/L1	Activation of dendritic cells	71]
Magnetite (Carboxymethyldextran Shell)	*HuH7* *HepG2* *PLC/PRF/5*	WB: ↑Pro-cath. B/Cathepsin B ratio ↑pmTOR/mTOR ↑LC3A/B-II/βactin ↑Rab7 IF: ↓cytoplasmic p53 WB: ↑Rab7 WB: ↑Pro-cath. B/Cathepsin B ratio ↓pmTOR/mTOR IF: ↓nuclear p53 ↑ cytoplasmic p53	Autophagy	72]

Abbreviations

↑ – Upregulated
→← – Colocalization
↓ – Downregulated
BMMs – Bone Marrow-derived Monocytes/Macrophages
CMS – Confocal Microscopy
D-SiO_2 – Dendritic-Silica Oxide
ELISA – Enzyme-Linked Immuno Sorbent Assay
FC – Flow cytometry
FMS – Fluorescence Microscopy
GSH – Glutathion
IF – Immunofluorescence
IP – Immunoprecipitation
IS – Immunostaining
LOS – Lipooligosacharide
MSCs – Mesenchymal Stem Cells
mTOR – Mammalian Target Of Rapamycin
NP – Nanoparticles
PDA – Polydopamine
PEG – Polyethylene glycol
PEI – Polyethylenimine
PMF – Pulsed Magnetic Field
qPCR – Quantitative Polymerase Chain Reaction
RANK – Receptor Activator Nf-κB
ROS – Reactive Oxygen Species
SPF – S-phase-Promoting Factor
SPIO-NPs – Superparamagnetic Iron Oxide Nanoparticles
TH – Tyrosine Hydroxylase
TLR4 – Toll-like Receptor 4
USPIO-NPs – Ultra-Small Superparamagnetic Iron Oxide Nanoparticles
VEGF – Vascular endothelial growth factor
WB – Western Blot

1.2.3 Hepatotoxicity and clearance of IONPs

The majority of literature related to nanomedicine studies shows that most nanomedicines are administered intravenously, leading to significant accumulation in the liver and spleen. This process is followed by NPs redistribution into the kidneys, heart, lungs, and other organs. This pattern of distribution determines the primary cell types interacting with the nanoparticles. Furthermore, the liver uptake of the nanomedicines and their excretion significantly impact NPs pharmacokinetics and pharmacodynamics (PK-PD).

Most IONPs used as MRI contrast agents, with diameters ranging from 30-200 nm, predominantly accumulate in the liver. Initially, IONPs accumulation was considered to be due to phagocytosis by macrophages like Kupffer cells activity. However, further research indicated that IONPs could directly interact with hepatocytes (Figure 4). Different solid nanomaterials are cleared by various cell types, not exclusively by Kupffer cells. Nanoparticles that are not absorbed during the first pass through the liver can re-enter system circulation and can be reabsorbed in a second pass [77, 78]. Eventually, nanoparticles ingested by hepatocytes and Kupffer cells are excreted via bile, although this is a prolonged process, with some IONPs remaining in the liver for extended periods.

Hepatic clearance of nanoparticles, particularly (IONPs), is directly linked with lysosomal accumulation and its critical impact on cellular functions. Lysosomal impairment, often linked with cell death and various pathologies, is a key factor in understanding the impact of IONPs, which are known to affect lysosomal kinetics significantly. Multiple initial research on IONPs indicated biocompatibility and an absence of cytotoxicity has been conducted. This was partially based on the understanding that iron is well-tolerated and regulated within the human body [7, 36]. However, following studies have revealed a range of toxicity responses associated with IONPs treatment, especially after longer exposure up to 3-5 days. These toxic effects have been observed in various cell

lines, including human monocytes and macrophages [7, 36]. Moreover, the overproduction of reactive oxygen species (ROS) and subsequent oxidative stress were discovered in these studies. Primarily, cellular uptake of IONPs leads to their accumulation and degradation in lysosomes, followed by iron ions release, which participates in uncontrolled redox reactions [73-76].

It is worth noting that initial studies did not fully recognize the cytotoxic impact of IONPs. However, cytotoxicity is not the only reason for the withdrawal of many IONP-based MRI contrast agents. In fact, ROS-driven cytotoxicity is a common effect of metal oxide nanoparticles, not just IONPs. *In vivo* studies have shown that IONPs also exhibit significant hepatotoxicity. The liver is a common target for drug-induced side effects, with hepatotoxicity being a major reason for drug withdrawals globally. Therefore, the hepatotoxicity of IONPs is a significant concern, aligning with broader patterns observed in drug safety and liver health.

Table 4. Summary of physicochemical properties of IONPs.

IONPs	Core size (nm)	Hydrodynamic diameter (nm)	Zeta potential (mV)	Magnetic moment (kA/m)	Shape	Coating	Potential application	Ref.
α-Fe_2O_3 Fe_3O_4	16.69±1.07 18,10±2,11	~ 220 ~ 280	NA NA	NA	Spherical	No coating	Bio-imaging, diagnostics, biomedicine	58]
SEI-10 SMG-10 SMG-30	10 10 30	17.2 ± 5.0 16.5 ± 4.7 35.8 ± 10.3	+29,28 -0,52 -0,52	NA	Spherical	PEI PEG PEG	Drug delivery, MRI, thermal ablation therapy, in vivo cell tracking, magnetic separation of cells and molecules	59]
Fe_3O_4 Fe_3O_4@PDA	48.3 62	NA NA	NA NA	NA	Spherical	No coating Polydopamine	Inflammation treatment	60]
Fe_2O_3 @D-SiO_2 Fe_3O_4 @D-SiO_2	~40 ~40	NA NA	NA NA	NA	Ellipsoidal	Dendritic Silica	Anti-cancer	61]
Ferumoxytol (Feraheme) Ferucarbotran (Resovist)	NA NA	19 -40	61 -23	NA	NA	NA	Osteoporosis treatment	62]
USPIO-NPs SPIO-NPs	~50 ~90	41.3 ± 5.9 112.6 ± 38.4	43.0 ± 9.5 45.2 ± 4.9	NA	Spherical	No coating	Hepatic disease diagnosis (MRI), cell tracking, drug delivery, magnetic transfections, treatment of	63]

							hyperthermia	
SPIONs	51.88	NA	8,7	NA	Spherical	No coating	Theranostic drug carrier, MRI contrast agent	64]
SPIONs	60	NA	NA	NA	NA	Carboxydextran	Imaging, sensing, drug delivery, hyperthermia, mechanical stimulation	65]
Ferucarbotran with PMF	60	60,6	-12,8	412	NA	Carboxydextran	Diagnostic tests, in vivo imaging, hyperthermia, drug delivery, magneto-mechanical actuation	66]
Resovist Feraheme	NA NA	62 30	NA	NA	NA	Carboxydextran Polyglucose sorbitol carboxymethyl ether	MRI, Iron deficiency	67]
SPIO nanocomposites	~97	90	28.4 ± 5.7	NA	Spherical	PEI	Anti-cancer nanotheranostics	68]
Magnetic IONPs-trastuzumab half-chains (MNP-HC)	~50	48.7 ± 1	-44,5 ± 9,9	NA	NA	Trastuzumab half-chains	Breast cancer treatment	69, 70]

mIONPsp-Xcc lipooligosaccharide (LOS) (TLR4 agonist)	6,56±1,19	20.85±6.49	-11,42±2,17	NA	Spherical	TLR4 agonist (lipooligosaccharide)	Cancer immunotherapy	71]
Magnetite	~200±20	non-fl.: 437; fluores.: 454	non-fl.: -15.02; fluores.: -16.31	412 [134]	NA	Carboxymethyl dextran	MRI	72]

NA – Not available
non-fl. – non-fluorescently labeled
fl. lab. – fluorescently labeled
PMF – Pulsed Magnetic Field
SPIO-NPs – Superparamagnetic Iron Oxide Nanoparticles
USPIO-NPs – Ultra-Small Superparamagnetic Iron Oxide Nanoparticles
LOS – Lipooligosacharide
TLR4 – Toll-like Receptor 4
PDA – Polydopamine
PEG – Polyethylene glycol
PEI – Polyethylenimine
D-SiO_2 – Dendritic-Silica Oxide

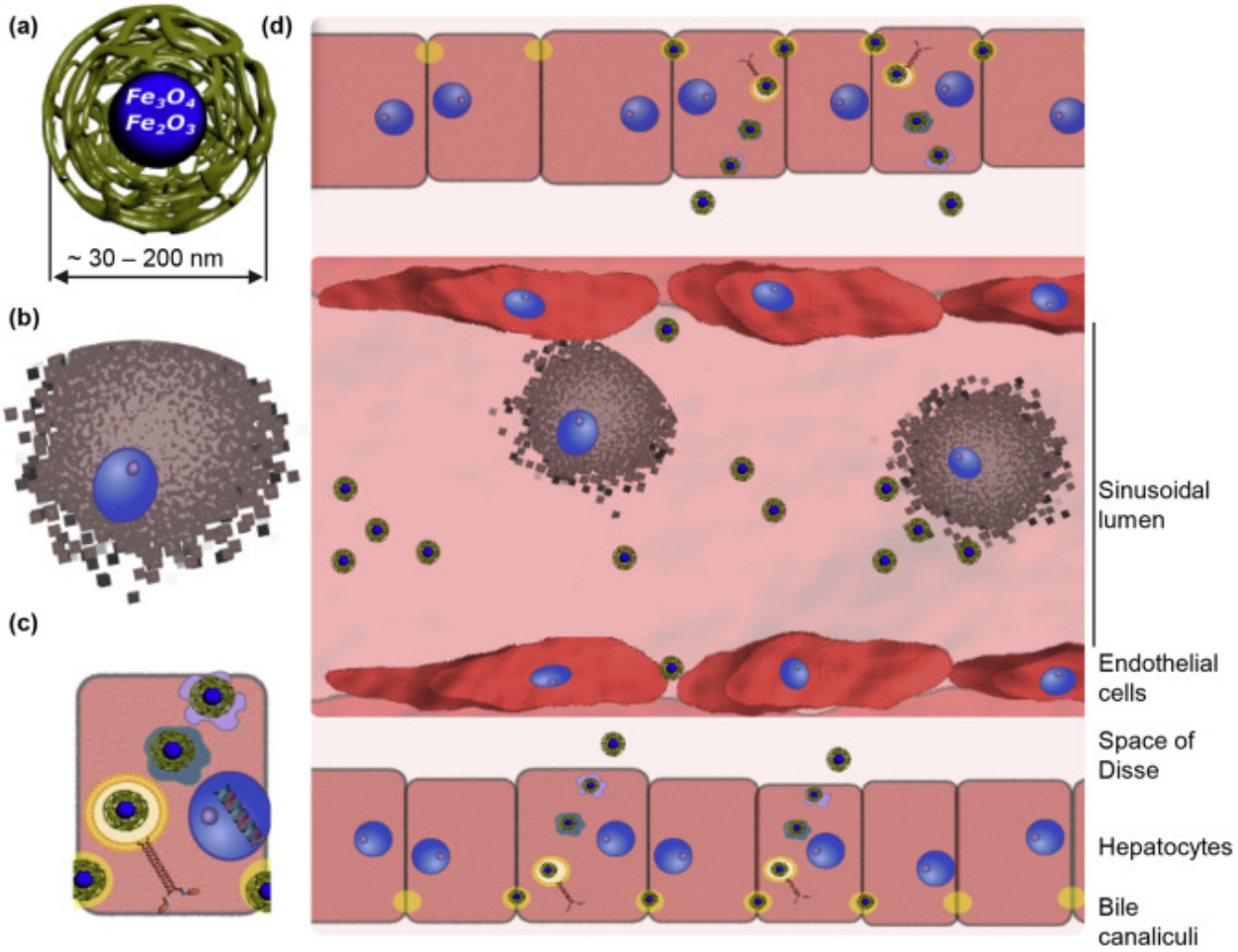

Figure 4. Liver cells interaction and elimination of iron oxide nanoparticles (IONPs). (a) Typical size of IONPs that are utilized in biomedical applications. (b) Kupffer cell. (c) Hepatocyte. (d) IONPs enter the hepatic sinusoid from systematic circulation and may be sequestered by Kupffer cells. Alternatively, depending on IONP physicochemical properties, nanoparticles may extravasate into the space of Disse and be engulfed by hepatocytes. Hepatocytes process and exocytose IONPs via bile canaliculi. This is the way for IONPs to travel through the hepatic ducts into the common bile duct. From the bile duct IONPs enter the entire gastrointestinal tract and are excreted in feces. *Reprinted from Adam Frtús, Barbora Smolková, Mariia Uzhytchak, Mariia Lunova, Milan Jirsa, Šárka Kubinová, Alexandr Dejneka, Oleg Lunov. Analyzing the mechanisms of iron oxide nanoparticles interactions with cells: A road from failure to success in clinical applications. Journal of Controlled Release, Volume 328, 2020, Pages 59-77, ISSN 0168-3659. https://doi.org/10.1016/j.jconrel.2020.08.036*

1.3 DNA nanostructures and their potential in biomedical applications

Self-assembled DNA nanostructures (DNs) are designed using specific techniques, where short DNA strands are folded and arranged in specific patterns to create complex 3D structures. DNA nanostructures can take various forms, such as DNA origami, wireframe structures, modular structures, etc. [13, 79-81].

In the field of biomedicine, DNs have promising applications in biosensing, drug delivery, cell modulation, and bioimaging in comparison with conventional NPs currently available [13, 14, 66, 79-81]. DNA nanostructures can be functionalized with various molecules, such as proteins, peptides, aptamers, or targeting ligands, to enhance their interactions with cells and improve their specificity and efficacy They can be designed to carry therapeutic cargo, such as drugs or nucleic acids, and deliver them to specific targets. DNs could be used as scaffolds for creating higher-order structures or as tools for studying fundamental cell biology processes [82-84]. There are certain advantages in DNs application such as greater biocompatibility and thus lower toxicity in contrast with NPs available in the biomedical market. However, for the successful translation of DNs to clinical applications, it is crucial to understand how they interact with living cells and their potential use in biomedical applications.

1.3.1 Types of DNA nanostructures

As mentioned before, several types of DNs have been used in biomedical research. For example, a DNA tetrahedron is a three-dimensional structure formed by folding DNA strands into a tetrahedral shape. Wireframe DNA structures are complex three-dimensional structures created by assembling DNA strands into wireframe-like shapes.

DNA origami in general refers to two-dimensional structures formed by folding a long single-stranded DNA molecule into a desired shape using short staple strands. Modular DNs are composed of small DNA "brick" motifs that can be assembled into larger, more complex structures [88-90]. DNA tiles are single-stranded DNA molecules that act as pixels in a two-dimensional array, allowing the creation of patterns and shapes [91] (Figure 5 a, c, d). [94] The structures of DNA boxes are designed to be opened via toehold-mediated strand displacement (TMSD), enabling the release of a cargo of interest. pH-sensitive DNA i-motifs are structures that can assemble and disassemble based on changes in pH, allowing for dynamic control over their shape [92, 93]. Different DNs structures, with potential use in drug delivery are pesented in Figure 5c, such as cholesterol-enhanced 6-helix bundle DNA nanostructures for preferential uptake in white blood cells over red blood cells and DNA origami sheet with MUC1-targeted aptamers for specific intracellular delivery of active RNase (Figure 5 d). There are many others, though the brief description of DNs used for this study is presented further.

Specifically designed DNs were utilized in this study: K10 and EE (Figure 5 b), DNA nanostructures coated with oligolysine-based peptides, including two aurein 1.2 sequences, enabling endosomal escape without serum proteins [95]. It has been reported that upon exposure to a serum-containing medium, a protein corona formed around the DNs [42, 43, 96]. This protein corona significantly reduces DNs ability to escape endolysosomal structures, resulting in accumulation in lysosomes, a common fate for unmodified nanostructures [97-99].

Even though DNs have been intensively studied, there are specific interactions between DNs and living cells, which are still not well-defined. There is an important aspect to consider the formation of a protein corona around DNs, when they come into contact with physiological fluids. As mentioned before, the protein corona consists of proteins and

other biomolecules that interact with the surface of the DNs, forming a multilayered shell.

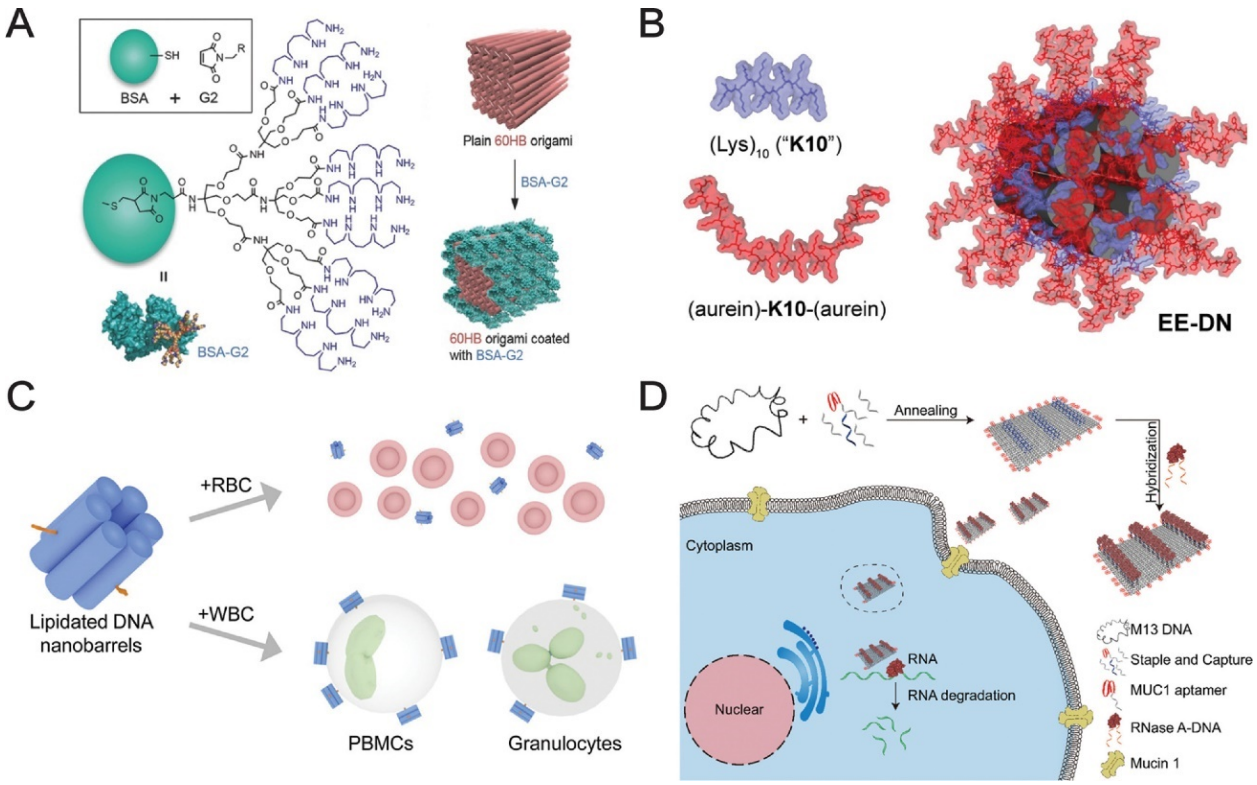

Figure 5. DNA nanostructures for biological applications. (a) BSA modified with positively charged dendrimers to adhere to a 60-helix bundle (60HB) nanostructure enables enhanced nanostructure stability, uptake, and immunoquiescence. (b) Oligolysine-based peptide coating featuring two functional aurein 1.2 sequences that exhibit endosomal escape of the coated DNA nanostructure (EE-DN) in the absence of serum proteins. (c) Cholesterol-bearing 6-helix bundle DNA nanostructures facilitate targeted uptake in white blood cells compared to red blood cells. (d) A DNA origami sheet bearing MUC1-targeted aptamers capable of targeted intracellular delivery of active RNase A. *Reprinted from Adam Frtús, Barbora Smolková, Mariia Uzhytchak, Mariia Lunova, Milan Jirsa, Skylar J.W. Henry, Alexandr Dejneka, Nicholas Stephanopoulos, Oleg Lunov. The interactions between DNA nanostructures and cells: A critical overview from a cell biology perspective, Acta Biomaterialia, Volume 146, 2022, Pages 10-22, ISSN 1742-7061, https://doi.org/10.1016/j.actbio.2022.04.046*

The presence of the protein corona can affect the function and efficiency of surface modifications on the DNs, such as chemical moieties, targeting ligands, and antibodies. Therefore, understanding the protein

corona formation is crucial for the successful design and optimization of DNs [42-44, 96, 100].

Another important factor is the physical interaction between the functionalized DNs and the surface receptors of cells. Ligand interactions with cell surface proteins play a significant role in determining the subsequent cell entry of exogenous materials and regulating the intracellular fate of various materials. While DNA molecules alone cannot cross the cell membrane, 3D DNs have been shown the ability to efficiently enter the intracellular matrix [42-44, 96, 100]. Therefore, studying the physical parameters that modulate the cellular interaction and processing of DNs is essential for the efficient targeting of cell surface receptors. The cellular uptake of DNA nanostructures can occur through various mechanisms, such as clathrin-mediated endocytosis, caveolin-dependent endocytosis, and scavenger receptor-mediated endocytosis [101] (Figure 6). The specific entry mechanism can impact the efficiency and intracellular processing of the nanostructures [102-106].

Furthermore, the geometry parameters of DNs, such as size, shape, and aspect ratio, can also influence their cellular uptake and therapeutic efficacy. For example, particles with rod-like geometry have shown higher cellular binding efficacy compared to spherically-shaped particles, while spherically-shaped particles have demonstrated higher uptake efficiency compared to rod-shaped ones. Overall, understanding the interactions between DNs and cells from a cell biology perspective is crucial for optimizing the design and functionality of DNs in biomedical applications [107]. It involves studying the formation of the protein corona, the physical interaction between DNs and cell surface receptors, and the influence of DN geometry on cellular uptake and therapeutic efficacy.

In the field of DNA nanostructures (DNs), a thorough examination of how these structures interact with cells is essential for their effective use in biomedical applications. Currently, research predominantly focuses on how cells uptake DNs and where these structures localize within the

cell, paying less attention to the functional impacts DNs might have on cellular processes [108]. This research gap has occurred due to the relatively recent exploration of DNs in biomedical contexts in general. There has been notable progress in understanding the influence of DNs' size and shape on their cellular uptake and internal distribution. Yet, it remains unclear how DNs might specifically alter cellular signaling pathways [89, 108-112].

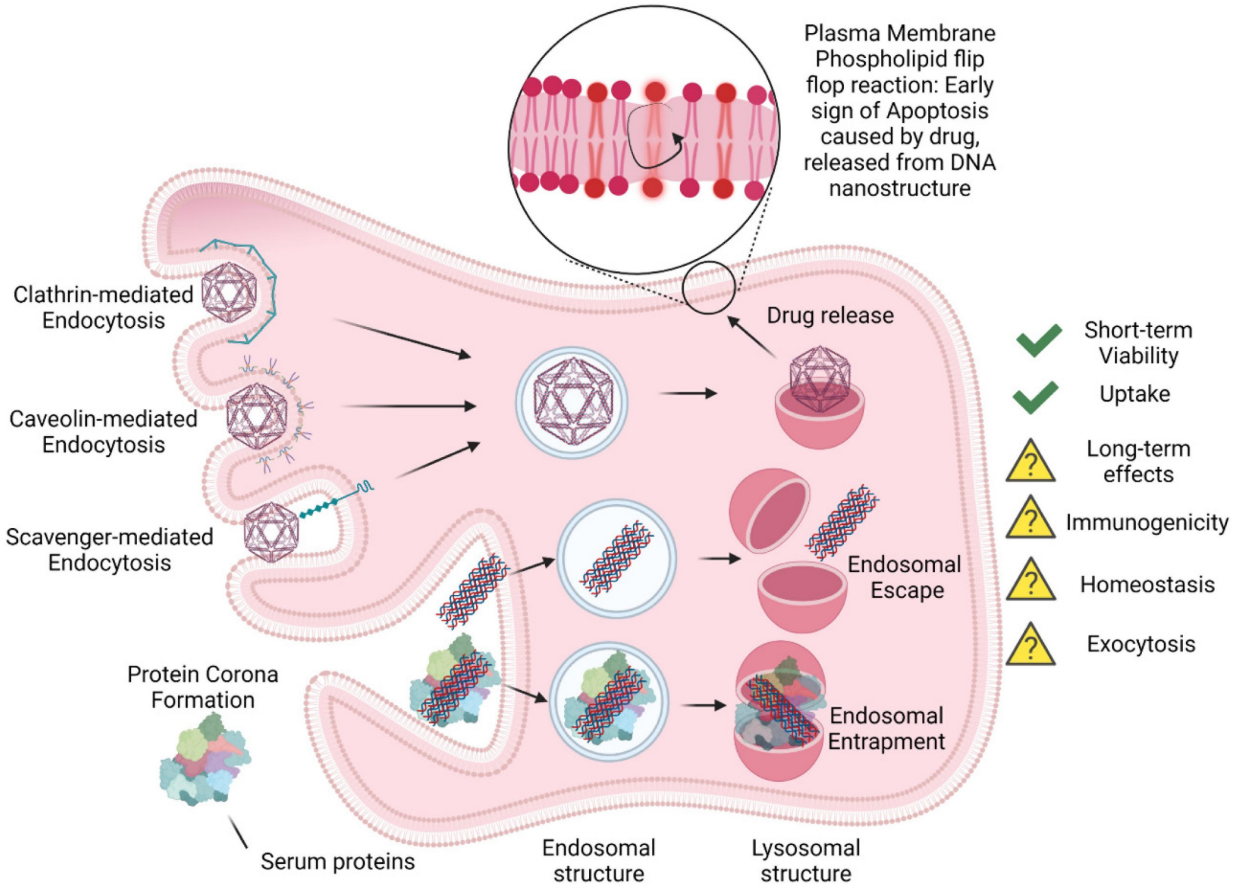

Figure 6. Schematic summary of DNA nanostructures interaction with living cells. *Reprinted from Adam Frtús, Barbora Smolková, Mariia Uzhytchak, Mariia Lunova, Milan Jirsa, Skylar J.W. Henry, Alexandr Dejneka, Nicholas Stephanopoulos, Oleg Lunov. The interactions between DNA nanostructures and cells: A critical overview from a cell biology perspective, Acta Biomaterialia, Volume 146, 2022, Pages 10-22, ISSN 1742-7061, https://doi.org/10.1016/j.actbio.2022.04.046*

The field of DNA nanotechnology, despite these research gaps, has shown significant promise, particularly in areas like biosensing, drug delivery, cell modulation, and bioimaging. DN-based biosensors are recognized for their precise design, specificity, and economical aspects of synthesis [9, 113-119]. In drug delivery, DNs offer new avenues for carrying and releasing pharmaceuticals. They also have the potential to precisely modulate cell behavior and are crucial in advanced DNA-PAINT imaging techniques. However, a deeper understanding of the interactions between DNs and cells, especially regarding long-term impacts, signaling pathways, immune responses, and elimination processes, is crucial for furthering these applications. The use of DNA nanotechnology in creating tunable hydrogel systems also opens up new possibilities in tissue engineering and controlled interactions between cells and their surrounding matrix. These DNA hydrogels, due to their programmable nature, allow for finely tuned cellular interactions. Yet, challenges such as scaling up production in a cost-effective manner, susceptibility to degradation by nucleases, and potential toxic or immunogenic effects remain to be addressed [42, 43, 100, 120, 121].

1.3.3 Potential cytotoxicity of DNA nanostructures

The biomedical advantage of DNA nanostructures (DNs) is often considered due to DNA's natural origin, their biodegradability, biocompatibility, and minimal toxic effects [98, 99, 122, 123]. However, this assumption of being a "naturalistic fallacy," might not always mean natural and safe, as many natural molecules can be toxic or immunogenic. For instance, while cell-free DNA is normally present in healthy individuals, elevated levels are linked to various pathologies and may have cytotoxic properties. DNA released during cellular injury can activate innate immunity response, leading to inflammation [124-126].

Preliminary studies indicate some biocompatibility and effective clearance of DNs, but there's no comprehensive analysis of their potential toxicity. Most studies show low cytotoxicity for DNs not loaded with drugs, but these are limited to short exposure times, usually under 48 hours. The long-term effects, especially considering the potential toxicity of degradation products and metabolization by-products, remain unclear, especially in *in vivo* models [98, 99, 122, 123].

Another limitation is the low variety of cell lines used in toxicological assessments, which may not accurately represent diverse biological responses. Genetic background in commonly used cell lines like MCF-7 and HeLa can lead to variable responses to treatments, highlighting the urge for a thorough cell line authentication [127]. Furthermore, the majority of studies don't use primary cell cultures, which more closely mimic *in vivo* conditions and could provide more reliable results on nanoformulation toxicity [128, 129].

In summary, while DNs show promise in biomedical applications, their safety profile requires careful and systematic evaluation, considering both the nanostructures themselves and their degradation products, across a diverse range of cell models [7, 130, 131].

1.4. Challenges and perspectives

In order to make a significant input into biomedical research, the nanomedicine field itself has undergone certain scientific reconsiderations and groundbreaking findings recently. During the past three decades, there has been enormously intensive and efficient progress in the nanotechnology field and its utilization in clinics. The scientific society went from micro- and nanoparticle discovery to the development of effective drug delivery agents during these years. Currently, there is an ongoing discussion regarding the lack of experimental data on bio-nanotechnology literature, mostly due to reproducibility issues. Talking

about the lack of characterization and standardization of custom-synthesized nanoparticles, we are facing a disturbing truth – the translational gap between nanoparticle production and introduction to animal and human models. There are no direct answers to these challenging questions, thus, the scientific society is assigned to reveal hidden details in molecular mechanisms of biodegradation, cytotoxicity effects, and the therapeutic impact of nano-agents on living organisms.

This PhD thesis is dedicated to investigating how different nanoparticles with various organic surface functionalizations interact with hepatic cells, their cell machinery, kinetics, and metabolic pathways in general. The problem of using different surface coating and core structures of nanoparticles became a cornerstone in modern biomedical and nanotechnology research since there has been no unified cellular response to nanoparticle treatment. So far, a variety of cellular responses to nano-treatment have been described and thoroughly investigated, such as regulated cell death, regulation and expression of certain proteins and genes, the interaction between organelles, and overall toxicity. All the abovementioned issues drag the attention of a scientific society, to uncover specific mechanisms and pathways, which are orchestrating certain cellular mechanisms. However, the main drawbacks such as out-of-target issues, cytotoxicity, and efficient drug delivery remain highly debatable and problematic among the scientific community. Undoubtedly, there is a strong necessity for fundamental research for a better understanding of the NPs fate in the living organism, its impact on cell biology and cell signaling, cellular toxicity and cell death related to it, and finally NPs clearance and its biodegradability.

2. Aims of the study

This work explores in detail the uptake mechanisms by the cell and their dependencies on the physical properties of the nanoparticle (size, shape) and its surface chemistry (chemical functions, charge, and polarity).

There has been selected a set of IONPs (200 nm, 60 nm sphere, cubic) as a model of current nano-drugs utilized in MRI, magnetic drug delivery, and hyperthermia. As a novel and promising nanomaterial, we used DNA nanostructures

This work analyzes in detail how nanoparticles are processed within the cell (transport mechanisms, association with organelles, degradation), and the responses of the cell to nanoparticle incorporation. These studies are conducted by employing time-resolved confocal microscopy on cultured cells, complemented by confocal experiments with ultra-high spatial resolution on fixed and live cells. Additional methodologies include flow cytometry, reverse transcription polymerase chain reaction (RT-PCR) for quantifying gene expression, Western blotting (WB) for protein detection and quantification, and immunofluorescence (IF) for visualizing the distribution of proteins and other antigens in cell samples. Conducting these experiments, this study aims to achieve a mechanistic description, in molecular terms, of the response of cultured cells to nanoparticles, which is the first important step toward an understanding of the effects of nanoparticles on the entire organism. On this background, it is very important to gain insight not only into the interaction between distinctly designed nanoparticles with primary cells and tumor cell lines, but also to identify possible receptors and target molecules, identify cell functions that may be targeted by nanoparticles, and validate the findings *in vivo* models.

3. Experimental part methods

This research is cross-disciplinary, demanding a diverse range of methodologies to effectively address the abovementioned research objectives. To provide a clearer understanding, we outline some of the major methods utilized in our study. Please kindly refer to the comprehensive descriptions available in the attached scientific papers, provided in Appendices I -IV.

3.1.Cell cultures

We utilized three distinct cell lines in our experiments: Huh7 cells, obtained from the Japanese Collection of Research Bioresources (JCRB), Alexander (PLC/PRF/5) cells from the American-Type Culture Collection (ATCC), and the human hepatoblastoma cell line HepG2, also sourced from ATCC. To establish optimal growth conditions, these cells were cultured in Eagle's minimal essential medium (EMEM, ATCC), supplemented with 10% fetal bovine serum (FBS, Thermo Fisher Scientific), and Penicillin/Streptomycin (Thermo Fisher Scientific), following the manufacturer's recommended protocols. The cell cultures were maintained in a controlled environment with 5% CO2 at a constant temperature of 37°C. We ensured the freshness of the cell culture by changing the medium once a week. In addition, we implemented routine screening for mycoplasma contamination across all cell lines using the MycoAlert Mycoplasma Detection Kit (Lonza), adhering to standard laboratory procedures.

3.2. Protein extraction and Western blot analysis

To investigate the cellular signaling at the protein level, we employed a methodical approach to extract proteins as follows. Whole cell lysates were extracted using RIPA buffer (Merck Millipore) supplemented with protease and phosphatase inhibitor cocktails (Sigma Aldrich), following the manufacturer's guidelines and our previously established protocols (see Appendix III-IV for detailed procedures). Cells were harvested from the culture plates by scraping, then centrifuged at 500g for 5 minutes, washed with PBS, and centrifuged again at 500g for 5 minutes. Subsequently, the cell pellet was resuspended in 50μl of RIPA buffer containing the specified inhibitors and incubated at 4°C for 30 minutes. Following this incubation period, the samples were centrifuged at 12,000g for 15 minutes, and the resulting supernatants were collected. The concentration of the extracted lysates was determined using the Micro BCA (Bicinchoninic acid) assay.

Equal amounts of protein lysates were subjected to separation via SDS-PAGE (sodium dodecyl sulfate-polyacrylamide gel electrophoresis). Subsequently, the separated proteins were transferred onto polyvinylidene fluoride (PVDF) membranes. These membranes were then blocked with an appropriate blocking buffer for 1 hour at room temperature. After blocking, they were incubated overnight at 4°C with primary antibodies targeting specific proteins, as detailed in Appendix III-IV, VI. Following the primary antibody incubation, the membranes were probed with the corresponding secondary antibodies for 1 hour at room temperature.

The specifications, including catalog numbers, dilutions, and antibody clones, are provided in Appendix III-IV, VI. Signal detection was accomplished using the GBOX CHEMI XRQ imaging system (Syngene), and chemiluminescence signals were captured using the GeneTools acquisition software (Syngene). Subsequent densitometric quantification of the blot signals was performed using GeneTools (Syngene) and ImageJ (NIH) software.

3.3. Microscopy

This study employed various microscopic techniques to investigate cellular features. For routine cellular morphology observation, we utilized optical light microscopy with the IM-2FL epi-fluorescent system (Optika Microscopes). This system is equipped with a white 8W LED light source (X-LED8), and a 100W HBO mercury burner, and offers various imaging modalities including brightfield, phase contrast, and fluorescence filters (UV, B, and G). The fluorescence capability allowed for highly sensitive and specific visualization of cellular compartments. Notably, the IM-2FL epi-fluorescent system was employed for detecting apoptosis using the Dead Cell Apoptosis Kit (Thermo Fisher Scientific) (see Appendix I).

To achieve higher-resolution imaging, two types of confocal microscopy were employed. Firstly, a Nikon Diaphot 200 microscope in conjunction with the BioRad MRC 1024 laser scanning imaging system was utilized. This system is equipped with a Krypton/Argon laser emitting three co-aligned excitation lines at 488nm, 568nm, and 647nm. Precise manipulation of samples was carried out using the Eppendorf micromanipulator 5171, adapted to the Nikon Diaphot 200 microscope. Fluorescent images were acquired using the Lasersharp 2000 v5.2 acquisition software (BioRad). Subsequent image processing and quantification were performed using the ImageJ system (NIH) and Laser-Sharp 2000 software (BioRad). This system was utilized in the following experimental work in Appendices I-II:

In addition, we employed state-of-the-art high-resolution spinning disk confocal microscopy, specifically the IXplore SpinSR system from Olympus, to achieve exceptionally detailed cell visualization. This cutting-edge system comprises two key components: the inverted microscope IX83 (Olympus) and the spinning disc confocal unit CSUW1-T2S SD (Yokogawa). To facilitate fluorophore excitation, we employed laser diodes at three distinct wavelengths, namely 405nm, 488nm, and 561nm.

Confocal images were acquired at a resolution of 2048 x 2048 pixels, or at 1024 x 1024 pixels for super-resolution images, using two digital CMOS cameras, specifically the ORCA-Flash4.0 V3 models by Hamamatsu. The acquisition of fluorescent confocal images was executed through the CellSens software developed by Olympus. Subsequent image processing and quantitative analysis were conducted using the ImageJ software developed by NIH.

For a more comprehensive understanding of our imaging system, detailed information can be found in Appendices III-IV, VI.

3.4. Spectro-fluorometric analysis

To measure absorbance, luminescence, or fluorescence signals from a larger number of samples, we employed the Tecan microplate reader SpectraFluorPlus (Tecan). This system allows for the utilization of various filter combinations for excitation, emission, or absorbance measurements. This system was utilized in the following experimental work in Appendix I

- Cell viability using WST-1 assay (Roche) or AlamarBlue reagent (TFS)
- Measurement of protein concertation by micro-BCA assay (TFS)

3.5. Statistical analysis

Quantitative results are presented as mean ± standard error of the mean (SEM). To assess the statistical significance of group differences, we employed ANOVA followed by either Fisher's, LSD, or Newman-Keuls tests, as appropriate. Statistically significant differences were defined as *P < 0.05. For a comprehensive explanation of the statistical analysis, please refer to Appendix I-IV, VI.

4. Results & Discussion

4.1. Physicochemical characterization of IONPs

The physicochemical properties of IONPs are fully detailed in Appendices I, II, III, IV, V. For detailed information see (Table 5). For this study were utilized fluorescent and non-fluorescent carboxymethyl dextran-coated iron oxide nanoparticles, custom designed IONs with different physicochemical parameters. The size is a significant parameter as particles with a diameter comparable to liver sinusoidal fenestrations can penetrate the space of Disse and interact directly with hepatocytes. The physicochemical analysis revealed that both fluorescent and unlabeled nanoparticles had a similar hydrodynamic diameter, which doubled in size after incubation in a medium with serum, by forming a protein corona. Both fluorescent and unlabeled nanoparticles have a negative zeta potential of approximately -2 mV. This potential remained similar after incubation with the medium. The formation of a protein corona, which is crucial in determining cellular responses to nanoparticles, was observed and was independent of nanoparticle concentration.

Additional physicochemical properties, such as average size and zeta potential measurements were done using a Zetasizer Nano. The nanoparticles were incubated in various media to study their interactions with proteins and other biomolecules.

Table 5. Physicochemical properties of IO-cubes and IO-clusters (*Dh* – hydrodynamic diameter; *Ms* – saturation magnetization, ζ - zeta potential, FL-fluorescent).

Sample	**Core type**	**Core size (nm)**	**Coating**	***Dh* (nm)**	***Ms* (emu/g)**	**ζ-potential (mV)**
IO-cubes	Magnetite	36±8	PEG	142	75(1)	N/A
IO-clusters	Magnetite	38±10	PEG	140	78(1)	N/A
SPION (60)	Magnetite/ Maghemite	4.2	Carboxydextran	62	N/A	-14.4
SPIONs (200)	Magnetite	N/A	Carboxymethyldextran	200±20	N/A	-1.76
SPIONs (200) FL	Magnetite	N/A	Carboxymethyldextran	200±20	N/A	-1.82

4.2. IONPs interaction with living cells

4.2.1 Controlling cellular uptake via magneto-mechanical modulation of IONPs

Within decades NPs were actively used for biological and clinical applications as contrast agents for MRI (magnetic resonance imaging), cell labeling, gene, and drug delivery. However, there appeared to be a necessity for effective loading and invention of a specific cargo to avoid the out-of-target issue. Fast and efficient uptake and controlled drug delivery became a cornerstone in improving intracellular transportation [132, 133]. However, certain cell types have limited phagocytic capacity, resulting in poor intracellular SPION uptake and reduced sensitivity for imaging purposes.

We aimed to address the challenge of efficient superparamagnetic iron oxide nanoparticles (SPIONs) uptake by cells and explore the potential use of pulsed magnetic fields to enhance cellular uptake. To investigate this, a custom pulsed magnetic field source capable of producing high-intensity magnetic fields was designed [134]. For a detailed description of the MF device please visit Appendix I. The experiments were conducted using Huh7 hepatic cells, and it was

observed that the application of pulsed magnetic fields significantly increased the uptake of SPIONs by the cells. This enhancement was evident across different SPIONs concentrations and resulted in a reduction in the time required for efficient uptake (Figure 7).

In order to assess the concentration-dependent uptake of SPIONs, cells were pre-incubated with various SPIONs concentrations and exposed to 10 magnetic pulses at 10-second intervals with a magnetic strength of approximately 7 T. Control cells, without magnetic stimulation, were imaged 10 minutes after pre-incubation with the same SPIONs concentration. Confocal images of the cells were captured and quantified.

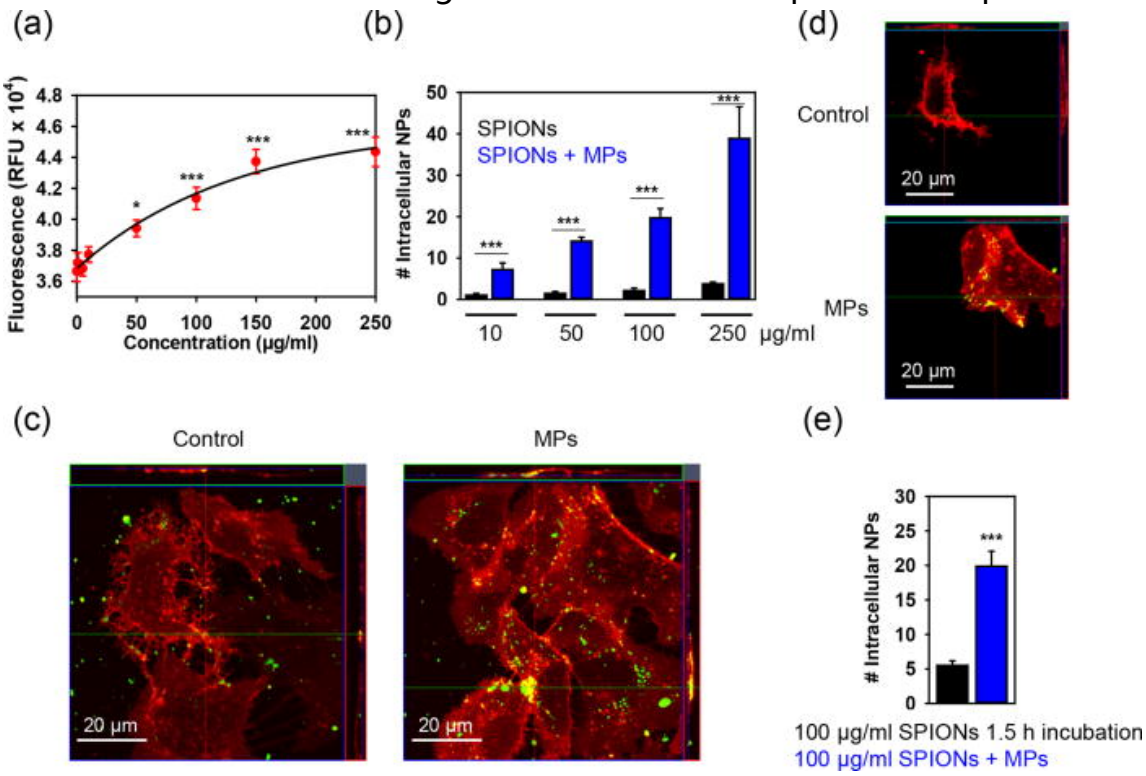

Figure 7. (a) Uptake kinetics of SPIONs by Huh7 cells in the absence of the pulsed magnetic field. The cells were incubated with different concentrations of SPIONs for 1.5 h and then washed, and the particle uptake was analyzed by measuring fluorescence intensity. (b) Quantification of concentration-dependent SPION uptake. Cells were pre-incubated with different concentrations of SPIONs for 1 min and exposed to 10 magnetic pulses (MPs) of ~7 T at 10 s intervals. Control cells were visualized 10 min after pre-incubation with the same concentration of SPIONs, without MP treatment. (c)

Confocal images of cells pre-incubated with SPIONs (250 μg Fe/ml, green) for 1 min and exposed to 10 magnetic pulses (MPs) of ~7 T at 10 s intervals. Control cells were visualized 10 min after pre-incubation with the same concentration of SPIONs, without MP treatment. Cell membranes were labeled with CellMaskTM Deep Red (red). (d) Representative images were used to quantify the number of SPION inside cells incubated at a concentration of 250 μg Fe/ml (e) The number of internalized nanoparticles after exposure to 10 magnetic pulses (MPs) of ~7 T at 10 s intervals. Control cells were visualized 1.5 h after pre-incubation with the same concentration of SPIONs, without MP treatment. Data are expressed as mean ±SEM of at least three independent experiments (n=12–24); ***p<0.001.. *Reprinted from M. Uzhytchak, A. Lynnyk, V. Zablotskii, N. M. Dempsey, A. L. Dias, M. Bonfim, M. Lunova, M. Jirsa, š. Kubinová, O. Lunov, A. Dejneka; The use of pulsed magnetic fields to increase the uptake of iron oxide nanoparticles by living cells. Appl. Phys. Lett. 11 December 2017; 111 (24): 243703. https://doi.org/10.1063/1.5007797 with the permission of AIP Publishing.*

The data revealed a concentration-dependent effect, with higher NPs concentrations leading to increased uptake by the cells. Furthermore, the application of pulsed magnetic fields demonstrated an additional enhancement in NPs uptake compared to cells without magnetic stimulation. The intensity and duration of the pulsed magnetic field were found to influence the efficiency of uptake, indicating the potential of this approach for improving SPION delivery to cells (Figure 8).

To ensure the safety of the enhanced uptake method, cell viability and potential adverse effects were investigated. The results indicate that exposure to SPIONs combined with pulsed magnetic fields does not impact cell viability, induce lysosomal permeabilization, or disrupt mitochondrial function. This suggests that the intense pulsed magnetic fields used in the study do not have acute toxic effects on the cells. Viability assay results are presented in Appendix I, II, and IV.

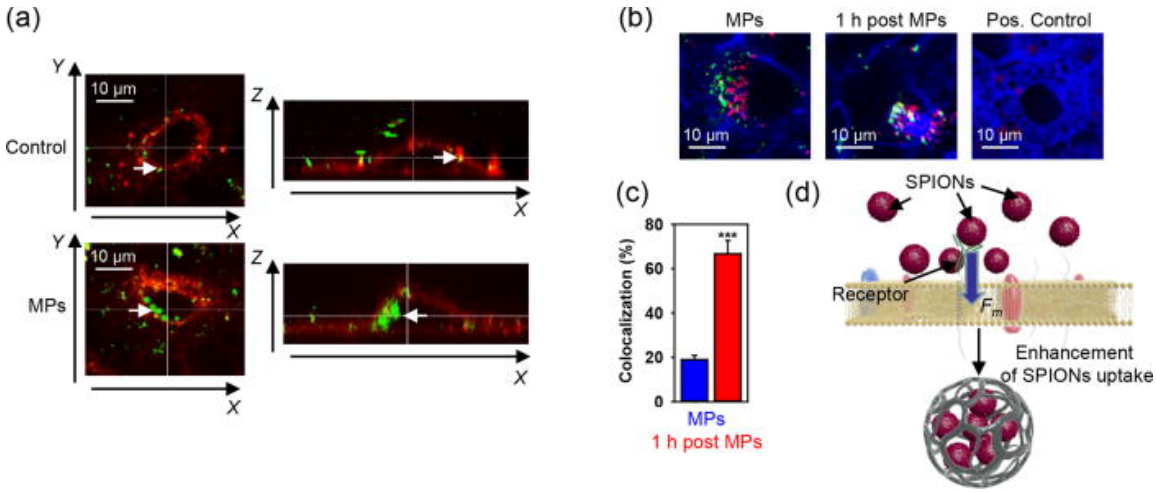

Figure 8. (a) Comparison of the uptake of SPIONs in the presence and absence of magnetic pulses. Confocal orthogonal images of cells pre-incubated with SPIONs (250 μg Fe/ml, green) for 1 min and exposed to 10 magnetic pulses (MPs) of ~7 T at 10 s intervals are shown. Control cells were visualized 10 min after pre-incubation with the same concentration of SPIONs, without MP treatment. Cell membranes were labeled with CellMask Deep Red (red). (b) Colocalization of lysosomes and SPIONs. Cells were pre-incubated with SPIONs (250 μg Fe/ml, green) for 1 min and exposed to MF. Images were captured by confocal microscopy either immediately or 1 h after magnetic pulses cell membranes-CellMask (blue), lysosomes-LysoTrackerVR Red DND-99 (red), nanoparticles-(green), and colocalization (yellow)]. As a positive control, cells were treated with 10% ethanol for 30 min. (c) Quantification of colocalization analysis was performed using ImageJ. The data are expressed as mean ±SEM; n=22 cells; ***p<0.001. (d) Scheme of magnetically assisted SPION uptake.. *Reprinted from M. Uzhytchak, A. Lynnyk, V. Zablotskii, N. M. Dempsey, A. L. Dias, M. Bonfim, M. Lunova, M. Jirsa, š. Kubinová, O. Lunov, A. Dejneka; The use of pulsed magnetic fields to increase the uptake of iron oxide nanoparticles by living cells. Appl. Phys. Lett. 11 December 2017; 111 (24): 243703. https://doi.org/10.1063/1.5007797 with the permission of AIP Publishing.*

4.2.2. Remote apoptosis

Further, cells were loaded with superparamagnetic iron oxide nanoparticles (SPIONs) to investigate lysosomal and mitochondrial integrity as well as apoptosis induction. The main hypothesis states that PMF application would induce mechanical stress on SPION-loaded lysosomes, leading to their leakage and dysfunction based on multiple studies [135-141]. Since NPs treatment without PMF does not impact cell

survival rate (Figure 9), it was confirmed that lysosomal increased size is concentration dependant with PMF applied and might lead to lysosomal mechanical damage. Additionally, early signs of poptosis were detected through Annexin V/propidium iodide labeling, which revealed significant phosphatidylserine exposure. For a detailed description please refer to Appendix II.

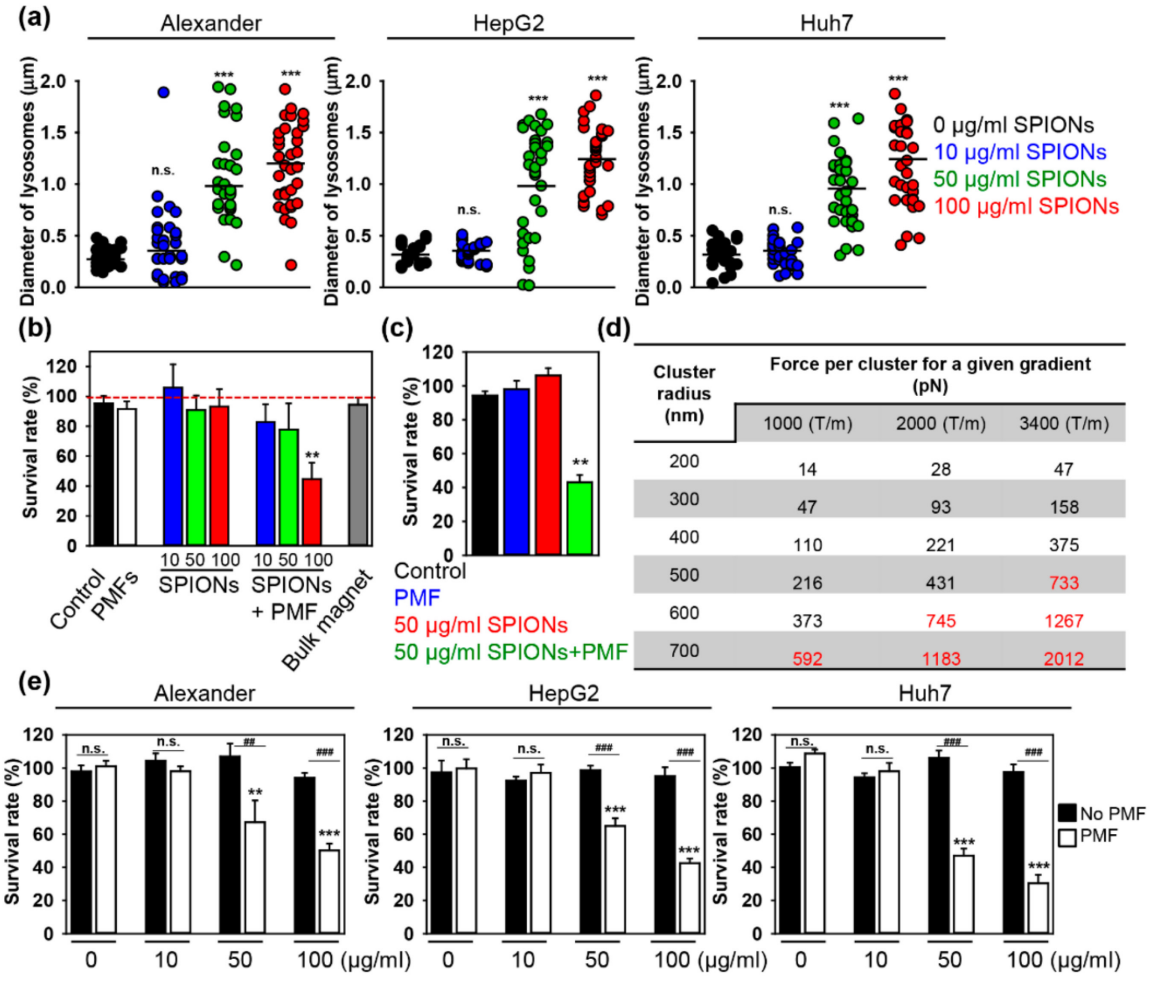

Figure 9. Cell viability, lysosomal size upon SPION uptake (a) Assessment of the lysosomal size upon SPION uptake. Huh7, HepG2, and Alexander cells were treated for 1.5 h with indicated concentrations of SPIONs. (b) Huh7 cells were pre-incubated with different concentrations of SPIONs (10, 50, 100 µg Fe/mL) for 1.5 h. (c) Huh7 cells were pre-incubated with SPIONs (50 µg Fe/mL) for 1.5 h. (d) Estimations of the magnetic gradient force exerted on clusters of SPIONs. (e) Huh7, HepG2, and Alexander cells were

pre-incubated with different concentrations of SPIONs (10, 50, 100 μg Fe/mL) for 1.5 h. After, cells with incorporated nanoparticles were exposed to PMF (10 pulses of ~ 8 T at intervals of 10 s). The 24 h cell viability was assessed by the WST-1 assay. The data were normalized to control values (no particles, no PMF exposure) and expressed as means ± SDs, $n = 3$ each. ** $p < 0.01$ and *** $p < 0.001$ denote significant differences concerning control (no particles, no PMF treatment). *Reprinted from Oleg Lunov, Mariia Uzhytchak, Barbora Smolková, Mariia Lunova, Milan Jirsa, Nora M. Dempsey, André L. Dias, Marlio Bonfim, Martin Hof, Piotr Jurkiewicz, et al. 2019. "Remote Actuation of Apoptosis in Liver Cancer Cells via Magneto-Mechanical Modulation of Iron Oxide Nanoparticles" Cancers 11, no. 12: 1873. https://doi.org/10.3390/cancers11121873*

To further support the hypothesis that cell death is influenced by the magnetic force on SPIONs clusters, experiments with cells loaded with 50 μg Fe/mL SPIONs and subjected to 8 T PMF were conducted. These conditions also resulted in LMP, loss of ΔmΦ, and following apoptosis. The lysosomal damage was studied more specifically by assessing cathepsin B release, a hallmark of LMP [148-151]. Immunofluorescent labeling showed cathepsin B release into the cytosol in SPION-loaded cells treated with 8 T PMF, along with the presence of swollen lysosomes. This finding, coupled with AO destabilization assay results, confirmed significant lysosomal destabilization upon PMF treatment [152-154] (Figure 10). Finally, reactive oxygen species (ROS) accumulation was checked, a known mediator of LMP-dependent apoptosis. Using fluorescent probes, a dose-dependent increase in both total ROS and superoxide in SPION-loaded cells treated with PMF, was monitored, indicating mitochondrial membrane permeabilization and dysfunction [148-151]. Furthermore, the impact of PMF on mitochondrial function was investigated using JC-1 staining to assess mitochondrial membrane potential (ΔmΦ). In healthy cells, JC-1 accumulates in mitochondria, shifting from green to red fluorescence as ΔmΦ increases. On the other hand, in cells with compromised mitochondria, JC-1 leaks into the cytosol, leading to reduced red fluorescence [142-144]. The results revealed a notable decrease in JC-1 red fluorescence in SPION-loaded cells exposed to 5 T PMF, indicating mitochondrial dysfunction and loss of ΔmΦ. This mitochondrial

impairment was observed after LMP initiation. For more detailed results please refer to Appendix II. To confirm apoptotic cell death, caspase-3 activity was measured, which is a key apoptotic marker [145-147]. Obtained results showed increased caspase-3 activity in SPION-loaded cells treated with 5 T PMF, confirming apoptosis induction

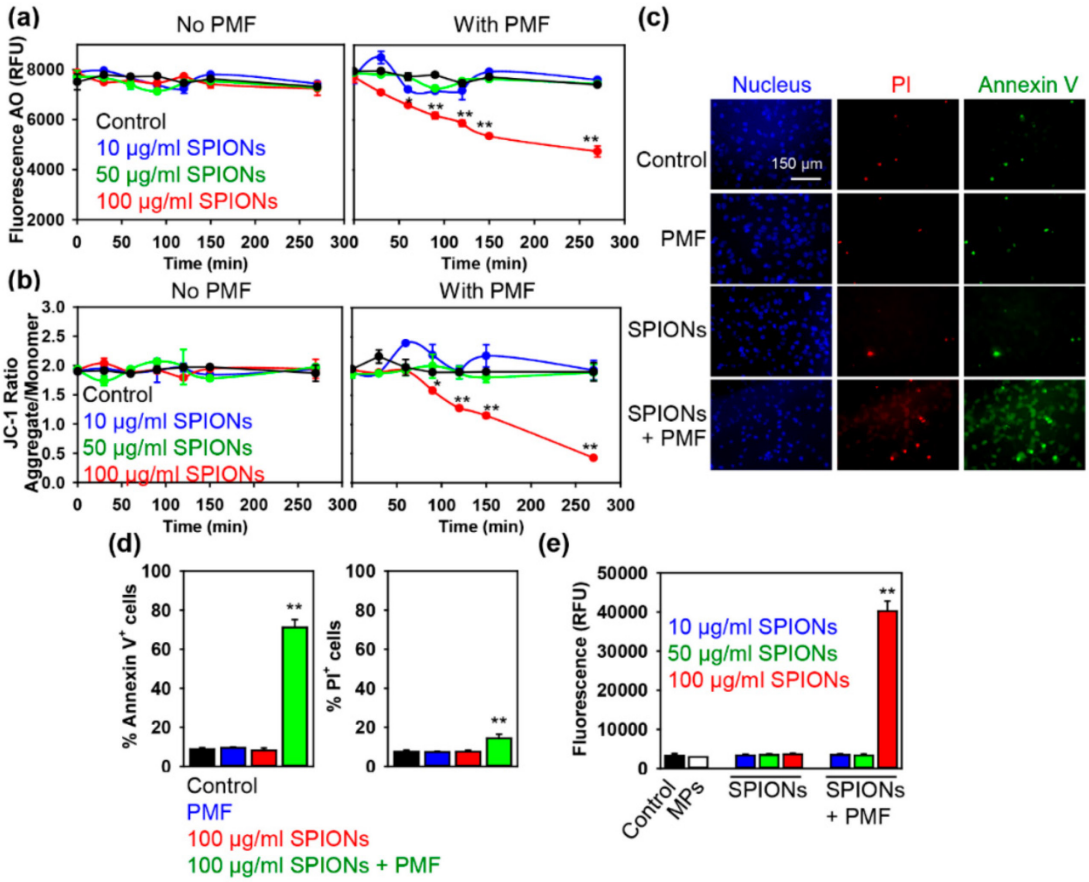

Figure 10. Lysosomal integrity, mitochondria membrane potential, and apoptosis assessment upon SPION treatment using MF. (a) Huh7 cells were pre-incubated with different concentrations of SPIONs (10, 50, 100 µg Fe/mL) for 1.5 h. After cells with incorporated nanoparticles were exposed to PMF (10 pulses of ~5 T at intervals of 10 s) and stained with acridine orange (AO), the fluorescence intensity was measured using a fluorescent microplate reader. The data are expressed as means ± SEMs, n = 3 each. * $p < 0.05$ and ** $p < 0.01$ denote significant differences concerning controls (no particles, no PMF treatment). (b) Huh7 cells were treated as in (a). After PMF treatment cells were stained with 2 µM JC-1 for 30 min and analyzed by fluorescent microplate reader. The

data are expressed as means ± SEMs, n = 3 each. * p < 0.05 and ** p < 0.01 denote significant differences concerning controls (no particles, no PMF treatment). (c) Huh7 cells were pre-incubated with SPIONs 100 μg Fe/mL for 1.5 h. After that cells with incorporated nanoparticles were exposed to PMF (10 pulses of ~5 T at intervals of 10 s); then, 4 h after treatment cells were labeled with Hoechst nuclear stain—blue dye, annexin V—green dye, and propidium iodide (PI)—red dye. Labeled cells were imaged with fluorescence microscopy. Representative images from three independent experiments are shown. (d) Apoptosis assessment in PMF-treated Huh7 cells. Cells were treated as in (c); then, 4 h after the treatment cells were labeled with Hoechst nuclear stain, annexin V, and propidium iodide. Fluorescence microscopy was used to visualize fluorescently stained cells. The percentage of Annexin V and PI-positive cells was calculated with ImageJ (NIH). The data are expressed as means ± SEMs, n = 3 each. ** p < 0.01 denotes significant differences concerning control (no particles, no PMF treatment). (e) Huh7 cells were pre-incubated with different concentrations of SPIONs (10, 50, 100 μg Fe/mL) for 1.5 h. After that, cells with incorporated nanoparticles were exposed to PMF (10 pulses of ~5 T at intervals of 10 s), and then caspase-3 activity was assessed using an ApoStat detection kit (R&D Systems) and analyzed with a fluorescent microplate reader. The data are expressed as means ± SEMs, n = 3 each. ** p < 0.01 denotes significant differences concerning control (no particles, no PMF treatment). *Reprinted from Oleg Lunov, Mariia Uzhytchak, Barbora Smolková, Mariia Lunova, Milan Jirsa, Nora M. Dempsey, André L. Dias, Marlio Bonfim, Martin Hof, Piotr Jurkiewicz, et al. 2019. "Remote Actuation of Apoptosis in Liver Cancer Cells via Magneto-Mechanical Modulation of Iron Oxide Nanoparticles" Cancers 11, no. 12: 1873. https://doi.org/10.3390/cancers11121873*

To summirize, the investigation revealed the localization of NPs within lysosomes, inducing significant changes in lysosomal size and morphology across three cell lines. Lysosomal acidification was particularly impaired in Alexander and Huh7 cells, with Huh7 cells presenting the most significant disruption. In general, this study demonstrates that employing a PMF, which can generate a sufficiently strong magnetic gradient force on SPIONs, effectively causes lysosomal cathepsin B to leak into the cytoplasm (Figure 11), [155, 156]. This leakage, which occurs at a minimal effective force of approximately 500 pN, initiates a chain of events starting with lysosomal membrane permeabilization, followed by mitochondrial damage, and ultimately

leading to the execution of apoptosis and cell death [157]. Additionally, this method has been successfully tested in a three-dimensional culture that closely resembles *in vivo* conditions, highlighting its potential applicability.

Despite these promising results, we acknowledge certain limitations of the presented system. The field gradient from the pulsed field source diminishes rapidly with distance from the coil, which currently limits its full potential in actual in vivo applications. Nevertheless, the magnetic field created by the described system should theoretically penetrate deep tissue. Moreover, the magnetic field gradient it generates is anticipated to be sufficiently strong. To adapt the PMF system fully for *in vivo* testing, extensive further research and adjustments are necessary. However, it's crucial to note that previous studies employing alternating or dynamic magnetic fields to disrupt membranes in SPION-loaded cancer cells did not provide validation *in vivo* or three-dimensional culture settings for magnetic field-induced cell death [158, 159].

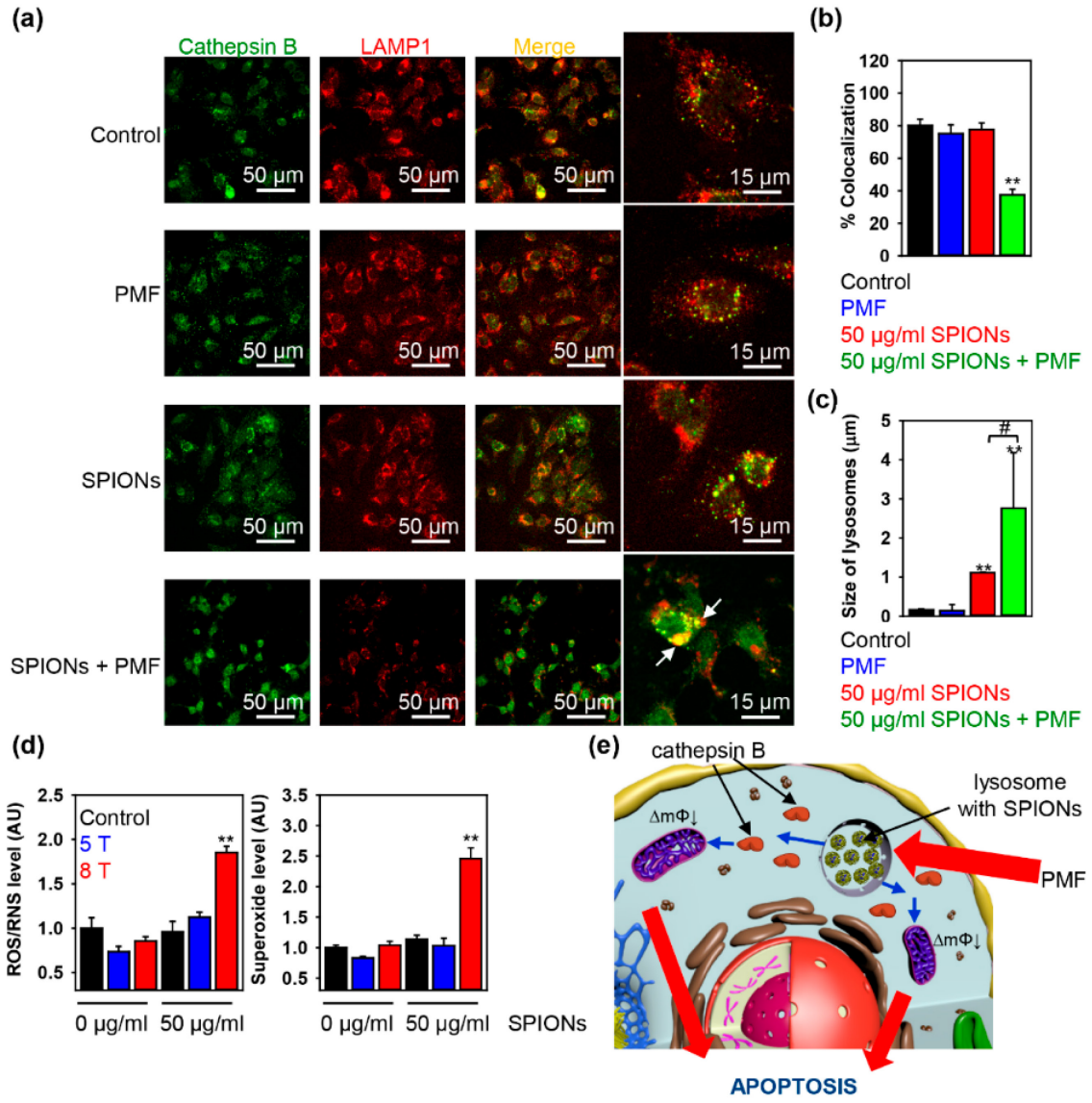

Figure 11. Apoptotic activation under PMF treatment of SPION-loaded cells is mediated by LMP a) Huh7 cells were pre-incubated with SPIONs 50 µg Fe/mL for 1.5 h. After incubation, cells with incorporated nanoparticles were exposed to PMF (10 pulses of ~8 T at intervals of 10 s), and then 4 h after treatment, cells were analyzed by confocal microscopy using LAMP1 antibody as a marker of lysosomes (red) and cathepsin B (green). Colocalization is shown in yellow. Colocalization analysis of cathepsin B and LAMP1 from images (a) is presented in (b). ** $p < 0.01$ denotes significant differences concerning control (no particles, no PMF treatment). (c) Assessment of the lysosomal size upon PMF treatment. (d) Intracellular ROS/superoxide ($O2^{-}$) production upon PMF treatment. (e) Principle of remote induction of apoptosis by PMF. Schematic representation of lysosomal membrane permeabilization by SPIONs in a pulsed

magnetic field. *Reprinted from Oleg Lunov, Mariia Uzhytchak, Barbora Smolková, Mariia Lunova, Milan Jirsa, Nora M. Dempsey, André L. Dias, Marlio Bonfim, Martin Hof, Piotr Jurkiewicz, et al. 2019. "Remote Actuation of Apoptosis in Liver Cancer Cells via Magneto-Mechanical Modulation of Iron Oxide Nanoparticles" Cancers 11, no. 12: 1873. https://doi.org/10.3390/cancers11121873*

4.2.3. Cellular interactions of IONPs

Once IONPs are introduced into biological systems they rapidly interact with the proteins, forming a protein corona. These formations usually consist of dynamically adsorbed proteins, which are critical for determining the biological identity of nanoparticles. The protein corona consists of an initial weak bound "soft" layer, which is further replaced by a more stable "hard" corona, formed out of proteins with higher binding affinities. This dynamic exchange is regulated by the Vroman effect, representing the competitive displacement of proteins in which low-molecular-weight (MW) proteins arriving first at a surface are displaced by relatively higher MW proteins over time.

The intracellular processing of IONPs is particularly relevant given their potential integration into the body's iron metabolism. Unlike physiological iron uptake mechanisms, macrophages can internalize IONPs via scavenger receptors, leading to lysosomal accumulation. The biodegradation of IONPs within lysosomes is a protracted process, with nanoparticles persisting in the body for an extended period, potentially disrupting cellular signaling pathways.

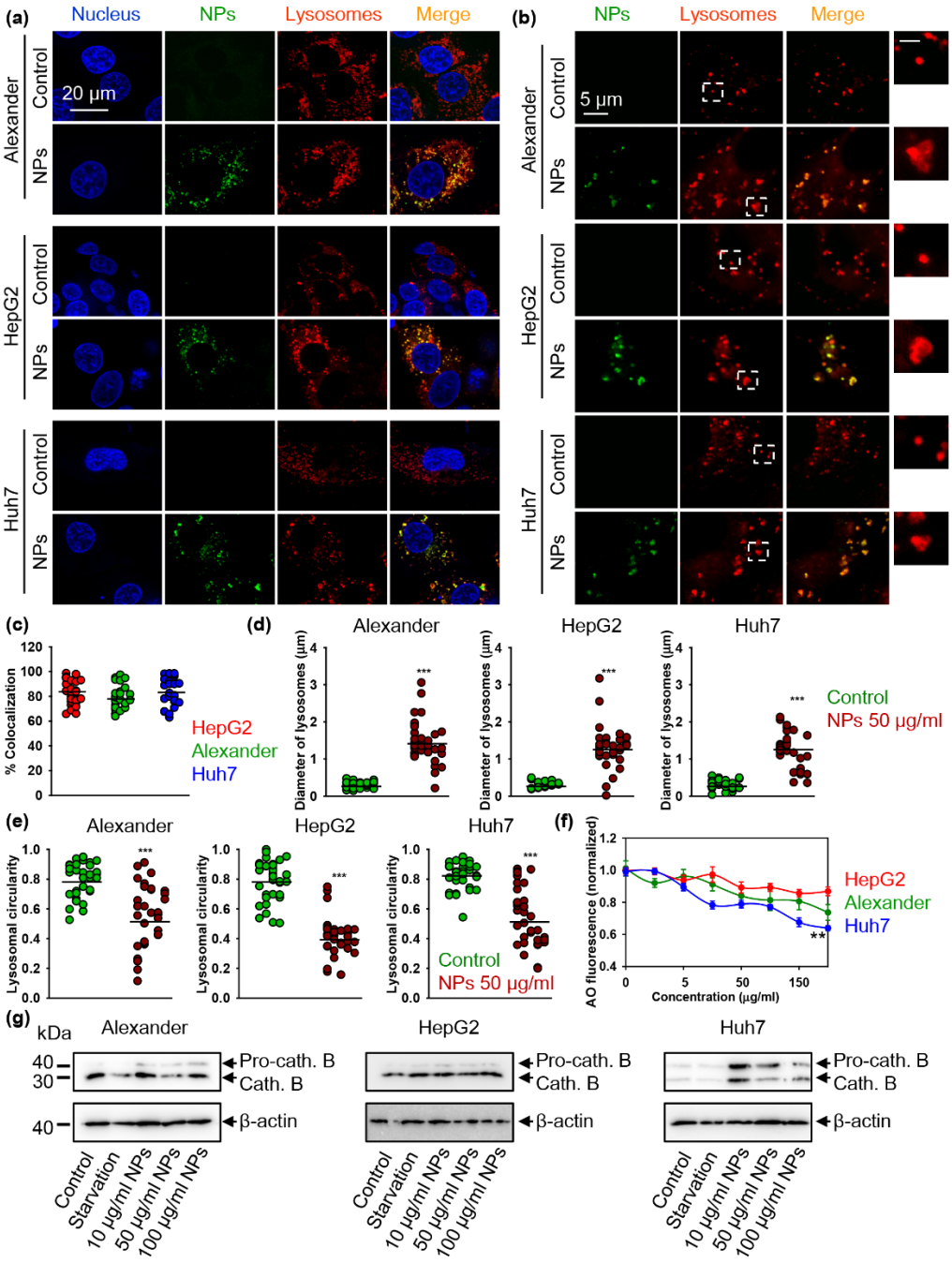

Figure 12. Lysosomal impairment induced by nanoparticles. (a) Localization of fluorescently labeled nanoparticles (green) in lysosomal compartments. Cells were treated for 12 h with nanoparticles 50 µg Fe/mL and labeled with LysoTracker™ Red DND-99 (red). Nuclei were stained with hoechst 33342 nuclear stain (blue). A merge of green and red gives a yellow color. (b) IXplore SpinSR Olympus super-resolution microscopy of lysosomes. Cells were treated for 12 h with nanoparticles 50 µg Fe/mL

(green) and labeled with LysoTracker™ Red DND-99 (red). The scale bar for the zoomed insert is 1 μm. (c) Colocalization analysis of nanoparticles and lysosomes from images (a) is presented. Quantifications performed using ImageJ are presented as means of n = 25 cells. (d) Measurements of the lysosomal diameter upon nanoparticle uptake. Super-resolution images (b) were quantified using ImageJ software. Quantifications are presented as means of n = 34 cells. (***) p < 0.001 denotes significant differences concerning control (no particle treatment). (e) Assessment of lysosomal circularity out of super-resolution images (b). Circularity was calculated using ImageJ software. Quantifications are presented as means of n = 34 cells. (***) p < 0.001 denotes significant differences concerning control (no particle treatment). (f) Lysosomal integrity as measured by acridine orange (AO) red fluorescence decrease. Cells were treated with indicated concentrations of nanoparticles for 24 h, stained with AO and then the fluorescence intensity was measured using a fluorescent microplate reader. The data are expressed as mean ± SEM, n = 3 each. (**) p < 0.01 denotes significant differences. (g) Nanoparticles impair the maturation of pro-cathepsin B in Alexander and Huh7 cells but not in HepG2. Cells were stimulated with nanoparticles at indicated concentrations for 12 h. Expression of cathepsin B was analyzed by immunoblotting. Positive control—serum starvation for 12 h. Actin denotes loading control. Densitometric quantification of blots is shown in Figure S7 of Supplemental Materials. *Reprinted from Mariia Uzhytchak, Barbora Smolková, Mariia Lunova, Milan Jirsa, Adam Frtús, Šárka Kubinová, Alexandr Dejneka, and Oleg Lunov. 2020. "Iron Oxide Nanoparticle-Induced Autophagic Flux Is Regulated by Interplay between p53-mTOR Axis and Bcl-2 Signaling in Hepatic Cells" Cells 9, no. 4: 1015. https://doi.org/10.3390/cells9041015*

Presented study (see Appendix III) has demonstrated that nanoparticles (NPs) can promote cytoskeletal remodeling independently of oxidative stress. In this study, significant changes in the cytoskeleton, particularly in f-actin and β-tubulin structures were observed, after 24 hours of NP exposure, as initially detected by conventional confocal microscopy. It was shown, that IONPs may cause delayed cytotoxic effects in different cell types, primarily through the excessive production of reactive oxygen species. Presented results indicate that cells, subjected to sub-lethal doses of various NPs, undergo noticeable morphological changes. Interestingly, these changes occur even at nanoparticle concentrations that do not trigger oxidative stress. Further, it becomes evident that sub-lethal exposure to iron oxide NPs results in their

accumulation within lysosomes (Figure 12). This accumulation leads to changes in lysosomal size and shape and a gradual decline in lysosomal functionality. This impairment has been found to support autophagic flux. This is consistent with the presented results. For detailed specifications see Appendix III, IV.

Moreover, the sub-cellular distribution and activity of mTOR were assessed, revealing no change in HepG2 cells but a decrease in nuclear mTOR phosphorylation in Alexander cells and an increase in cytosolic mTOR activity in Huh7 cells. This suggests that NPs may affect mTOR signaling differently within cell types, with potential for cancer prognosis due to the association of increased mTOR nuclear localization with poor prognosis in various cancer types.

A critical factor in these different cellular responses appears to be the expression and sub-cellular distribution of the p53 protein within different cell lines. Huh7 cells, for instance, exhibit the highest levels of p53, predominantly localized in the nucleus, in contrast to HepG2 cells where p53 is mainly cytosolic (Figure 13). This variation is further complicated by the fact that Huh7 and Alexander cells have mutated forms of p53, which is known to enhance mTOR activity, potentially influencing autophagic flux and lysosomal function in general. Those findings also highlight the role of Bcl-2, an anti-apoptotic and anti-autophagic protein, in modulating cellular responses to NPs. HepG2 cells, which express higher levels of Bcl-2, show resistance to lysosomal dysfunction and destabilization upon NP treatment, potentially contributing to their chemoresistance. This resistance is also linked to mild cytoskeletal reorganization in HepG2 cells, which can alter autophagy execution. In contrast, the mutated p53 and elevated mTOR phosphorylation in Alexander and Huh7 cells predispose them to lysosomal dysfunction induced by NPs. However, the impaired autophagy execution in Alexander cells, compared to Huh7, might be related to the NP-induced alterations in p53 localization, underscoring the complex

interplay between p53, mTOR signaling, and autophagic regulation in these cells. This complex interplay highlights the need to consider specific molecular and genetic backgrounds while evaluating the impact of NPs on cellular functions.

The following lysosomal dysfunction influences the sub-cellular distribution of proteins like pmTOR and p53, with progressive lysosomal impairment initiating autophagic flux, further facilitated by nuclear protein p53. In contrast, cytosolic p53 and elevated Bcl-2 levels are known to inhibit autophagy (Figure 13).

To investigate p53 sub-cellular localization across various cell lines, including Huh7, HepG2, and Alexander cells, cells were fixed, treated with IONPs, and stained for p53. Further analysis involved assessing the expressions of pmTOR and mTOR in the whole cell lysates with the following densitometric quantification of the pmTOR/mTOR ratio. However, in Alexander cells treated with NPs, there is an observed increase in cathepsin B and LC3 levels, but without the lipidated form of LC3. Notably, these cells exhibit high cytoplasmic levels of p53 following NP treatment. The subcellular localization of p53 is crucial, as it differentially affects autophagic flux; cytoplasmic p53 is known to inhibit autophagy, whereas nuclear p53 activates it. These findings align with previous results, suggesting that autophagic flux in Alexander cells is disrupted following NP treatment.

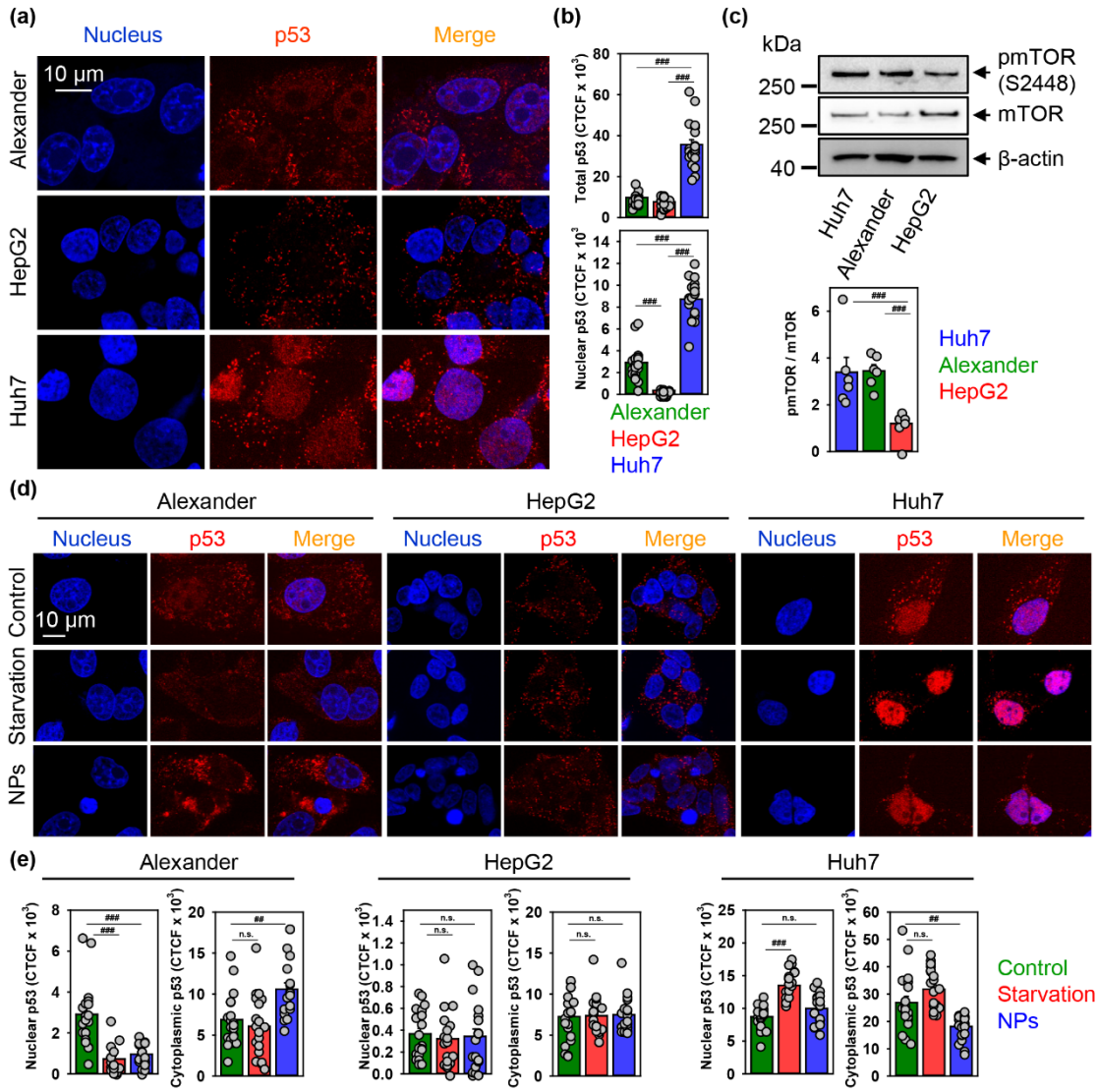

Figure 13. Nanoparticles affect p53 nuclear shuttling. (a–b) Representative confocal microscopic images and quantification of p53 sub-cellular localization in distinct cell lines. Huh7, HepG2, and Alexander cells were fixed and immunostained for p53 (red). Nuclei were stained with Hoechst 33342. Labeled cells were then imaged using spinning disk confocal microscopy (a). Quantification of p53 cellular fluorescence (b) was done by ImageJ and presented as means of n = 20 cells. (###) $p < 0.001$ denotes significant differences. (c) Expressions of pmTOR and mTOR were analyzed in whole cell lysates of HepG2, Huh7, and Alexander cells by immunoblotting. Actin—control of equal protein loading. The graphs show densitometric quantification of pmTOR/mTOR ratio. Quantification was performed using ImageJ. The data are expressed as mean ± SEM, n = 5–6. (###) $p < 0.001$ denotes significant differences. (d–e) Representative confocal microscopic images and quantification of p53 sub-cellular localization in distinct cell

lines upon nanoparticle treatment. Cells were treated for 12 h with nanoparticles 50 μg Fe/mL, fixed, and immunostained for p53 (red). Labeled cells were then imaged using spinning disk confocal microscopy (d). Positive control—serum starvation for 12 h. *Reprinted from Mariia Uzhytchak, Barbora Smolková, Mariia Lunova, Milan Jirsa, Adam Frtús, Šárka Kubinová, Alexandr Dejneka, and Oleg Lunov. 2020. "Iron Oxide Nanoparticle-Induced Autophagic Flux Is Regulated by Interplay between p53-mTOR Axis and Bcl-2 Signaling in Hepatic Cells" Cells 9, no. 4: 1015. https://doi.org/10.3390/cells9041015*

4.2.4 IONPs bias autophagic flux in hepatic cells

The following nanoparticle-cell interactions continue with the initial binding of nanoparticles to cell surface receptors and membranes, leading to nanoparticle uptake primarily through endocytosis. This internalization process is influenced by both specific interactions, such as ligand-receptor binding, and nonspecific forces, including hydrophobic or electrostatic interactions. Endocytosis covers several mechanisms: phagocytosis, clathrin-mediated, caveolin-mediated, clathrin/caveolae-independent endocytosis, and micropinocytosis, its pathway primarily dependent on the cell type and nanoparticle characteristics. Further, nanoparticles are sequestered into endocytic vesicles, which are transported into different intracellular structures for sorting and trafficking. The fate of these nanoparticles is heavily influenced by factors such as the protein corona, nanoparticle aggregation, and the physicochemical properties of the nanoparticles themselves. IONPs treatment ends up in the development of mature endolysosomes, identified by Rab7/LAMP1-vesicles. This was evidenced by a significant increase in Rab7/LAMP1 colocalization across all tested cell lines, explaining the formation of endocytic vesicles upon NP exposure. It was observed that in HepG2 and Huh7 cells, NPs treatment also led to increased expression in the overall Rab7 protein levels, contrasting with the Alexander cells, where Rab7 expression remained unchanged (Figure 14). Moreover, the dose and exposure duration of nanoparticles do not significantly impact endosomal

nanoparticle distribution, which is primarily covered by the dynamics of the endocytic process. Endocytic vesicles subsequently merge with early endosomes, transporting nanoparticles to specific organelles. These endosomes can either fuse back with the plasma membrane or progress to lysosomes, where the engulfed nanoparticles may undergo degradation. However, some nanoparticles can provoke lysosomal degradation through endosomal escape, which is discussed further. Furthermore, the study examined the impact of NP treatment on cathepsins B, enzymes regulated by lysosomes and associated with lysosomal dysfunction. While HepG2 cells showed no significant change in cathepsins B expression, Alexander and Huh7 cells exhibited increased expression and altered conversion of cathepsins B, indicating lysosomal dysfunction. Overall, the findings underscore the importance of lysosomes in the cellular processing of NPs, revealing cell-specific responses that highlight the intricate relationship between nanomaterials and cellular signaling pathways. Observed lysosomal changes and autophagy modulation upon IONPs treatment further revealed that NPs can influence autophagy through lysosome-dependent mechanisms, potentially dysregulating autophagic flux or inhibiting autophagosome degradation. The results (see Appendix III) showed the impact of NPs on the activity of key autophagy-related proteins, indicating elevated LC3 protein levels in Alexander and Huh7 cells post IONPs treatment, and therefore autophagic activity The downregulation of mTOR phosphorylation in Alexander cells corresponds with autophagic induction, given mTOR's role as an autophagy inhibitor when activated. Contrarily, Huh7 cells showed NPs-induced autophagic flux, evidenced by the accumulation of lipid-conjugated LC3. The use of bafilomycin A1 further confirmed autophagy activation in Huh7 cells by increasing LC3-positive. Interestingly, this study found that IONPs led to elevated mTOR phosphorylation in Huh7 cells but not in HepG2 cells, which showed no

significant change in LC3 levels or mTOR phosphorylation, indicating a cell-specific response to NP treatment.

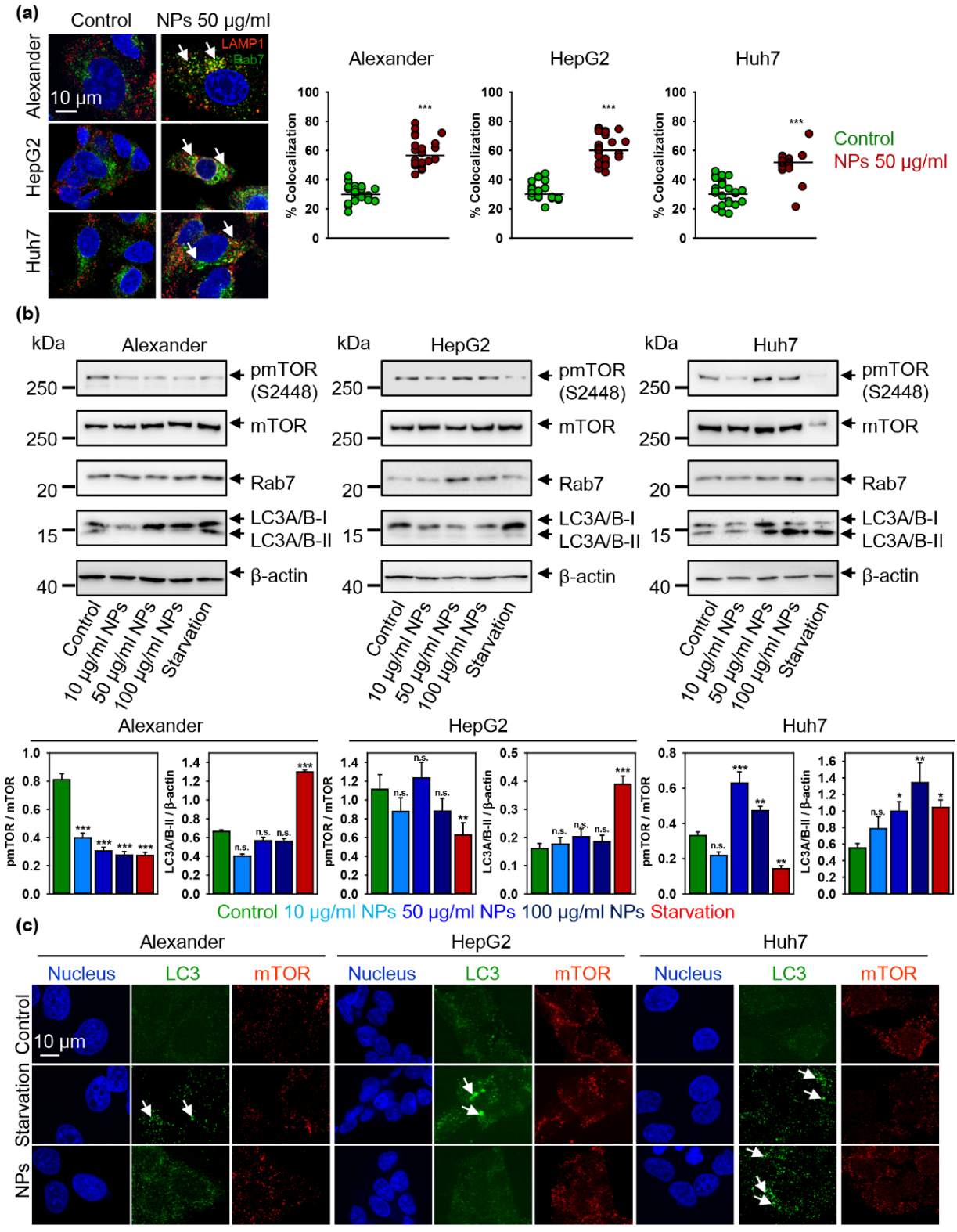

Figure 14. Nanoparticle treatment-induced autophagic flux is cell line dependent. (a) Colocalization analysis of nanoparticles and Rab7 protein. Cells were treated for 12 h with nanoparticles 50 μg Fe mL−1, fixed and immunostained for LAMP1 (red) and Rab7 (green). Labeled cells were then imaged using spinning disk confocal microscopy. Colocalization quantifications were done in ImageJ and presented as means of n = 25 cells. (***) $p < 0.001$ denotes significant differences concerning control (no particle treatment). (b) Cells were stimulated with nanoparticles at indicated concentrations for 12 h. Expressions of pmTOR, mTOR, Rab7 and LC-3 were analyzed by immunoblotting. Positive control—serum starvation for 12 (Alexander, Huh7) and 14 (HepG2) h. Actin denotes loading control. Graphs show the densitometric quantification of blots. (*) $p < 0.05$, (**) $p < 0.01$ and (***) $p < 0.001$ denotes significant differences concerning control (no particles treatment). (c) Confirmation of autophagic flux by formation of cellular autophagosome punctae containing LC3-II. Cells were treated for 12 h with nanoparticles 50 μg Fe mL−1, fixed and immunostained for mTOR (red) and LC3 (green). Labeled cells were then imaged using spinning disk confocal microscopy. Arrows indicate the formation of cellular autophagosome punctae. Positive control—serum starvation for 12 (Alexander, Huh7) and 14 (HepG2) h. Nuclei were stained with Hoechst 33342. *Reprinted from Mariia Uzhytchak, Barbora Smolková, Mariia Lunova, Milan Jirsa, Adam Frtús, Šárka Kubinová, Alexandr Dejneka, and Oleg Lunov. 2020. "Iron Oxide Nanoparticle-Induced Autophagic Flux Is Regulated by Interplay between p53-mTOR Axis and Bcl-2 Signaling in Hepatic Cells" Cells 9, no. 4: 1015. https://doi.org/10.3390/cells9041015*

To summarize the presented data, an accumulation of nanoparticles in lysosomal compartments leads to progressive impairment of lysosomal function. The resulting lysosomal dysfunction probably affects the sub-cellular localization of pmTOR and p53 (Figure 15). Progressive lysosomal dysfunction leads to the initiation of autophagic flux, which is supported by nuclear p53, however, cytosolic p53 and high levels of Bcl-2 inhibit autophagy.

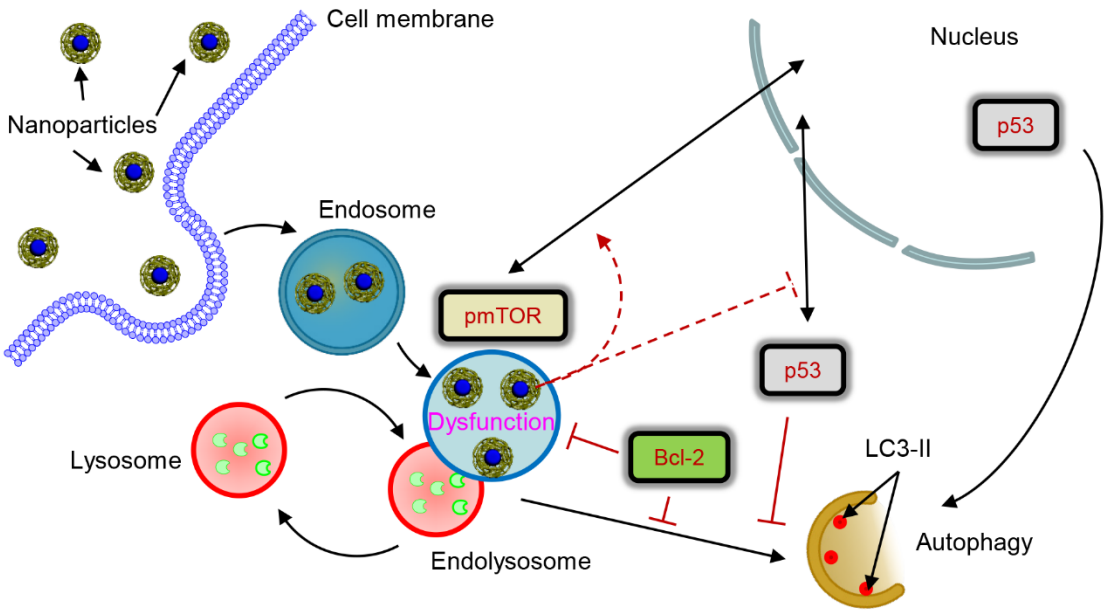

Figure 15. Scheme of lysosomal dysfunction upon nanoparticle treatment. *Reprinted from Mariia Uzhytchak, Barbora Smolková, Mariia Lunova, Milan Jirsa, Adam Frtús, Šárka Kubinová, Alexandr Dejneka, and Oleg Lunov. 2020. "Iron Oxide Nanoparticle-Induced Autophagic Flux Is Regulated by Interplay between p53-mTOR Axis and Bcl-2 Signaling in Hepatic Cells" Cells 9, no. 4: 1015. https://doi.org/10.3390/cells9041015*

4.2.5 Distinct IONPs induce progressive lysosomal membrane permeabilization.

It has been observed that most of the IONPs have the potential to induce adverse effects such as toxicity, inflammation, and oxidative stress in a range of cell types, including both cancerous and normal cells.

Exposure of three hepatic cell lines to either IO-cubes or IO-clusters for 24 hours induced early apoptotic signs. Phosphatidylserine translocation to the outer membrane was confirmed with annexin V labeling, without increased membrane permeability in Alexander and HepG2 cells. Caspase-3 activity was significantly increased in all tested cell lines, indicating apoptosis initiated by IO-clusters (Figure 16).

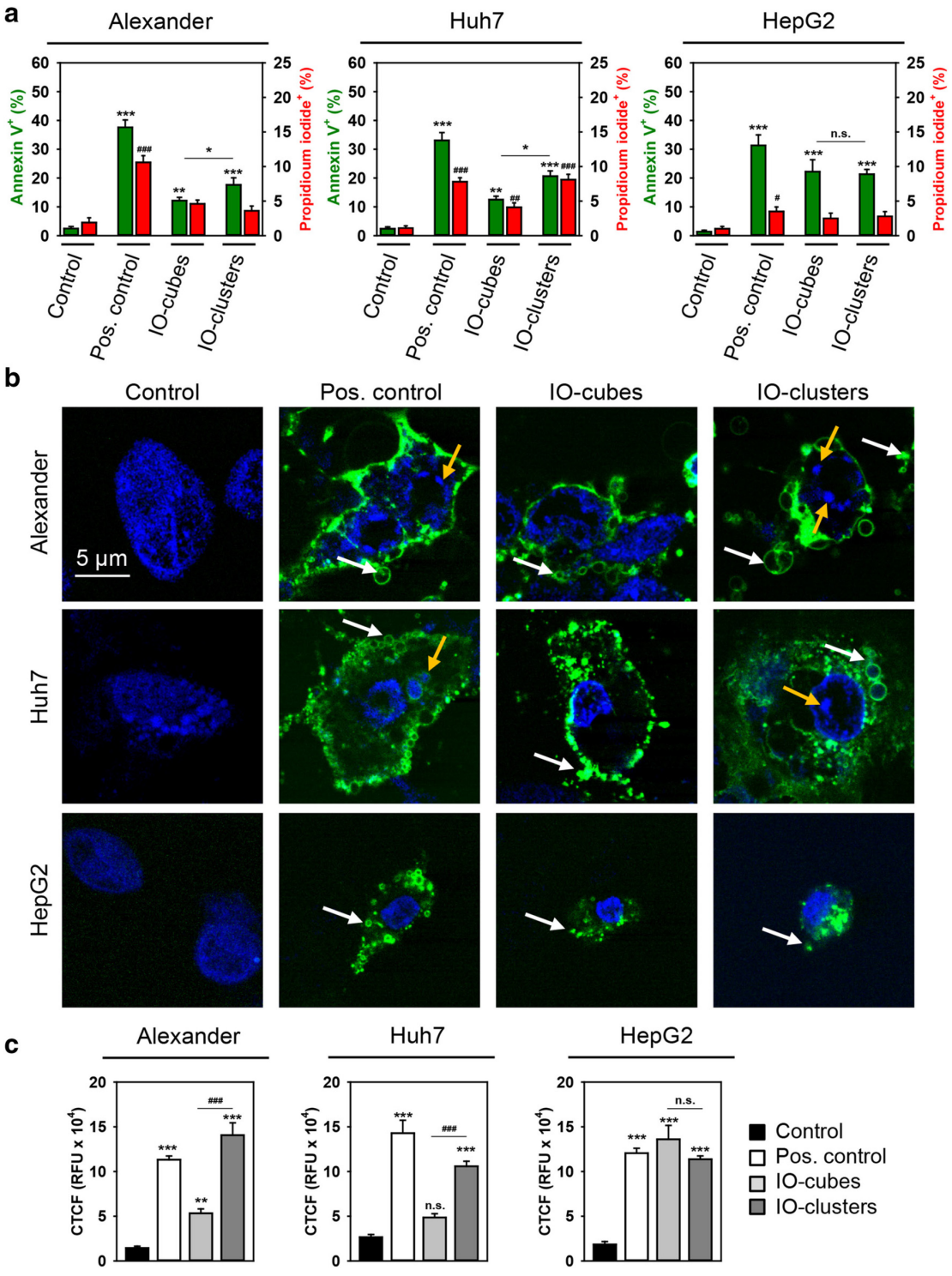

Figure 16. Analysis of apoptotic cell death upon treatment with IO-cubes and IO-clusters. (a) Cells were stimulated with IO-cubes or IO-clusters (100 µg/mL) for 24 h and labeled with annexin V – green dye, propidium iodide – red dye, hoechst 33342 nuclear stain blue. Cells treated with 2 µM staurosporine for 3 h served as a positive control. (b)

Cells were stimulated with IO-cubes or IO-clusters (100 μg/mL) for 24 h and then labeled with hoechst 33342 nuclear stain (blue) and annexin V (green). Cells treated with 2 μM staurosporine for 3 h served as a positive control. Labeled cells were then imaged using high-resolution spinning disk confocal microscopy (Spin SR, Olympus). (c) Caspase-3 activation in hepatic cell lines. Alexander, HepG2, and Huh7 cells were stimulated with IO-cubes or IO-clusters (100 μg/mL) for 24 h, and incubated with fluorescein-conjugated pan-caspase inhibitor (VAD-FMK). *Reprinted from Levada, K., Pshenichnikov, S., Omelyanchik, A. et al. Progressive lysosomal membrane permeabilization induced by iron oxide nanoparticles drives hepatic cell autophagy and apoptosis. Nano Convergence 7, 17 (2020).* https://doi.org/10.1186/s40580-020-00228-5

Lysosomes are primarily recognized for their role in breaking down a variety of biomolecules and materials ingested by cells, positioning them as the central degradation hubs within cellular architecture. The regulation of lysosome-mediated degradation is influenced by factors such as nutrient availability and cellular signaling. Moreover, they are involved in nutrient sensing, transcriptional regulation, and metabolic homeostasis. As reported, lysosomal pivotal role as decision-making centers might orchestrate key cellular processes including secretion, plasma membrane repair, cellular growth, survival, signaling, and energy metabolism. Therefore, lysosomes are considered a crucial metabolic hub in complex nanoparticle-induced cellular signaling dynamics.

As was reported, the cytotoxic effects of IONs start from oxidative stress caused by redox cycling and the generation of reactive oxygen species (ROS). Since mitochondria are a significant intracellular source of ROS, these processes usually lead to lipid peroxidation and DNA damage. Further, it has been described that the ION exposure leads to mitochondrial dysfunction since it has been associated with various cell death signaling pathways, including necrosis and apoptosis. Mitochondrial fragmentation and circularization were observed in treated cells, indicating ROS-induced oxidative stress and mitochondrial dysfunction (Figure 17). Following, the IONs have been confirmed as inducers of autophagy. The study hypothesized that disturbances in

autophagic flux might explain the apoptosis triggered by IO-cubes and IO-clusters across various hepatic cell lines. The formation of LC3-II, a marker of autophagy, was significantly induced by IO-cubes in Alexander and Huh7 cells, but not in HepG2 cells. In contrast, IO-clusters did not affect LC3 lipidation. Additionally, the expression of RIP1, a necroptosis marker was assessed, to rule out necroptotic pathways. Neither IO-cubes nor IO-clusters significantly altered RIP1 expression in any of the utilized cell lines It was found that IO-cubes induced autophagic death in Alexander and Huh7 cells, while IO-clusters triggered apoptosis in the same cell lines. In HepG2 cells, treatment with either type of nanoparticle resulted in apoptosis. This differential cell death response could be linked to the high levels of Bcl-2 in HepG2 cells, which is known to block autophagy, thereby predisposing these cells to apoptosis rather than autophagic death upon nanoparticle treatment.

The initiation of ION-induced autophagy at the lysosomal level, paired with evidence of nanoparticle-induced lysosomal membrane permeabilization (LMP). The results proposed that the distinct patterns of cell death between the cell lines might start from differing levels of LMP induced by IONs treatments. It was evident, that both IO-cubes and IO-clusters caused lysosomal destabilization across all examined hepatic cell lines, marked by the formation of large, swollen lysosomes, a clear indicator of compromised lysosomal integrity (Figure 18). Furthermore, a comparative analysis using LysoTracker fluorescent intensity measurements highlighted that IO-clusters precipitated a progressively greater extent of LMP than IO-cubes in Alexander and Huh7 cells. This observation suggests a mechanism by which these nanoparticles might induce differential cell death pathways. In contrast, both nanoparticles induced a similar degree of LMP in HepG2 cells, leading exclusively to apoptotic outcomes. These findings underscore the critical role of lysosomal destabilization in dictating the cellular response to nanoparticle

exposure. The progression of LMP appears to be a pivotal factor in determining whether cells undergo autophagic death or apoptosis.

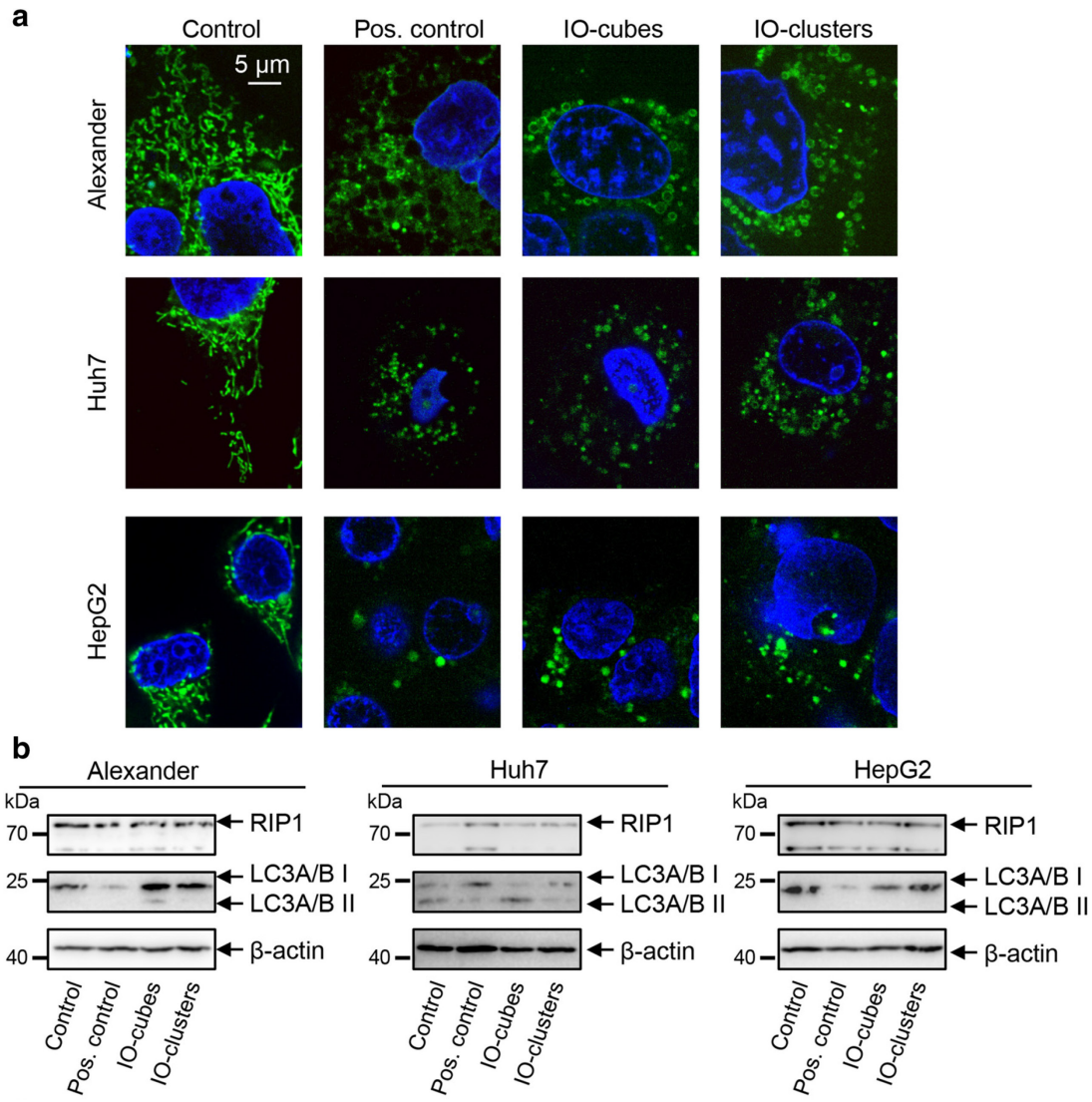

Figure 17. Mitochondrial morphology and immunoblot data. (a) Alteration of mitochondrial morphology by IO-cubes and IO-clusters treatment. Cells were ith MitoTracker® green. Treatment with 20 % ethanol for 20 min served as a positive control. Nuclei were labeled with hoechst 33342 nuclear stain (blue). Labeled cells were then imaged using high-resolution spinning disk confocal microscopy (Spin SR, Olympus). (b) Cells were stimulated with IO-cubes or IO-clusters (100 µg/mL) for 24 h and analyzed by immunoblotting. Actin – control of equal protein loading. Cells treated with 2 µM staurosporine for 3 h served as a positive control. *Reprinted from Levada, K., Pshenichnikov, S., Omelyanchik, A. et al. Progressive lysosomal membrane permeabilization induced by iron oxide*

nanoparticles drives hepatic cell autophagy and apoptosis. Nano Convergence 7, 17 (2020). https://doi.org/10.1186/s40580-020-00228-5

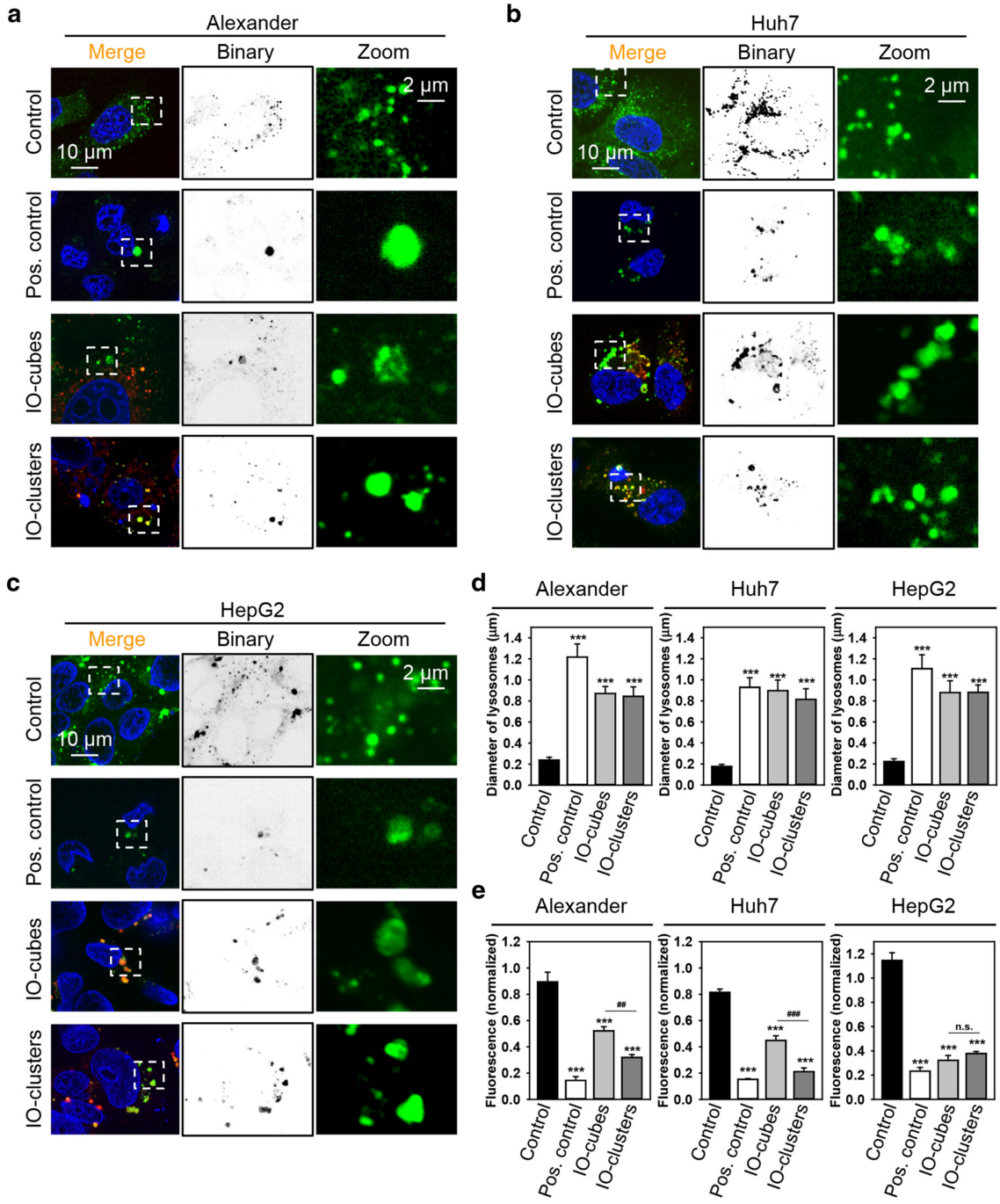

Figure 18. Lysosomal integrity upon IO-cubes and IO-clusters treatment. IO-cubes and IO-clusters treatment affects lysosomal integrity. Alexander (a), HepG2 (b), and Huh7 (c) cells were treated with fluorescently labeled (red) IO-cubes or IO-clusters (100 μg/mL) for 24 h and stained with LysoTracker (green), yellow indicates colocalization of fluorescently labeled nanoparticles with lysosomes. Positive control – 20

% ethanol for 20 min. Nuclei were labeled with hoechst 33342 nuclear stain (blue). Labeled cells were then imaged using high-resolution spinning disk confocal microscopy (Spin SR, Olympus). d Assessment of the lysosomal size upon IO-cubes or IO-clusters (100 μg/mL) uptake. e Alexander, HepG2, and Huh7 cells were exposed to IO-cubes or IO-clusters (100 μg/mL), then stained with LysoTracker and analyzed by laser scanning confocal microscopy. As a positive control, cells were treated with 20 % ethanol for 20 min. *Reprinted from Levada, K., Pshenichnikov, S., Omelyanchik, A. et al. Progressive lysosomal membrane permeabilization induced by iron oxide nanoparticles drives hepatic cell autophagy and apoptosis. Nano Convergence 7, 17 (2020).* https://doi.org/10.1186/s40580-020-00228-5

To summarize complex cellular interactions of IONs and SPIONs, mitochondrial function, and cell death mechanisms, the study explains the potential mechanisms underlying NPs cytotoxicity and the cellular responses to nanoparticle exposure, with implications for understanding nanoparticle toxicity (Figure 19). It shows the critical role of mitochondrial dysfunction and autophagic flux perturbations in determining the fate of hepatic cells exposed to NPs, leading to diverse outcomes such as autophagic death or apoptosis.

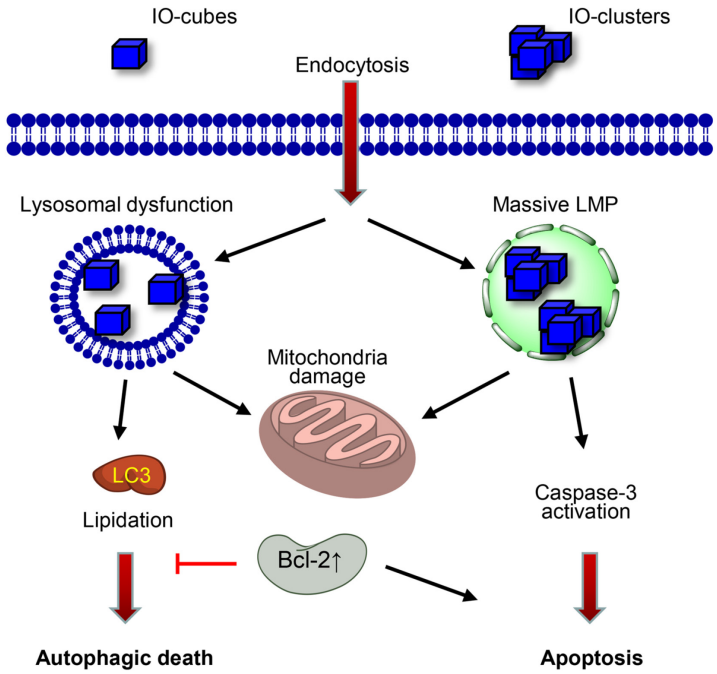

Figure 19. Scheme of cell signaling activation after stimulation with IO-cubes or IO-clusters. *LMP* lysosomal membrane permeabilization. *Reprinted from Levada, K., Pshenichnikov, S., Omelyanchik, A. et al. Progressive lysosomal membrane permeabilization*

induced by iron oxide nanoparticles drives hepatic cell autophagy and apoptosis. Nano Convergence 7, 17 (2020). https://doi.org/10.1186/s40580-020-00228-5

4.3. DNA nanostructures (DNs) interaction with living cells

4.3.1 Physicochemical characterization of DNs

The 6HB nanostructure, known for its selective interaction with different cell types and potential to remodel lipid membranes, was investigated for its ability to facilitate endosomal escape, so far unknown property of DNs functionalized with a specific endosomal escape peptide. The 6HB has a simple structure of six strands that form through an annealing process, resulting in a rigid, monomeric assembly of approximately 7 x 6 nm^2 in size. Those DNs were additionally investigated for the effect of coating with cationic oligolysine peptides, specifically a $(Lys)_{10}$ peptide (K10) and an endosome escape-enhancing peptide (EE), to enhance its stability in biological media. Characterization techniques included native agarose gel electrophoresis, atomic force microscopy (AFM), and dynamic laser light scattering (DLS) (Figure 20). These methods confirmed the effective coating of the nanostructures by the peptides through electrostatic interactions and provided insights into their size distribution, with minimal aggregation. The hydrodynamic diameters measured by DLS indicated an increase in size due to peptide coatings, aligning with the theoretical size predictions. Further, the structural stability of the DNs in physiological conditions was evaluated using a temperature-induced unfolding assay, relying on fluorescence resonance energy transfer (FRET) between incorporated fluorescent dyes. The analysis showed that the 6HB structures remained stable and assembled in a physiological buffer, maintaining their integrity over time. Considering the tendency of nanomaterials to be sequestered by the liver upon intravenous injection, the study also aimed to understand the

interactions between DNs and hepatocytes, utilizing HepG2, Huh7, and Alexander cell lines as models.

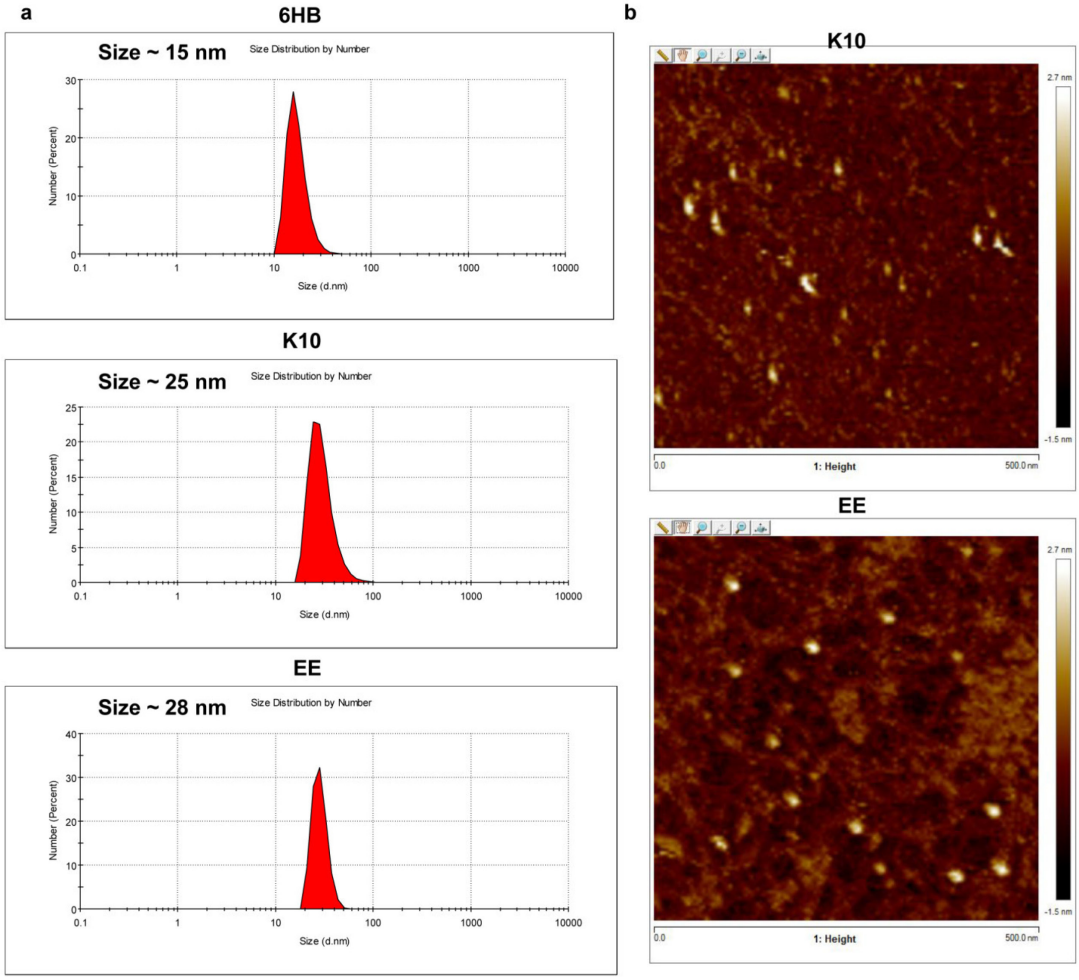

Figure 20. Size distribution of different DNs. Characterization of the particles dissolved in PBS was measured with a Zetasizer Nano (Malvern Instruments). AFM characterization of the K10 and EE DNs. *Reprinted from Barbora Smolková, Tara MacCulloch, Tyler F. Rockwood, Minghui Liu, Skylar J. W. Henry, Adam Frtús, Mariia Uzhytchak, Mariia Lunova, Martin Hof, Piotr Jurkiewicz, Alexandr Dejneka, Nicholas Stephanopoulos, and Oleg Lunov. ACS Applied Materials & Interfaces* ***2021*** *13 (39), 46375-46390* https://doi.org/10.1021/acsami.1c14401

4.3.2 Uptake of different DNs

The composition of the "hard" corona, which remains relatively stable and stays relevant to biomedical applications, is typically

dominated by high-affinity proteins such as apolipoproteins, fibrinogen, and albumin. The nature of the protein corona is influenced by numerous nanoparticle properties, including size, shape, surface charge, and the chemical functionalization of the nanoparticle surface, as well as by the composition of the surrounding biological fluid. The formation of the protein corona is a dynamic interaction that significantly alters the physicochemical properties of nanoparticles, such as their hydrodynamic diameter and colloidal stability. Moreover, this process can modulate the biological activity of the adsorbed proteins, potentially leading to altered protein conformations, impaired biological functions, and unintended cellular interactions. Critically, the presence of the protein corona significantly alters the targeting capability of functionalized nanoparticles, leading to a loss of specificity and efficacy in therapeutic and diagnostic applications. Despite its significance, the implications of protein corona formation were initially overlooked in the development of nanoparticle-based biomedical applications, underscoring the need for a deeper exploration of the nano-bio interface to leverage the potential of nanotechnology in clinics fully.

Further quantitative analysis of the protein corona composition was conducted through Fluorescence Correlation Spectroscopy (FCS), a sophisticated optical technique used for characterizing the dynamics of fluorescent particles in solution. The DNs, following incubation in either HBSS or EMEM supplemented with 10% FBS, were analyzed by FCS to analyze the mean diffusion time, to measure the hydrodynamic radius, the presence, and thickness of the protein corona on the DNs surface.

Each type of DNs at a concentration of 50 nM, was incubated in two different media: Hank's Balanced Salt Solution (HBSS) and Eagle's Minimum Essential Medium (EMEM), supplemented with 10% fetal bovine serum (FBS). The dissociated proteins were then subjected to polyacrylamide gel electrophoresis, a technique renowned for its ability to resolve proteins based on their molecular weight. The gels were

subsequently stained with Coomassie blue, a dye from AppliChem known for its sensitivity and specificity in protein visualization, to allow for the qualitative assessment of the protein corona (Figure 21).

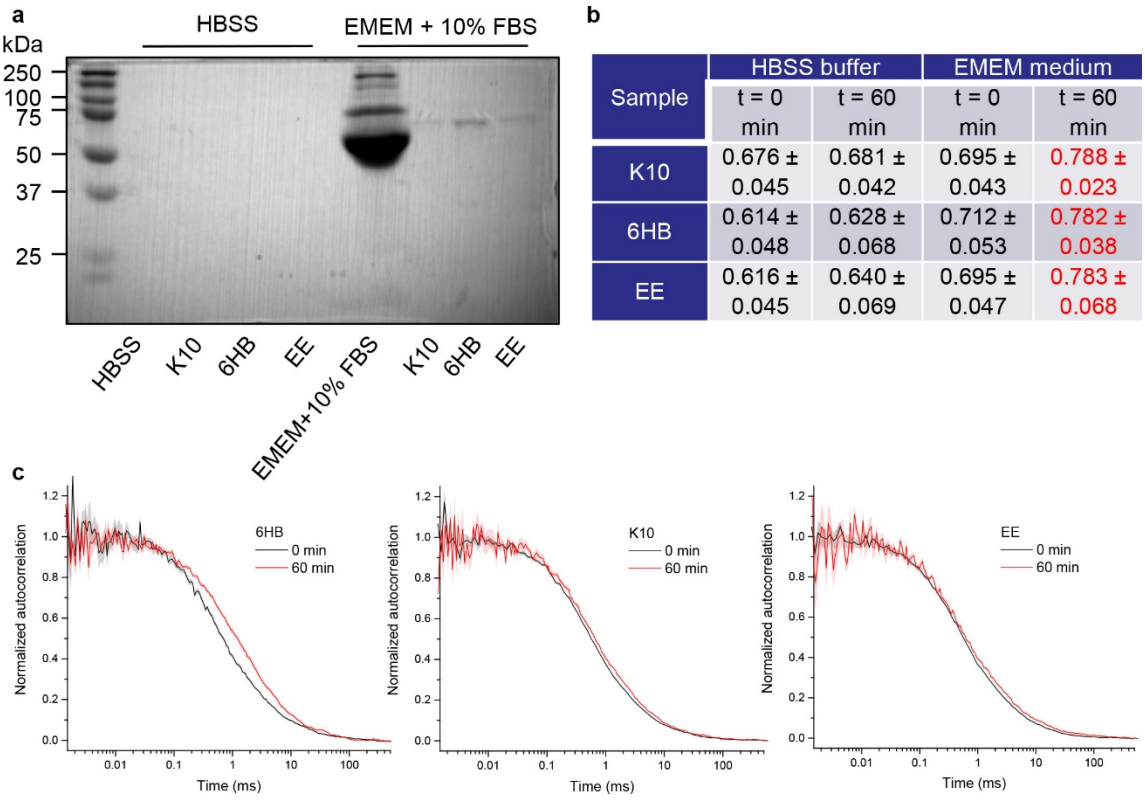

Sample	HBSS buffer		EMEM medium	
	t = 0 min	t = 60 min	t = 0 min	t = 60 min
K10	0.676 ± 0.045	0.681 ± 0.042	0.695 ± 0.043	0.788 ± 0.023
6HB	0.614 ± 0.048	0.628 ± 0.068	0.712 ± 0.053	0.782 ± 0.038
EE	0.616 ± 0.045	0.640 ± 0.069	0.695 ± 0.047	0.783 ± 0.068

Figure 21. DN−protein interaction. (a) Different types of DNs at a concentration 50 nM were incubated either in HBSS or in EMEM medium (ATCC) supplemented with 10% fetal bovine serum (FBS, Thermo Fisher Scientific) for 2 h at 37 °C. The DNs were centrifuged and washed with PBS. Elution and denaturation in the sample loading buffer were used to detach proteins associated with the particles. Afterward, proteins were separated by gel electrophoresis. Gels were stained with Coomassie blue (AppliChem). (b and c) Analysis of the protein corona on the particles assessed by Fluorescence Correlation Spectroscopy (FCS). Different types of DNs were incubated either in HBSS, or in EMEM medium (ATCC) supplemented with 10% fetal bovine serum (FBS, Thermo Fisher Scientific), and the mean diffusion time was measured by FCS. (b) Table summarizing diffusion times of different DNs incubated in different buffer conditions in milliseconds. The data are presented as mean ± SE, n = 3. The mean diffusion time is given in milliseconds (ms). (c) Examples of autocorrelation curves obtained for the

diffusion of fluorescently labeled particles in EMEM medium supplemented with 10% fetal bovine serum. The measurements were performed immediately after adding the particles to the medium and after 60 min after addition. *Reprinted from Barbora Smolková, Tara MacCulloch, Tyler F. Rockwood, Minghui Liu, Skylar J. W. Henry, Adam Frtús, Mariia Uzhytchak, Mariia Lunova, Martin Hof, Piotr Jurkiewicz, Alexandr Dejneka, Nicholas Stephanopoulos, and Oleg Lunov. ACS Applied Materials & Interfaces* ***2021*** *13 (39), 46375-46390* https://doi.org/10.1021/acsami.1c14401

Obtained autocorrelation curves generated from FCS data represent the diffusion behavior of fluorescently labeled DNs in the EMEM with 10% FBS. The curves were recorded both immediately after the introduction of DNs into the medium and after incubation for 60 minutes, providing temporal resolution to the dynamics of protein corona formation on the DNs in a serum-supplemented media.

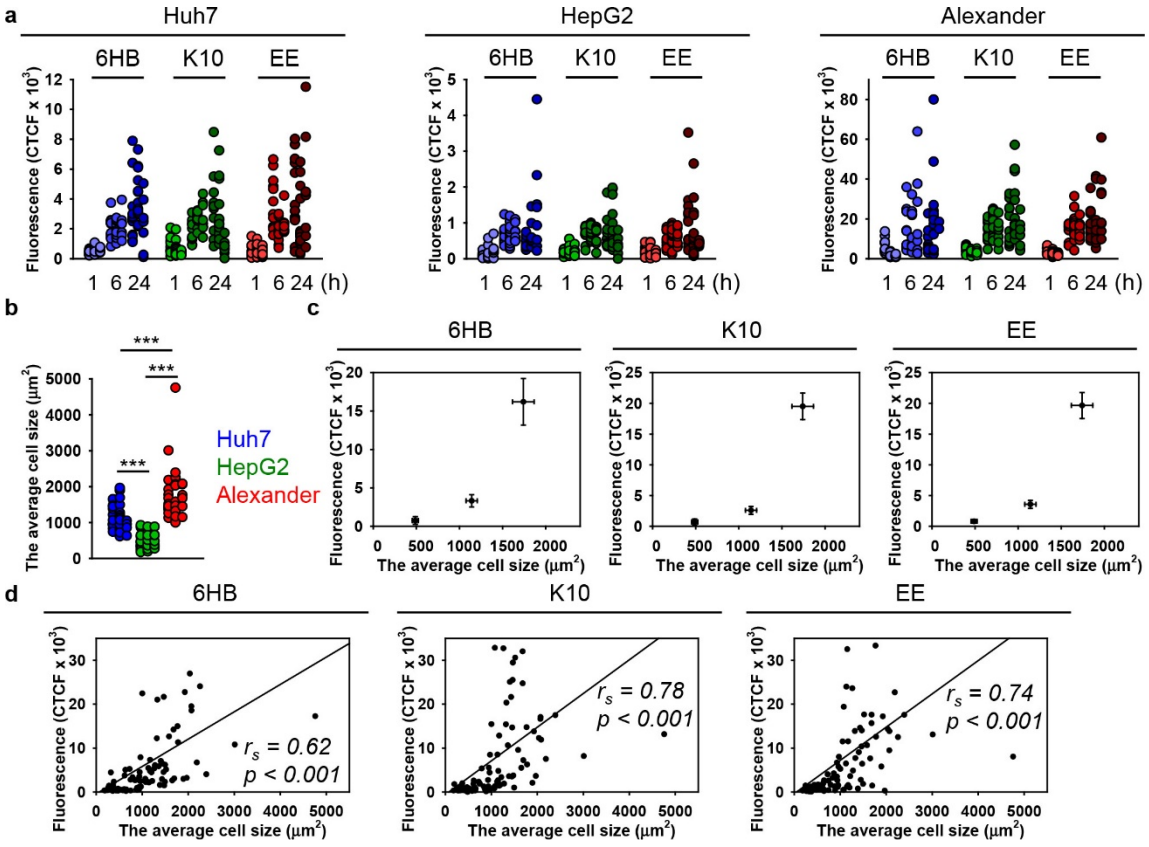

Figure 22. Uptake kinetics assessment of different DNs. (a) Alexander, HepG2, and Huh7 cell lines were treated with a 50 nM concentration of different DNs for 1, 6,

and 24 h. After treatment, cells were fixed with 4% paraformaldehyde (VWR) and labeled with CellBrite Blue (Biotium) plasma membrane stain. Stained cells were imaged using spinning disk confocal microscopy IXplore SpinSR (Olympus, Tokyo, Japan). The intracellular DNs were measured as corrected total cell fluorescence (CTCF) of the full area of interest using ImageJ software (NIH). Data are expressed out of at least three independent experiments (n = 28−34 cells). (b) Assessment of cell size in Huh7, HepG2, and Alexander cells. Cells were stained with CellMask Green (Thermo Fisher Scientific) plasma membrane stain. Nuclei were counterstained with Hoechst 33342 (Thermo Fisher Scientific). Stained cells were imaged using spinning disk confocal microscopy IXplore SpinSR (Olympus, Tokyo, Japan). The average cell area was measured using ImageJ software (NIH) and is presented as a means of n = 30 cells. (***) P < 0.001 denotes significant differences. (c) Cellsize-dependent DNs uptake. The intracellular DNs presented as CTCF after 24 h treatment with 50 nM concentration of different DNs were plotted versus corresponding cell size. (d) Linear correlation between cell size and DNs uptake. Each black point represents confocal microscopy measured single-cell DN uptake plotted against corresponding cell size. The uptake is expressed as CTCF after 24 h treatment with 50 nM concentration of different DNs. Correlation coefficients and P values were calculated using SigmaPlot 13 software (Systat Software, Inc.). *Reprinted from Barbora Smolková, Tara MacCulloch, Tyler F. Rockwood, Minghui Liu, Skylar J. W. Henry, Adam Frtús, Mariia Uzhytchak, Mariia Lunova, Martin Hof, Piotr Jurkiewicz, Alexandr Dejneka, Nicholas Stephanopoulos, and Oleg Lunov. ACS Applied Materials & Interfaces* ***2021*** *13 (39), 46375-46390* *https://doi.org/10.1021/acsami.1c14401*

In order to analyze uptake kinetics Alexander, HepG2, and Huh7 cell lines were treated with a 50 nM concentration of different DNs for 1, 6, and 24 h (Figure 22). Upon treatment, DNs were rapidly internalized by all cell lines within the first hour, with the following uptake up to 24 hours. It is worth noting, that Alexander cells showed the highest uptake rates, which was correlated with their larger cell size in comparison to Huh7 and HepG2 cells. Quantitative measurements established the average cell sizes as 1700 μm^2 for Alexander, 1100 μm^2 for Huh7, and 500 μm^2 for HepG2, explaining the impact of cell size on DNs uptake efficiency. This result is consistent with literature suggesting the importance of cell size in the cellular uptake of nanomaterials.

4.3.3 Protein Corona Inhibits Endosomal Escape of Functionalized DNA Nanostructures

Further, this study (see Appendix VI) focused on the cellular uptake and processing of DNA nanostructures (DNs). Results revealed certain variability of DN uptake efficiency among the cell lines, with Alexander cells exhibiting the most efficient uptake. Interestingly, within each cell line, DN uptake efficiency did not significantly vary, regardless of the functional modifications. Additionally, an analysis of cellular morphology revealed size and shape differences among the cell lines, which could potentially influence DN uptake efficiency. Moreover, all types of DNs were internalized by the cell lines within one hour, with the process continuing for up to 24 hours. Alexander cells consistently displayed the highest DN internalization rate. The linear relationship between cell size and DN uptake across all DN types indicates that cell size is a crucial factor in DN internalization rates.

A series of colocalization analyses were conducted on Huh7, HepG2, and Alexander cells to investigate intracellular kinetics. Cells were exposed to various DNs at a concentration of 50 nM for 6 hours, under both nutrient-rich conditions (10% FBS EMEM) and in the absence of serum (0% FBS EMEM). Following the incubation period, the cells were stained with the lysosomal marker LysoTracker Blue DND-22, (Figure 23). To quantitatively assess the degree of colocalization between the DNs and lysosomes, the Pearson's correlation coefficient was calculated for each fluorophore pair, DNA-Lysosomes, and DNA-pHrodo. For detailed protocol see Appendix VI. The obtained results demonstrate interactions between DNs and cellular lysosomes, suggesting a notable affinity of DNs for lysosomes within different cell lines and under different culture conditions. The overall dynamics of endolysosomal escape exhibited by elastin-like polypeptide-encapsulated DNA nanocarriers (EE-DNs) were

notably increased in serum-enriched media. This observation was consistent across all three studied cell lines. The observed increase in colocalization within serum conditions compared to serum-free medium suggests enhanced retention of EE-DNs in endo-/lysosomal vesicles upon serum exposure.

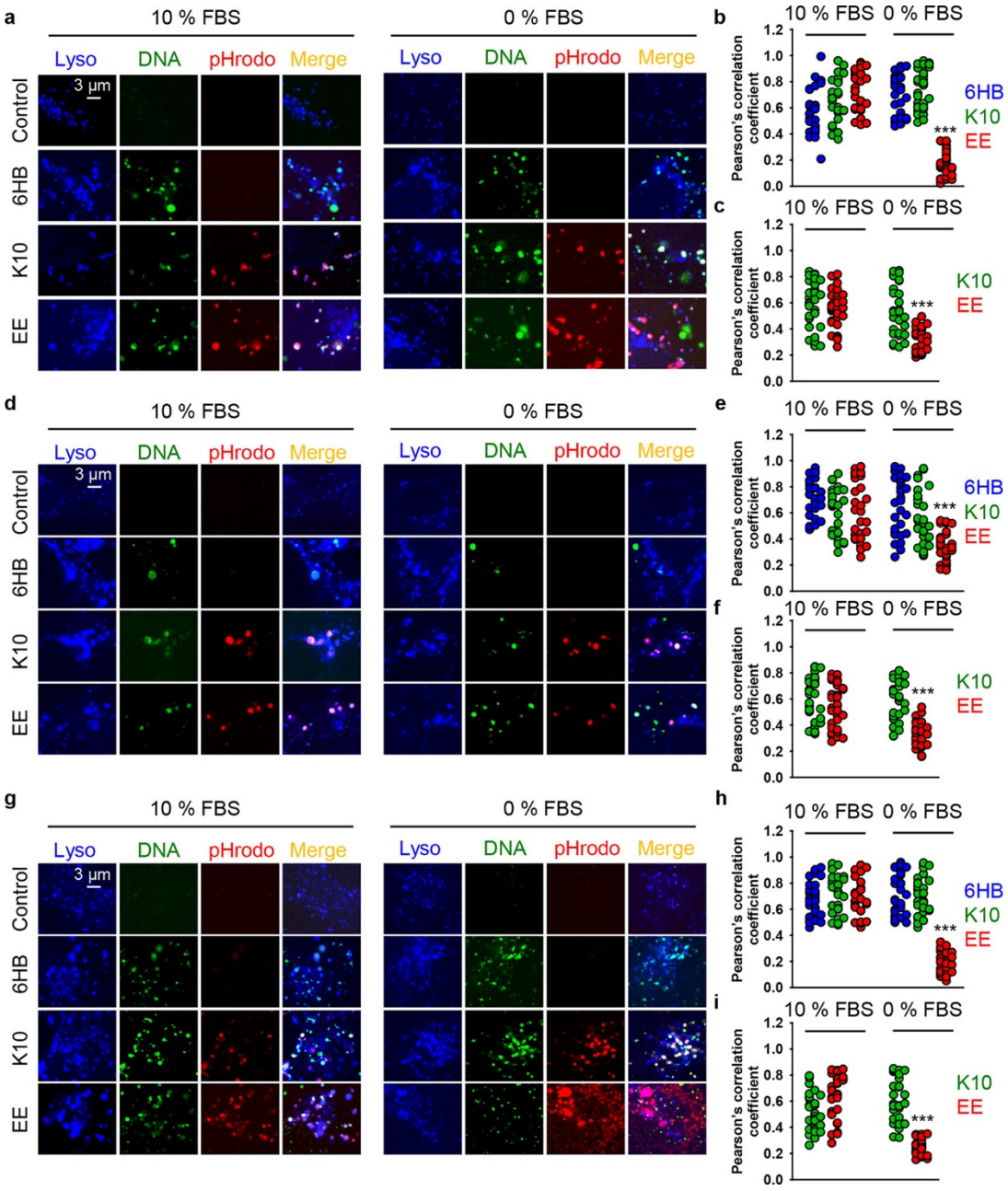

Figure 23. Colocalization analysis of different DNs. (a–c) Huh7 cells were treated with different types of DNs (at 50 nM concentration) for 6 h either in full medium (10% FBS EMEM) or in serum-free medium (0% FBS EMEM). After incubation, cells were

labeled with lysosomal marker LysoTracker Blue DND-22 (b) DNA−Lysosomes or (c) DNA−pHrodo was calculated using the Coloc 2 tool available in ImageJ software (NIH) and is presented as means of n = 30 cells. (***) P < 0.001 denotes significant differences. (d−f) HepG2 cells were treated with different types of DNs (at 50 nM concentration) for 6 h either in full medium (10% FBS EMEM) or in serum-free medium (0% FBS EMEM). (e) DNA−Lysosome or (f) DNA−pHrodo was calculated using the Coloc 2 tool available in ImageJ software (NIH) and is presented as means of n = 30 cells. (***) P < 0.001 denotes significant differences. (g−i) Alexander cells were treated with different types of DNs (at 50 nM concentration) for 6 h either in full medium (10% FBS EMEM) or in serum-free medium (0% FBS EMEM). (h) DNA−Lysosomes or (i) DNA−pHrodo was calculated using the Coloc 2 tool available in ImageJ software (NIH) and is presented as means of n = 30 cells. (***) P < 0.001 denotes significant differences. *Reprinted from Barbora Smolková, Tara MacCulloch, Tyler F. Rockwood, Minghui Liu, Skylar J. W. Henry, Adam Frtús, Mariia Uzhytchak, Mariia Lunova, Martin Hof, Piotr Jurkiewicz, Alexandr Dejneka, Nicholas Stephanopoulos, and Oleg Lunov. ACS Applied Materials & Interfaces* ***2021*** *13 (39), 46375-46390* *https://doi.org/10.1021/acsami.1c14401*

Analysis showed similar colocalization patterns for both 6HB-DNs and EE-DNs with endo-/lysosomes, indicating a complex interaction between DN constructs and serum components that do not significantly differ with the inclusion of elastin-like polypeptides. The stability of DNs suggests a strong interaction between the DNA and peptide elements of EE-DNs, potentially affecting their endo-/lysosomal retention and cellular processing.

Further, this study investigated the effect of the protein corona on the escape efficiency of DNs functionalized with an endolysosomal escape enhancer. For detailed discription please refer to the Appendix VI. Given that uptake continues up to 24 hours, an optimal time point for endolysosomal escape assessment was identified as 6 hours to avoid biased effects from autophagy. The study utilized a 13-residue peptide, aurein 1.2, known to enhance endolysosomal escape and improve cytosolic delivery of proteins. Aurein 1.2, is capable of disrupting endolysosomal membranes without rupturing cell membranes or notable cytotoxicity. Results demonstrated that aurein 1.2-decorated DNs in serum-free medium successfully escaped from endosomes/lysosomes

into the cytoplasm in all three cell lines after 6 hours of treatment. However, in the presence of serum, the endolysosomal escape of EE-DNs was significantly diminished, with DNs remaining inside endo-/lysosomal vesicles.

The study also explored the specificity of aurein 1.2 as an endolysosomal escape enhancer by comparing it with a highly charged deca-lysine (K10) peptide and scrambled aurein 1.2 sequences. Neither alternative peptide facilitated noticeable endolysosomal escape, underscoring the sequence-dependent effectiveness of aurein 1.2.

Overall, these results underscore the significant role of cell size in the uptake of DNs and the stability of these nanocarriers within lysosomal compartments. The obtained data reveal a specific pattern of EE-DNs uptake and their engagement with cellular endo-/lysosomal systems. The understanding of the dynamics between serum components and EE-DNs is essential for the development and use of DNA nanocarriers in the biomedical field, particularly where serum presence is a major factor.

5. Conclusions

Presented work resulted in 8 publications published in indexed peer-reviewed journals, several conference contributions, and lectures.

This interdisciplinary work merges various scientific disciplines like nanomedicine, including pharmaceutical sciences, cell biology, engineering, chemistry, and materials science. The integration of these fields promotes innovation though complicates the translation of nanomedicines to clinical applications due to differing methodologies and focus areas. The research further explores the interactions between nanoparticles and cellular systems, noting that nanoparticles are primarily internalized through endocytic pathways and localized in lysosomes. The fate of nanoparticles and the ability of engineered nanoparticles to impact lysosomal degradation are particularly relevant to *in vivo* biomedical applications. The liver's function is pivotal in nanoparticle metabolism and potential hepatotoxicity might be deeply explored in nanomedicine research. The thesis also addresses the lack of comprehensive understanding regarding the role of lysosomal dysfunction in adverse drug reactions (ADRs) associated with nanomedicines. The limited data available call for further investigation into the interaction between nanomedicines and altered lysosomal functions in disease states.

In this dissertation, the hepatic accumulation of iron oxide nanoparticles (IONPs) and their interaction with liver cells have been critically examined, revealing a complex interplay of biological processes that may lead to hepatotoxicity. Initially described as biocompatible due to their iron composition, IONPs were supposed to mimic natural iron processes in the body. However, further research has demonstrated a range of toxic effects, particularly with longer exposure time, primarily attributed to their interaction with cellular lysosomes. The liver, as the

central organ for metabolism and detoxification, is a primary site for IONP accumulation. The size and surface characteristics of IONPs significantly influence their biodistribution, with particles larger than 6–8 nm being predominantly sequestered in the liver and spleen. Despite initial assumptions of efficient clearance by liver cells, studies indicate that IONPs can persist within the liver for extended periods, raising concerns about hepatotoxicity, especially under compromised liver function (Figure 24).

Based on these results, the work further investigated the impact of cellular genetic background on the response of liver tumor cells to IONPs. The study highlights that the cellular outcome, either apoptosis or autophagy upon IONP exposure, is significantly influenced by the expression levels of Bcl-2 protein. In HepG2 cells, high Bcl-2 expression directs the response towards apoptosis, facilitated by lysosomal membrane permeabilization (LMP). For instance, in Alexander and Huh7 cells, the response to IONPs varies, with the nature of LMP critically affecting the cell death pathway. Since, Bcl-2, a key protein involved in the regulation of apoptotic pathways, it was found to significantly influence the cellular response to IONP treatment. In hepatoblastoma-derived HepG2 cells, characterized by high Bcl-2 expression, an increased predisposition towards apoptosis was observed upon NPs exposure. This response is connected to Bcl-2's ability to inhibit autophagy. Therefore, directing the cellular response toward apoptotic death, is a pathway further regulated by lysosomal membrane permeabilization (LMP). This indicates that Bcl-2 expression levels critically modulate the balance between apoptosis and autophagy in the presence of IONPs, with high Bcl-2 expression regulating apoptosis. On the other hand, in hepatocellular carcinoma Alexander and Huh7 cells, the cellular response to IONPs was more variable, influenced by the severity of LMP and the differential expression of Bcl-2 and p53. These proteins play a crucial role in determining the fate of cells, with p53's sub-cellular localization being

particularly significant. Those findings suggest that the treatment with IONPs in Alexander cells leads to an increase in cathepsin B and LC3 levels, indicative of autophagic processes, yet without the expected lipidation of LC3, pointing to an impaired autophagic flux. This impairment correlates with an increase in cytoplasmic p53 levels, highlighting p53 role in autophagy regulation. This explains that cytoplasmic p53 is known to inhibit autophagy, while nuclear p53 promotes it. The differential response of cells to IONPs, based on the expression and localization of Bcl-2 and p53, provides significant information related to the complex interplay between nanoparticle characteristics, cellular genetic background, and the molecular interplay between apoptosis and autophagy pathways.

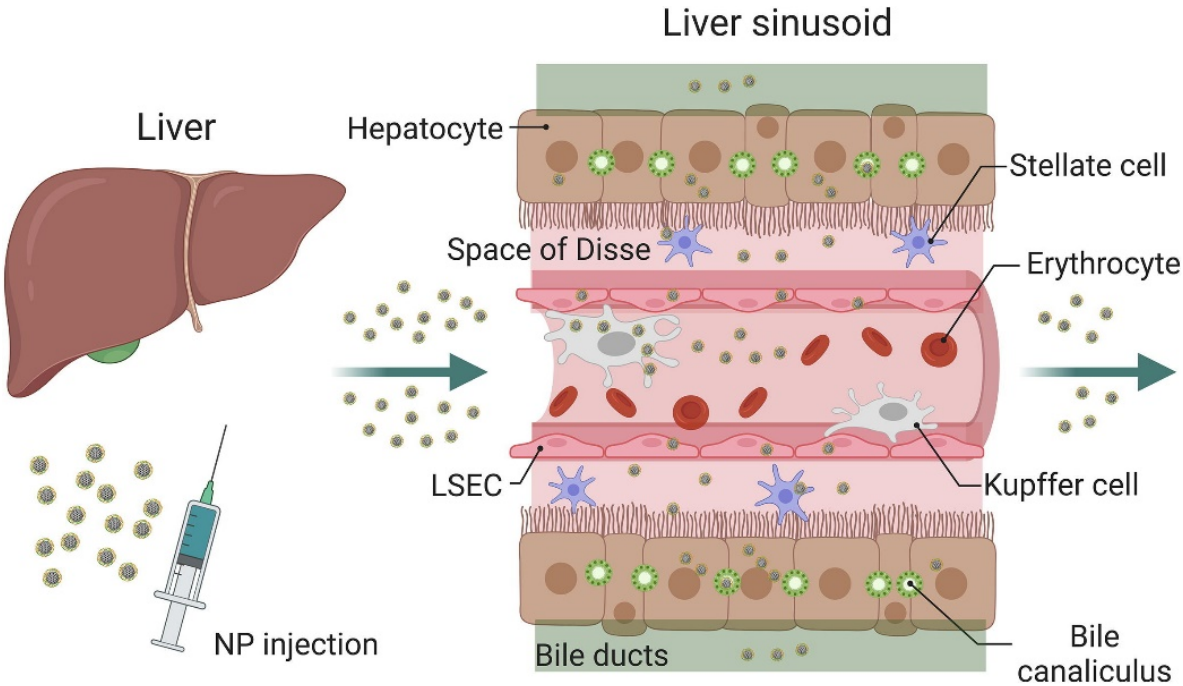

Figure 24. Scheme of processing and clearance of injected nanoparticles (NPs) by the liver. *Reprinted from Mariia Uzhytchak, Barbora Smolková, Mariia Lunova, Adam Frtús, Milan Jirsa, Alexandr Dejneka, Oleg Lunov. Lysosomal nanotoxicity: Impact of nanomedicines on lysosomal function. Advanced Drug Delivery Reviews, Volume 197, 2023. 114828, ISSN 0169-409X.* https://doi.org/10.1016/j.addr.2023.114828

This research underscores the importance of considering the genetic and molecular profiles of tumor cells in designing targeted nanomedicine strategies for liver cancer treatment. The findings suggest that sub-lethal exposure to IONPs leads to lysosomal accumulation and functional impairment, contributing to altered autophagic flux. The role of lysosomal dysfunction in regulating cellular responses to IONPs, mediated by proteins such as Bcl-2 and p53, highlights the necessity of integrating genetic factors into the development of nanoparticle-based therapies.

In summary, the thesis emphasizes the need for a more integrated, biology-focused approach in the design and development of nanomedicines, highlighting the challenges in clinical translation. It advocates for continued adherence to scientific rigor, ethical research practices, and a focus on patient safety and treatment efficacy in the advancement of the field. The thesis aims to provide a comprehensive overview of the current state of nanomedicine research, emphasizing the necessity for interdisciplinary collaboration and a deeper understanding of biological interactions to develop safe and effective nanotherapeutics.

List of Figures

List of Tables

List of Abbreviations

SPIONs, superparamagnetic iron oxide nanoparticles;

NPs, nanoparticles;

FDA, Food and Drug Administration;

LAMP1, lysosome-associated membrane protein 1;

LAMP2A, lysosomal-associated membrane protein 2A;

LC3B, microtubule-associated protein 1 light chain 3B;

LMP, lysosomal membrane permeabilization;

MRI, magnetic resonance imaging;

mTOR, mechanistic/mammalian target of rapamycin;

ADE, adverse drug effect;
ADME, absorption, distribution, metabolism and elimination;
ADR, adverse drug reaction;
ALT, alanine aminotransferase;
API, active pharmaceutical ingredient;
APCs, antigen-presenting cells;
AST, aspartate aminotransferase;
BAX, Bcl-2-associated X protein;
BBB, the blood-brain barrier;
BID, the BH3 interacting-domain death agonist;
CKD, chronic kidney disease;
CAM, cell adhesion molecule;
CMA, conditional marketing authorization mass;
CME, clathrin-mediated endocytosis;
CLIC/GEEC,clathrin-independent/dynamin-independent endocytosis;
CNS, central nervous system;
CSFB, blood-cerebrospinal fluid barrier;
DCs, dendritic cells;
DILI, drug-induced liver injury;
ECM, extracellular matrix;
EEA1, Early Endosome Antigen 1;
EMA, European Medicines Agency;
EPR, enhanced permeability and retention;
ER, endoplasmic reticulum;
ERK, extracellular signal-regulated kinase;
ERTs, enzyme replacement therapies;
EUA, emergency use authorization;
FDA, Food and Drug Administration;
FEME, fast endophilin-mediated endocytosis;
HUVECs, human umbilical vein endothelial cells;

HSP42, heat shock protein 42;
ICAM-1, intercellular adhesion molecule 1;
ID, injected dose;
ICV, intracerebroventricular;
I.V., intravenous;
LAMP1, lysosome-associated membrane protein 1;
LAMP2A, lysosomal-associated membrane protein 2A;
LC3B, microtubule-associated protein 1 light chain 3B;
LMP, lysosomal membrane permeabilization;
LSDs, lysosomal storage disorders;
MAPK, mitogen-activated protein kinase;
MEK, mitogen-activated protein kinase kinase;
MHC, major histocompatibility complex;
MMP, mitochondrial membrane permeabilization;
MPS, mononuclear phagocytic system;
MPTP, mitochondrial permeability transition pore;
MRI, magnetic resonance imaging;
mTOR, mechanistic/mammalian target of rapamycin;
mTORC1, mechanistic target of rapamycin complex 1;
NK cells, natural killer cells;
NLRP3, NLR family pyrin domain containing 3;
NPs, nanoparticles;
NPC1, Niemann-Pick type C1 protein;
NF-κB, nuclear factor-κB;
NF-κB/AP-1, nuclear factor-κB/activator protein 1;
PAMAM, poly(amidoamine);
PD, pharmacodynamics;
PDMS, poly(dimethylsiloxane);
PEG, poly(ethylene glycol);
PEI, poly(ethylenimine);
PK, pharmacokinetics;

PLGA, poly-(lactide-co-glycolide);
PECAM-1, platelet-endothelial CAM-1;
Rab5, RAS-associated protein RAB5A;
ROS, reactive oxygen species;
SARS-CoV-2, severe acute respiratory syndrome coronavirus 2;
siRNA, small interfering RNA;
TFEB, transcription factor EB;
TLR4, Toll-like receptor 4;
UPR, unfolded protein response;
UPS, ubiquitin proteasomal system;
v-ATPase, vacuolar-type proton adenosine triphosphatase;

List of Publications

The list consists of 25 publications, excluding conferences abstracts. The total number of citations (19th of April, 2024) is 431, H- index 13 according to Scopus database, and 374, H-index 12, according to Web of Science (WoS).

- **Uzhytchak, M.,** Smolková, B., Frtús, A. *et al.*. *Sci Rep* **13**, 10818 (2023).

- **Uzhytchak, M.,** Smolkova, B., Lunova, M., et al., , *Adv. Drug Delivery Rev.*, 2023, vol. 197, p. 114828.

- Frtús, A.; Smolková, B.; **Uzhytchak, M.;** Lunova, M.; Jirsa, M.; Petrenko, Y.; Dejneka, A.; Lunov, O. *ACS Biomater. Sci. Eng.* 2023, 9, 5, 2408–2425

- **Uzhytchak, M.;** Lunova, M.; Smolkova, B., Jirsa, M.; Dejneka, A.; Lunov, O. *Nanoscale Adv.,* 2023,**5**, 4250-4268

- Frtús, A.; Smolková, B.; **Uzhytchak, M.;** Lunova, M.; Jirsa, M.; Henry, S.J.W.; Dejneka, A.; Stephanopoulos, N.; Lunov, O. *Acta Biomater.* **2022**, *146*, 10–22.

- Smolková B., MacCulloch T., Rockwood T. F., Liu M., Henry S. J. W., Frtús A., **Uzhytchak M.,** Lunova, M. Hof, P. Jurkiewicz, A. Dejneka, N. Stephanopoulos, and O. Lunov, *ACS Appl. Mater. Interfaces* 2021, 13, 39, 46375–46390. IF 9.229

- Lunova M., Kubovciak J., Smolková B., **Uzhytchak M.,** Michalova K., Dejneka A., Strnad P., Lunov O., Jirsa M. *Int. J. Mol. Sci*. 2021, 22(5), 2560. IF 5.924

- Frtús A., Smolková B., **Uzhytchak M.,** Lunova M., Jirsa M., Hof M., Jurkiewicz P., Lozinsky V.I., Wolfová L., Petrenko Y., Kubinová Š. Dejneka A., Lunov O. *Pharmaceuticals* 2020, 13(12), 430. IF 5.863

- Smolková, B. Frtús, A., **Uzhytchak, M.,** Lunova, M., Kubinová, Š., Dejneka, A., Lunov, O. *Int. J. Mol. Sci.* 2020, 21, 6226. IF 5.924

- Frtús A, Smolková B, **Uzhytchak M,** Lunova M, Jirsa M, Kubinová Š, Dejneka A, Lunov O. *J. Control. Release* 2020; 328: 59. IF 9.776

- Omelyanchik, A., Gurevich, A., Pshenichnikov, S., Kolesnikova, V., Smolkova, B., **Uzhytchak, M.,** ... Rodionova, V. *Journal of Magnetism and Magnetic Materials* 2020, 166991. IF 2.993

- Levada, K., Pshenichnikov, S., Omelyanchik, A. ...Lunova M., Jirsa M., Smolková B., **Uzhytchak M.,** Dejneka A., Lunov O. *Nano Convergence* 2020,7, 17. IF 8.526

- **Uzhytchak, M.;** Smolková, B.; Lunova, M.; Jirsa, M.; Frtús, A.; Kubinová, Š.; Dejneka, A.; Lunov, O. *Cells* 2020, 9, 1015. IF 6.6

- Víšová, I.; Smolková, B.; **Uzhytchak, M.;** Vrabcová, M.; Chafai, D.E.; Houska, M.; Pastucha, M.; Skládal, P.; Farka, Z.; Dejneka, A.; Vaisocherová-Lísalová, H. *Biomolecules* 2020, 10, 1146. IF 4.879

- Víšová, I.; Smolková, B.; **Uzhytchak, M.;** Vrabcová, M.; Zhigunova, Y.; Houska, M.; Surman, F.; de los Santos Pereira, A.; Lunov, O.;

Dejneka, A.; Vaisocherová-Lísalová, H. *Macromol. Biosci*. 2020, 20, 1900351– 1900359. IF 4.979

- Lunova M., Smolková B., **Uzhytchak M.,** Janoušková K.Ž., Jirsa M., Egorova D., Kulikov A., Kubinová Š., Dejneka A., Lunov O. *Cell. Mol. Life Sci*. 2020, 77, 2815–2838. IF 9.261

- Lunov, O.; **Uzhytchak, M.;** Smolková, B.; Lunova, M.; Jirsa, M.; Dempsey, N.M.; Dias, A.L.; Bonfim, M.; Hof, M.; Jurkiewicz, P.; Petrenko, Y.; Kubinová, Š.; Dejneka, A. *Cancers* 2019, 11, 1873. IF 6.126

- Jelinek, M.; Kocourek, T.; Jurek, K.; Jelinek, M.; Smolková, B.; **Uzhytchak, M.;** Lunov, O. *Nanomaterials* 2019, 9, 451. IF 4.324

- O. Lunov, B. Smolková, A. Lynnyk, **M. Uzhytchak,** Š. Kubinová, A. Dejneka, *Jemná mechanika a optika* 2019, 64/5, 127 - 129.

- Smolková, B.; **Uzhytchak, M.;** Lynnyk, A.; Kubinová, Š.; Dejneka, A.; Lunov, O., *J. Funct. Biomater*. 2019, 10, 2.

- Lunova, M.; Smolková, B.; Lynnyk, A.; **Uzhytchak, M.;** Jirsa, M.; Kubinová, Š.; Dejneka, A.; Lunov, O. *Cancers* 2019, 11, 82. IF 6.126

- Smolkova, B., Lunova, M.; Lynnyk, A.; **Uzhytchak, M.;** Churpita, O.; Jirsa, M.; Kubinova, S.; Lunov, O.; Dejneka, A., *Cell Physiol. Biochem* 2019. 52(1): p. 119-140. IF 5.5

- **Uzhytchak, M.;** Lynnyk, A.; Zablotskii, V.; Dempsey, N.M.; Dias, A.L.; Bonfim, M.; Lunova, M.; Jirsa, M.; Kubinova, S.; Lunov, O., et al. *Appl. Phys. Lett.* 2017, *111*, 243703.

- Bláha, M., **Uzhytchak, M.,** Bondarenko, V., Policar, T. *Zool Anz*, 2017;
  267:151–154

- Samarin, A. M., Blecha, M., **Uzhytchak, M.,** Bytyutskyy, D., Zarski, D., Flajshans, M., & Policar, T., *Aquaculture*, 2016, **450**, 431–438.

List of Conferences

- **18th FEBS Young Scientists' Forum (YSF)/FEBS Congress 03.07.2018-12.07.2018** Oral presentation during the FEBS congress and a poster during YSF.

Topic: *Application of Iron oxide nanoparticles for the magnetic cell labelling and delivery vehicle within external pulsed magnetic field*

- **7th Young Professionals Workshop on Plasma Medicine Frontiers in Redox Biochemistry and Medicine (FiRBaM) 2018** Oral presentation.

  Topic: *Superparamagnetic iron oxide nanoparticles: friend or foe?*
- **The FEBS Congress 2019, Krakow, Poland**
  Poster session.

Topic: *Remote apoptosis resulted by external magnetic field in cancer cells loaded with magnetic nanoparticles as potential therapeutic method.*

- **The FEBS Congress 2021, virtual**
  Online

Topic: *Lysosome dysfunction induced by magnetic nanoparticles: is it an answer how to regulate the cell death remotely?*

List of Appendices

Appendix I

Uzhytchak, M.; Lynnyk, A.; Zablotskii, V.; Dempsey, N.M.; Dias, A.L.; Bonfim, M.; Lunova, M.; Jirsa, M.; Kubinova, S.; Lunov, O., et al. *The use of pulsed magnetic fields to increase the uptake of iron oxide nanoparticles by living cells.* ***Appl. Phys. Lett.*** 2017, 111, 243703.

Contribution: Design and realization of the experiments, interpretation of results, writing majority of the paper.

Appendix II

Lunov, O.; **Uzhytchak, M.;** Smolková, B.; Lunova, M.; Jirsa, M.; Dempsey, N.M.; Dias, A.L.; Bonfim, M.; Hof, M.; Jurkiewicz, P.; Petrenko, Y.; Kubinová, Š.; Dejneka, A. *Remote Actuation of Apoptosis in Liver Cancer Cells via Magneto-Mechanical Modulation of Iron Oxide Nanoparticles.* ***Cancers*** 2019, 11, 1873.

Contribution: Data acquisition and participation in the data interpretation and analysis, participation in writing and editing of the manuscript.

Appendix III

Uzhytchak, M.; Smolková, B.; Lunova, M.; Jirsa, M.; Frtús, A.; Kubinová, Š.; Dejneka, A.; Lunov, O. *Iron Oxide Nanoparticle-Induced Autophagic Flux Is Regulated by Interplay between p53-mTOR Axis and Bcl-2 Signaling in Hepatic Cells.* ***Cells*** 2020, 9, 1015.

Contribution: Design and realization of the experiments, interpretation of results, writing majority of the paper..

Appendix IV

Levada, K., Pshenichnikov, S., Omelyanchik, A. ...Lunova M., Jirsa M., Smolková B., **Uzhytchak M.,** Dejneka A., Lunov O. *Progressive lysosomal membrane permeabilization induced by iron oxide nanoparticles drives hepatic cell autophagy and apoptosis.* ***Nano Convergence*** 2020,7, 17. IF 8.526

Contribution: Data acquisition and participation in the data interpretation and analysis, participation in writing and editing of the manuscript.

Appendix V

Frtús A, Smolková B, **Uzhytchak M,** Lunova M, Jirsa M, Kubinová Š, Dejneka A, Lunov O. *Analyzing the mechanisms of iron oxide nanoparticles interactions with cells: A road from failure to success in clinical applications.* ***J. Control. Release*** 2020; 328: 59.

Contribution: Review of the literature, participation in interpretation of results, writing corresponding parts of the paper.

Appendix VI

Smolková B., MacCulloch T., Rockwood T. F., Liu M., Henry S. J. W., Frtús A., **Uzhytchak M.,** Lunova, M. Hof, P. Jurkiewicz, A. Dejneka, N. Stephanopoulos, and O. Lunov, *Protein Corona Inhibits Endosomal Escape of Functionalized DNA Nanostructures in Living Cells. ACS Appl. Mater. Interfaces* 2021, 13, 39, 46375–46390.

Contribution: Data acquisition and participation in the data interpretation and analysis, participation in writing and editing of the manuscript.

Appendix VII

Frtús, A.; Smolková, B.; **Uzhytchak, M.;** Lunova, M.; Jirsa, M.; Henry, S.J.W.; Dejneka, A.; Stephanopoulos, N.; Lunov, O. *The interactions*

between DNA nanostructures and cells: A critical overview from a cell biology perspective. ***Acta Biomater****.* 2022, *146*, 10–22.

Contribution: Data acquisition and participation in the data interpretation and analysis, participation in writing and editing of the manuscript.

Appendix VIII

Uzhytchak, M., Smolkova, B., Lunova, M., et al., *Lysosomal nanotoxicity: Impact of nanomedicines on lysosomal function.* ***Adv. Drug Delivery Rev.,*** 2023, vol. 197, p. 114828.

Contribution: Design and realization of the experiments, interpretation of results, writing majority of the paper.

References

1. Park, K., *The beginning of the end of the nanomedicine hype.* Journal of Controlled Release, 2019. **305**: p. 221-222.
2. Yang, V.C., *Personal perspectives and concerns over the so-called nanomedicine.* Journal of Controlled Release, 2019. **311**: p. 322-323.
3. *https://www.fda.gov/science-research/nanotechnology-programs-fda/nanotechnology-guidance-documents.*
4. *https://www.ema.europa.eu/en/news/european-medicines-agency-publishes-reflection-paper-general-issues-consideration-regarding-coated.*
5. Poon, W., et al., *A framework for designing delivery systems.* Nature Nanotechnology, 2020. **15**(10): p. 819-829.
6. Mitchell, M.J., et al., *Engineering precision nanoparticles for drug delivery.* Nature Reviews Drug Discovery, 2021. **20**(2): p. 101-124.
7. Frtús, A., et al., *Analyzing the mechanisms of iron oxide nanoparticles interactions with cells: A road from failure to success in clinical applications.* Journal of Controlled Release, 2020. **328**: p. 59-77.
8. Dawson, K.A. and Y. Yan, *Current understanding of biological identity at the nanoscale and future prospects.* Nature Nanotechnology, 2021. **16**(3): p. 229-242.
9. Wilhelm, S., et al., *Analysis of nanoparticle delivery to tumours.* Nature Reviews Materials, 2016. **1**(5): p. 16014.
10. Wang, J., Y.Y. Li, and G.J. Nie, *Multifunctional biomolecule nanostructures for cancer therapy.* Nature Reviews Materials, 2021. **6**(9): p. 766-783.
11. Kantamneni, H., et al., *Surveillance nanotechnology for multi-organ cancer metastases.* Nature Biomedical Engineering, 2017. **1**(12): p. 993-1003.

12. Cheng, C.J., et al., *A holistic approach to targeting disease with polymeric nanoparticles.* Nature Reviews Drug Discovery, 2015. **14**(4): p. 239-247.
13. Shi, J.J., et al., *Cancer nanomedicine: progress, challenges and opportunities.* Nature Reviews Cancer, 2017. **17**(1): p. 20-37.
14. Davis, M.E., Z. Chen, and D.M. Shin, *Nanoparticle therapeutics: an emerging treatment modality for cancer.* Nature Reviews Drug Discovery, 2008. **7**(9): p. 771-782.
15. Bobo, D., et al., *Nanoparticle-based medicines: A review of FDA-approved materials and clinical trials to date.* Pharm Res, 2016. **33**(10): p. 2373-87.
16. Fenton, O.S., et al., *Advances in biomaterials for drug delivery.* Advanced Materials, 2018. **30**(29): p. 1705328.
17. Caster, J.M., et al., *Investigational nanomedicines in 2016: a review of nanotherapeutics currently undergoing clinical trials.* Wiley Interdisciplinary Reviews-Nanomedicine and Nanobiotechnology, 2017. **9**(1): p. 1416.
18. Soundararajan, A., et al., *[Re-186]Liposomal doxorubicin (Doxil): in vitro stability, pharmacokinetics, imaging and biodistribution in a head and neck squamous cell carcinoma xenograft model.* Nuclear Medicine and Biology, 2009. **36**(5): p. 515-524.
19. Boswell, G.W., D. Buell, and I. Bekersky, *AmBisome (Liposomal amphotericin B): A comparative review.* Journal of Clinical Pharmacology, 1998. **38**(7): p. 583-592.
20. Iuliano, F., et al., *Phase II study of liposome encapsulated doxorubicin citrate complex, NPLD (Myocet (TM)) in myelofibrosis with myeloid metaplasia (MMM).* Blood, 2006. **108**(11): p. 1034a-1035a.
21. Silverman, J.A. and S.R. Deitcher, *Marqibo (R) (vincristine sulfate liposome injection) improves the pharmacokinetics and*

pharmacodynamics of vincristine. Cancer Chemotherapy and Pharmacology, 2013. **71**(3): p. 555-564.

22. Drummond, D.C., et al., *Development of a highly active nanoliposomal irinotecan using a novel intraliposomal stabilization strategy.* Cancer Research, 2006. **66**(6): p. 3271-3277.
23. Wang, Q., et al., *Pharmacokinetics, drug metabolism, and tissue distribution of CPX-351 in animals.* Nanomedicine-Nanotechnology Biology and Medicine, 2020. **30**: p. 102275.
24. Akinc, A., et al., *The Onpattro story and the clinical translation of nanomedicines containing nucleic acid-based drugs.* Nature Nanotechnology, 2019. **14**(12): p. 1084-1087.
25. Bhattacharyya, J., et al., *A paclitaxel-loaded recombinant polypeptide nanoparticle outperforms Abraxane in multiple murine cancer models.* Nature Communications, 2015. **6**: p. 7939.
26. Liu, Y., et al., *Topical ferumoxytol nanoparticles disrupt biofilms and prevent tooth decay in vivo via intrinsic catalytic activity.* Nature Communications, 2018. **9**: p. 2920.
27. Zou, P., et al., *Physicochemical characterization of iron carbohydrate colloid drug products.* AAPS Journal, 2017. **19**(5): p. 1359-1376.
28. Ahmed, U., P.S. Latham, and P.S. Oates, *Interactions between hepatic iron and lipid metabolism with possible relevance to steatohepatitis.* World Journal of Gastroenterology, 2012. **18**(34): p. 4651-4658.
29. Lunova, M., et al., *Hepcidin knockout mice fed with iron-rich diet develop chronic liver injury and liver fibrosis due to lysosomal iron overload.* Journal of Hepatology, 2014. **61**(3): p. 633-641.
30. Fernandez-Real, J.M. and M. Manco, *Effects of iron overload on chronic metabolic diseases.* Lancet Diabetes & Endocrinology, 2014. **2**(6): p. 513-526.
31. Liu, X.S., et al., *Safety considerations of cancer nanomedicine-A key step toward translation.* Small, 2020. **16**(36): p. 2000673.

32. Barenholz, Y., *Doxil (R) - The first FDA-approved nano-drug: Lessons learned.* Journal of Controlled Release, 2012. **160**(2): p. 117-134.
33. Gabizon, A., H. Shmeeda, and Y. Barenholz, *Pharmacokinetics of pegylated liposomal doxorubicin - Review of animal and human studies.* Clinical Pharmacokinetics, 2003. **42**(5): p. 419-436.
34. Solomon, R. and A.A. Gabizon, *Clinical pharmacology of liposomal anthracyclines: Focus on pegylated liposomal doxorubicin.* Clinical Lymphoma & Myeloma, 2008. **8**(1): p. 21-32.
35. Lyass, O., et al., *Correlation of toxicity with pharmacokinetics of pegylated liposomal doxorubicin (Doxil) in metastatic breast carcinoma.* Cancer, 2000. **89**(5): p. 1037-1047.
36. Toth, G.B., et al., *Current and potential imaging applications of ferumoxytol for magnetic resonance imaging.* Kidney International, 2017. **92**(1): p. 47-66.
37. Wells, S.A., et al., *Pharmacokinetics of ferumoxytol in the abdomen and pelvis: A dosing study with 1.5- and 3.0-T MRI relaxometry.* Radiology, 2020. **294**(1): p. 108-116.
38. McCullough, B.J., et al., *Ferumoxytol in clinical practice: Implications for MRI.* Journal of Magnetic Resonance Imaging, 2013. **37**(6): p. 1476-1479.
39. Bashir, M.R., et al., *Emerging applications for ferumoxytol as a contrast agent in MRI.* Journal of Magnetic Resonance Imaging, 2015. **41**(4): p. 884-898.
40. Rubin, R., *Black box warning for anemia drug.* Jama-Journal of the American Medical Association, 2015. **313**(17): p. 1704-1704.
41. *https://www.fda.gov/drugs/drug-safety-and-availability/fda-drug-safety-communication-fda-strengthens-warnings-and-changes-prescribing-instructions-decrease.*
42. Ke, P.C., et al., *A decade of the protein corona.* ACS Nano, 2017. **11**(12): p. 11773-11776.

43. Del Pino, P., et al., *Protein corona formation around nanoparticles - from the past to the future.* Materials Horizons, 2014. **1**(3): p. 301-313.
44. Ge, C.C., et al., *Towards understanding of nanoparticle-protein corona.* Archives of Toxicology, 2015. **89**(4): p. 519-539.
45. Onishchenko, N., D. Tretiakova, and E. Vodovozova, *Spotlight on the protein corona of liposomes.* Acta Biomater, 2021: p. 10.1016/j.actbio.2021.07.074.
46. Li, H.M., et al., *The protein corona and its effects on nanoparticle-based drug delivery systems.* Acta Biomaterialia, 2021. **129**: p. 57-72.
47. Salvati, A., et al., *Transferrin-functionalized nanoparticles lose their targeting capabilities when a biomolecule corona adsorbs on the surface.* Nature Nanotechnology, 2013. **8**(2): p. 137-143.
48. Rennick, J.J., A.P.R. Johnston, and R.G. Parton, *Key principles and methods for studying the endocytosis of biological and nanoparticle therapeutics.* Nature Nanotechnology, 2021. **16**(3): p. 266-276.
49. Behzadi, S., et al., *Cellular uptake of nanoparticles: Journey inside the cell.* Chemical Society Reviews, 2017. **46**(14): p. 4218-4244.
50. Rauch, J., et al., *Big signals from small particles: Regulation of cell signaling pathways by nanoparticles.* Chemical Reviews, 2013. **113**(5): p. 3391-3406.
51. Mosquera, J., I. Garcia, and L.M. Liz-Marzan, *Cellular uptake of nanoparticles versus small molecules: A matter of size.* Accounts of Chemical Research, 2018. **51**(9): p. 2305-2313.
52. Foroozandeh, P. and A.A. Aziz, *Insight into cellular uptake and intracellular trafficking of nanoparticles.* Nanoscale Research Letters, 2018. **13**: p. 339.

53. Anselmo, A.C. and S. Mitragotri, *Nanoparticles in the clinic: An update.* Bioengineering & Translational Medicine, 2019. **4**(3): p. e10143.
54. Lunov, O., et al., *Differential uptake of functionalized polystyrene nanoparticles by human macrophages and a monocytic cell line.* Acs Nano, 2011. **5**(3): p. 1657-1669.
55. Serpooshan, V., et al., *Effect of cell sex on uptake of nanoparticles: The overlooked factor at the nanobio interface.* ACS Nano, 2018. **12**(3): p. 2253-2266.
56. Uzhytchak, M., et al., *Iron oxide nanoparticle-induced autophagic flux is regulated by interplay between p53-mTOR axis and Bcl-2 signaling in hepatic cells.* Cells, 2020. **9**(4): p. 1015.
57. Sun, D.X., S. Zhou, and W. Gao, *What went wrong with anticancer nanomedicine design and how to make it right.* ACS Nano, 2020. **14**(10): p. 12281-12290.
58. Wang, L., et al., *Deciphering active biocompatibility of iron oxide nanoparticles from their intrinsic antagonism.* Nano Research, 2018. **11**(5): p. 2746-2755.
59. Feng, Q., et al., *Uptake, distribution, clearance, and toxicity of iron oxide nanoparticles with different sizes and coatings.* Sci Rep, 2018. **8**(1): p. 2082.
60. Li, X., et al., *Iron oxide nanoparticles promote the migration of mesenchymal stem cells to injury sites.* Int J Nanomedicine, 2019. **14**: p. 573-589.
61. Gu, Z., et al., *Mechanism of iron oxide-induced macrophage activation: The impact of composition and the underlying signaling pathway.* J Am Chem Soc, 2019. **141**(15): p. 6122-6126.
62. Liu, L., et al., *Bioactive iron oxide nanoparticles suppress osteoclastogenesis and ovariectomy-induced bone loss through regulating the TRAF6-p62-CYLD signaling complex.* Acta Biomater, 2020. **103**: p. 281-292.

63. He, C., et al., *Endoplasmic reticulum stress mediates inflammatory response triggered by ultra-small superparamagnetic iron oxide nanoparticles in hepatocytes.* Nanotoxicology, 2018. **12**(10): p. 1198-1214.
64. Liu, Y., et al., *Characterization of superparamagnetic iron oxide nanoparticle-induced apoptosis in PC12 cells and mouse hippocampus and striatum.* Toxicol Lett, 2018. **292**: p. 151-161.
65. Pedro, L., et al., *Impact of locally administered carboxydextran-coated super-paramagnetic iron nanoparticles on cellular immune function.* Small, 2019. **15**(20): p. e1900224.
66. Lunov, O., et al., *Remote actuation of apoptosis in liver cancer cells via magneto-mechanical modulation of iron oxide nanoparticles.* Cancers (Basel), 2019. **11**(12): p. 1873.
67. Jin, R.R., et al., *Iron oxide nanoparticles promote macrophage autophagy and inflammatory response through activation of toll-like Receptor-4 signaling.* Biomaterials, 2019. **203**: p. 23-30.
68. He, C.Y., et al., *Mitochondrial electron transport chain identified as a novel molecular target of SPIO nanoparticles mediated cancer-specific cytotoxicity.* Biomaterials, 2016. **83**: p. 102-114.
69. Truffi, M., et al., *Multivalent exposure of trastuzumab on iron oxide nanoparticles improves antitumor potential and reduces resistance in HER2-positive breast cancer cells.* Sci Rep, 2018. **8**(1): p. 6563.
70. Fiandra, L., et al., *Assessing the in vivo targeting efficiency of multifunctional nanoconstructs bearing antibody-derived ligands.* ACS Nano, 2013. **7**(7): p. 6092-102.
71. Traini, G., et al., *Cancer immunotherapy of TLR4 agonist-antigen constructs enhanced with pathogen-mimicking magnetite nanoparticles and checkpoint blockade of PD-L1.* Small, 2019. **15**(4): p. e1803993.

72. Uzhytchak, M., et al., *Iron oxide nanoparticle-induced autophagic flux Is regulated by interplay between p53-mTOR axis and Bcl-2 signaling in hepatic cells.* Cells, 2020. **9**: p. 1015.
73. Krishna, R., et al., *Doxorubicin encapsulated in sterically stabilized liposomes exhibits renal and biliary clearance properties that are independent of valspodar (PSC 833) under conditions that significantly inhibit nonencapsulated drug excretion.* Clinical Cancer Research, 1999. **5**(10): p. 2939-2947.
74. Smits, E.A.W., et al., *The availability of drug by liposomal drug delivery Individual kinetics and tissue distribution of encapsulated and released drug in mice after administration of PEGylated liposomal prednisolone phosphate.* Investigational New Drugs, 2019. **37**(5): p. 890-901.
75. He, H., et al., *Pharmacokinetics and pharmacodynamics modeling and simulation systems to support the development and regulation of liposomal drugs.* Pharmaceutics, 2019. **11**(3): p. 110.
76. van der Koog, L., T.B. Gandek, and A. Nagelkerke, *Liposomes and extracellular vesicles as drug delivery systems: A comparison of composition, pharmacokinetics, and functionalization.* Advanced Healthcare Materials, 2021: p. e2100639.
77. Ngo, W., et al., *Why nanoparticles prefer liver macrophage cell uptake in vivo.* Advanced Drug Delivery Reviews, 2022. **185**: p. 114238.
78. Boey, A. and H.K. Ho, *All roads lead to the liver: Metal nanoparticles and their implications for liver health.* Small, 2020. **16**(21): p. 2000153.
79. Ahrens, E.T. and J.W.M. Bulte, *Tracking immune cells in vivo using magnetic resonance imaging.* Nature Reviews Immunology, 2013. **13**(10): p. 755-763.
80. Lammers, T. and M. Ferrari, *The success of nanomedicine.* Nano Today, 2020. **31**.

81. Pelaz, B., et al., *Diverse applications of nanomedicine.* ACS Nano, 2017. **11**(3): p. 2313-2381.
82. Groeneveld, E. and C. de Mello Donegá, *The challenge of colloidal nanoparticle synthesis*, in *Nanoparticles: Workhorses of Nanoscience*, C. de Mello Donegá, Editor. 2014, Springer Berlin Heidelberg: Berlin, Heidelberg. p. 145-189.
83. Abedini, A., et al., *Recent advances in shape-controlled synthesis of noble metal nanoparticles by radiolysis route.* Nanoscale Res Lett, 2016. **11**(1): p. 287.
84. da Silva, A.G., et al., *Controlling size, morphology, and surface composition of AgAu nanodendrites in 15 s for improved environmental catalysis under low metal loadings.* ACS Appl Mater Interfaces, 2015. **7**(46): p. 25624-32.
85. Wang, P., et al., *Visualization of the cellular uptake and trafficking of DNA origami nanostructures in cancer cells.* J Am Chem Soc, 2018. **140**(7): p. 2478-2484.
86. Bastings, M.M.C., et al., *Modulation of the cellular uptake of DNA origami through control over mass and shape.* Nano Letters, 2018. **18**(6): p. 3557-3564.
87. Whitehouse, W.L., et al., *Cholesterol anchors enable efficient binding and intracellular uptake of DNA nanostructures.* Bioconjug Chem, 2019. **30**(7): p. 1836-1844.
88. Rothemund, P.W.K., *Folding DNA to create nanoscale shapes and patterns.* Nature, 2006. **440**(7082): p. 297-302.
89. Han, D., et al., *DNA origami with complex curvatures in three-dimensional space.* Science, 2011. **332**(6027): p. 342-346.
90. Douglas, S.M., et al., *Self-assembly of DNA into nanoscale three-dimensional shapes.* Nature, 2009. **459**(7245): p. 414-418.
91. Ke, Y., et al., *Three-dimensional structures self-assembled from DNA bricks.* Science, 2012. **338**(6111): p. 1177-1183.

92. Dong, Y.H., et al., *DNA functional materials assembled from branched DNA: Design, synthesis, and applications.* Chemical Reviews, 2020. **120**(17): p. 9420-9481.
93. Wang, X., et al., *Paranemic crossover DNA: There and back again.* Chemical Reviews, 2019. **119**(10): p. 6273-6289.
94. Burns, J.R., et al., *A biomimetic DNA-based channel for the ligand-controlled transport of charged molecular cargo across a biological membrane.* Nature Nanotechnology, 2016. **11**(2): p. 152-156.
95. Li, M., et al., *Discovery and characterization of a peptide that enhances endosomal escape of delivered proteins in vitro and in vivo.* Journal of the American Chemical Society, 2015. **137**(44): p. 14084-14093.
96. Cai, R. and C.Y. Chen, *The crown and the scepter: Roles of the protein corona in nanomedicine.* Advanced Materials, 2019. **31**(45): p. e1805740.
97. Jahanban-Esfahlan, A., et al., *Dynamic DNA nanostructures in biomedicine: Beauty, utility and limits.* Journal of Controlled Release, 2019. **315**: p. 166-185.
98. Keller, A. and V. Linko, *Challenges and perspectives of DNA nanostructures in biomedicine.* Angewandte Chemie-International Edition, 2020. **59**(37): p. 15818-15833.
99. Chandrasekaran, A.R., *Nuclease resistance of DNA nanostructures.* Nature Reviews Chemistry, 2021. **5**(4): p. 225-239.
100. Kharazian, B., N.L. Hadipour, and M.R. Ejtehadi, *Understanding the nanoparticle-protein corona complexes using computational and experimental methods.* International Journal of Biochemistry & Cell Biology, 2016. **75**: p. 162-174.
101. Walsh, A.S., et al., *DNA cage delivery to mammalian cells.* ACS Nano, 2011. **5**(7): p. 5427-5432.

102. Yong, K.W., et al., *Pointing in the right direction: Controlling the orientation of proteins on nanoparticles improves targeting efficiency.* Nano Letters, 2019. **19**(3): p. 1827-1831.
103. Yong, K.W., et al., *Engineering the orientation, density, and flexibility of single-domain antibodies on nanoparticles to improve cell targeting.* ACS Applied Materials & Interfaces, 2020. **12**(5): p. 5593-5600.
104. Johnston, A.P.R., et al., *Targeting cancer cells: Controlling the binding and internalization of antibody-functionalized capsules.* ACS Nano, 2012. **6**(8): p. 6667-6674.
105. Colombo, M., et al., *Tumour homing and therapeutic effect of colloidal nanoparticles depend on the number of attached antibodies.* Nature Communications, 2016. **7**: p. 13818.
106. Zhang, Q.Y. and B.M. Reinhard, *Ligand density and nanoparticle clustering cooperate in the multivalent amplification of epidermal growth factor receptor activation.* ACS Nano, 2018. **12**(10): p. 10473-10485.
107. Chithrani, B.D., A.A. Ghazani, and W.C.W. Chan, *Determining the size and shape dependence of gold nanoparticle uptake into mammalian cells.* Nano Letters, 2006. **6**(4): p. 662-668.
108. Cremers, G.A.O., et al., *Determinants of ligand-functionalized DNA nanostructure-cell interactions.* Journal of the American Chemical Society, 2021. **143**(27): p. 10131-10142.
109. Douglas, S.M., et al., *Self-assembly of DNA into nanoscale three-dimensional shapes.* Nature, 2009. **459**(7245): p. 414-418.
110. Castro, C.E., et al., *A primer to scaffolded DNA origami.* Nature Methods, 2011. **8**(3): p. 221-229.
111. Sobczak, J.P.J., et al., *Rapid folding of DNA into nanoscale shapes at constant temperature.* Science, 2012. **338**(6113): p. 1458-1461.
112. Benson, E., et al., *DNA rendering of polyhedral meshes at the nanoscale.* Nature, 2015. **523**(7561): p. 441-444.

113. Shi, J., et al., *Cancer nanomedicine: progress, challenges and opportunities.* Nat Rev Cancer, 2017. **17**(1): p. 20-37.
114. Gause, K.T., et al., *Immunological principles guiding the rational design of particles for vaccine delivery.* ACS Nano, 2017. **11**(1): p. 54-68.
115. Anchordoquy, T.J., et al., *Mechanisms and barriers in cancer nanomedicine: Addressing challenges, looking for solutions.* ACS Nano, 2017. **11**(1): p. 12-18.
116. Qin, S.Y., et al., *Drug self-delivery systems for cancer therapy.* Biomaterials, 2017. **112**: p. 234-247.
117. Cheng, Y.H., et al., *Meta-analysis of nanoparticle delivery to tumors using a physiologically based pharmacokinetic modeling and simulation approach.* ACS Nano, 2020. **14**(3): p. 3075-3095.
118. Sindhwani, S., et al., *The entry of nanoparticles into solid tumours.* Nature Materials, 2020. **19**: p. 566–575.
119. Frtus, A., et al., *Analyzing the mechanisms of iron oxide nanoparticles interactions with cells: A road from failure to success in clinical applications.* J Control Release, 2020. **328**: p. 59-77.
120. Ge, C., et al., *Towards understanding of nanoparticle-protein corona.* Arch Toxicol, 2015. **89**(4): p. 519-39.
121. Saptarshi, S.R., A. Duschl, and A.L. Lopata, *Interaction of nanoparticles with proteins: relation to bio-reactivity of the nanoparticle.* J Nanobiotechnology, 2013. **11**: p. 26.
122. Dey, S., et al., *DNA origami.* Nature Reviews Methods Primers, 2021. **1**(1): p. 13.
123. Xu, F., Q. Xia, and P.F. Wang, *Rationally designed DNA nanostructures for drug delivery.* Frontiers in Chemistry, 2020. **8**: p. 751.
124. Harman, C., *The fallacy of 'alternative' medicine.* Nature Reviews Nephrology, 2009. **5**(7): p. 361-361.

125. Singh, S. and E. Ernst, *Trick or treatment? : alternative medicine on trial*. 2009, London: Transworld.
126. *https://blogs.bmj.com/bmj/2012/08/15/edzard-ernst-the-natural-equals-safe-fallacy/.*
127. Ben-David, U., et al., *Genetic and transcriptional evolution alters cancer cell line drug response.* Nature, 2018. **560**(7718): p. 325-330.
128. Masters, J.R., *HeLa cells 50 years on: the good, the bad and the ugly.* Nature Reviews Cancer, 2002. **2**(4): p. 315-319.
129. Horbach, S.P.J.M. and W. Halffman, *The ghosts of HeLa: How cell line misidentification contaminates the scientific literature.* Plos One, 2017. **12**(10): p. e0186281.
130. Lunov, O., et al., *The effect of carboxydextran-coated superparamagnetic iron oxide nanoparticles on c-Jun N-terminal kinase-mediated apoptosis in human macrophages.* Biomaterials, 2010. **31**(19): p. 5063-5071.
131. Lunov, O., et al., *Lysosomal degradation of the carboxydextran shell of coated superparamagnetic iron oxide nanoparticles and the fate of professional phagocytes.* Biomaterials, 2010. **31**(34): p. 9015-9022.
132. Xie, J., et al., *Iron oxide nanoparticle platform for biomedical applications.* Curr Med Chem, 2009. **16**(10): p. 1278-94.
133. Pankhurst, Q., S. Jones, and J. Dobson, *Applications of magnetic nanoparticles in biomedicine: the story so far.* Journal of Physics D-Applied Physics, 2016. **49**(50).
134. Uzhytchak, M., et al., *The use of pulsed magnetic fields to increase the uptake of iron oxide nanoparticles by living cells.* Applied Physics Letters, 2017. **111**(24): p. 243703.
135. Kim, D.H., et al., *Biofunctionalized magnetic-vortex microdiscs for targeted cancer-cell destruction.* Nature Materials, 2010. **9**(2): p. 165-171.

136. Elbez, R., et al., *Nanoparticle induced cell magneto-rotation: monitoring morphology, stress and drug sensitivity of a suspended single cancer cell.* PLoS One, 2011. **6**(12): p. e28475.
137. Hapuarachchige, S., et al., *Non-temperature induced effects of magnetized iron oxide nanoparticles in alternating magnetic field in cancer cells.* PLoS One, 2016. **11**(5): p. e0156294.
138. Master, A.M., et al., *Remote actuation of magnetic nanoparticles for cancer cell selective treatment through cytoskeletal disruption.* Scientific Reports, 2016. **6**: p. 33560.
139. Zhang, E., et al., *Dynamic magnetic fields remote-control apoptosis via nanoparticle rotation.* ACS Nano, 2014. **8**(4): p. 3192-201.
140. Wong, W., et al., *Interplay of cell death signaling pathways mediated by alternating magnetic field gradient.* Cell Death Discov, 2018. **4**: p. 49.
141. Domenech, M., et al., *Lysosomal membrane permeabilization by targeted magnetic nanoparticles in alternating magnetic fields.* ACS Nano, 2013. **7**(6): p. 5091-5101.
142. Lynnyk, A., et al., *Manipulating the mitochondria activity in human hepatic cell line Huh7 by low-power laser irradiation.* Biomed Opt Express, 2018. **9**(3): p. 1283-1300.
143. Smolkova, B., et al., *Non-thermal plasma, as a new physicochemical source, to induce redox imbalance and subsequent cell death in liver cancer cell lines.* Cell Physiol Biochem, 2019. **52**(1): p. 119-140.
144. Lunova, M., et al., *Nanoparticle core stability and surface functionalization drive the mTOR signaling pathway in hepatocellular cell lines.* Sci Rep, 2017. **7**(1): p. 16049.
145. Krysko, O., L. de Ridder, and M. Cornelissen, *Phosphatidylserine exposure during early primary necrosis (oncosis) in JB6 cells as evidenced by immunogold labeling technique.* Apoptosis, 2004. **9**(4): p. 495-500.

146. Galluzzi, L., et al., *Molecular mechanisms of cell death: recommendations of the Nomenclature Committee on Cell Death 2018.* Cell Death Differ, 2018. **25**(3): p. 486-541.
147. Galluzzi, L., et al., *Molecular definitions of cell death subroutines: recommendations of the Nomenclature Committee on Cell Death 2012.* Cell Death and Differentiation, 2012. **19**(1): p. 107-120.
148. Boya, P. and G. Kroemer, *Lysosomal membrane permeabilization in cell death.* Oncogene, 2008. **27**(50): p. 6434-51.
149. Settembre, C., et al., *Signals from the lysosome: a control centre for cellular clearance and energy metabolism.* Nature Reviews Molecular Cell Biology, 2013. **14**(5): p. 283-296.
150. Boya, P., et al., *Lysosomal membrane permeabilization induces cell death in a mitochondrion-dependent fashion.* J Exp Med, 2003. **197**(10): p. 1323-34.
151. Erdal, H., et al., *Induction of lysosomal membrane permeabilization by compounds that activate p53-independent apoptosis.* Proceedings of the National Academy of Sciences of the United States of America, 2005. **102**(1): p. 192-197.
152. Pierzynska-Mach, A., P.A. Janowski, and J.W. Dobrucki, *Evaluation of acridine orange, lysotracker red, and quinacrine as fluorescent probes for long-term tracking of acidic vesicles.* Cytometry Part A, 2014. **85a**(8): p. 729-737.
153. Kirkegaard, T., et al., *Hsp70 stabilizes lysosomes and reverts Niemann-Pick disease-associated lysosomal pathology.* Nature, 2010. **463**(7280): p. 549-553.
154. Petersen, N.H.T., et al., *Transformation-associated changes in sphingolipid metabolism sensitize cells to lysosomal cell death induced by inhibitors of acid sphingomyelinase.* Cancer Cell, 2013. **24**(3): p. 379-393.
155. Kast, D.J. and R. Dominguez, *The cytoskeleton-autophagy connection.* Curr Biol, 2017. **27**(8): p. R318-R326.

156. Pu, J., et al., *Mechanisms and functions of lysosome positioning.* J Cell Sci, 2016. **129**(23): p. 4329-4339.
157. Gonzalez-Rodriguez, D., et al., *Mechanical criterion for the rupture of a cell membrane under compression.* Biophys J, 2016. **111**(12): p. 2711-2721.
158. Langhans, S.A., *Three-dimensional in vitro cell culture models in drug discovery and drug repositioning.* Front Pharmacol, 2018. **9**: p. 6.
159. Xu, X., M.C. Farach-Carson, and X. Jia, *Three-dimensional in vitro tumor models for cancer research and drug evaluation.* Biotechnol Adv, 2014. **32**(7): p. 1256-1268.